

**Imaging of Cenozoic climatic events and bottom  
water activities at the northeastern flank of  
Walvis Ridge: A correlation of seismic data  
with borehole data measurements**

**Dissertation**

zur Erlangung des Doktorgrades der Naturwissenschaften

im Fachbereich 5  
der Universität Bremen

vorgelegt von  
Thomas Bartels  
Bremen im  
Januar 2008

**Name:** Thomas Bartels

**Datum:** 3.1.2008

**Anschrift:** Moorbekring 23 F 22359, Hamburg

## **Erklärung:**

---

**Hiermit versichere ich, dass ich**

- 1. die Arbeit ohne unerlaubte fremde Hilfe angefertigt habe**
- 2. keine anderen als die von mir angegebenen Quellen und Hilfsmittel benutzt habe**
- 3. die den benutzten Werken wörtlich oder inhaltlich entnommenen Stellen als solche kenntlich gemacht habe**

Bremen, den

---

Unterschrift

## Table of contents:

<b>Zusammenfassung</b> .....	1
<b>Summary</b> .....	4
<b>1. Introduction</b> .....	6
1.1 General Introduction.....	6
1.2 Data.....	10
1.2.1 Seismic data / data acquisition.....	10
1.2.1.1 Processing of the multichannel GI-Gun data.....	11
1.2.1.2 Processing of the multichannel Watergun data.....	12
1.2.3 Echosounder (Parasound) data.....	15
1.2.4 Bathymetry (Hydrosweep) data.....	15
1.2.5 Borehole data.....	16
1.3 The paleoclimate (a general overview).....	18
1.4 The thermohaline circulation (a general overview).....	21
1.5 Role candidate.....	25
1.6 References.....	25
<b>2. A correlation of high resolution seismic data with ODP Leg 208 borehole measurements</b> .....	31
2.1 Abstract.....	31
2.2 Introduction.....	32
2.3 Data and methods.....	33
2.3.1 The seismic data.....	34
2.3.2 Calculation of synthetic seismograms.....	34
2.3.3 Editing of Grape Density Data.....	34
2.3.4 P-Wave velocity-models.....	36
2.3.5 Correlation of the synthetic seismograms with the seismic record.....	37
2.4 Description of the Sites.....	42
2.5 Discussion.....	52
2.5.1 Seismic characterization of target horizons.....	52
2.5.2 Sedimentary features on outer Walvis Ridge.....	54
2.6 Conclusions.....	55
2.7 Acknowledgements.....	58
2.8 References.....	58
<b>3. Seismic imaging of thin clay layers deposited during extreme Cenozoic climatic events</b> .....	61
3.1 Abstract.....	61
3.2 Introduction.....	62

3.3	Seismic data.....	64
3.4	Borehole data.....	66
3.5	Modelling.....	67
3.6	Results.....	70
3.7	Discussion.....	80
3.8	Conclusions.....	82
3.9	Acknowledgements.....	82
3.10	References.....	83
<b>4.</b>	<b>Cenozoic evolution of central Walvis Ridge paleotopography.....</b>	<b>85</b>
4.1	Abstract.....	85
4.2	Introduction.....	85
	4.2.1 Geologic setting.....	87
	4.2.2 Oceanographic Setting.....	87
4.3	Methods.....	88
	4.3.1 Seismic data.....	88
	4.3.2 Model of the paleotopography and age determination.....	89
4.4	Results .....	90
	4.4.1 Model of the paleotopography.....	90
	4.4.2 Seismic data.....	93
	4.4.3 Ages of the channel structures.....	94
4.5	Discussion.....	97
4.6	Conclusions.....	99
4.7	Acknowledgements.....	99
4.8	References.....	100
<b>5.</b>	<b>The Walvis Kom: A pathway for AABW from the Cape Basin to the Angola Basin?.....</b>	<b>103</b>
5.1	Abstract.....	103
5.2	Introduction.....	103
5.3	Methods.....	106
	5.3.1 Seismic data.....	106
	5.3.2 Sediment echo-sounder profiling .....	107
	5.3.3 Swath mapping data.....	107
5.4	Results.....	107
	5.4.1 Bathymetry.....	107
	5.4.2 Seismic and echo-sounder profiles.....	109
	5.4.3 Stratigraphy.....	119
5.5	Discussion.....	120



5.6	Conclusion.....	125
5.7	Acknowledgements.....	126
5.8	References.....	126
<b>6.</b>	<b>Final conclusions .....</b>	<b>131</b>
<b>7.</b>	<b>Acknowledgements.....</b>	<b>133</b>

## Zusammenfassung

Die Untersuchung der Sedimentationsprozesse und der paläoozeanographischen Entwicklung im Bereich des Walfisch Rückens, wurde über eine Korrelation mariner seismischer Daten der R/V Meteor Expedition M49/1 mit Tiefsee Bohrdaten des ODP (*Ocean Drilling Program*) Leg 208 durchgeführt. Die R/V Meteor Expedition M 49/1 diente dabei der Vorerkundung potentieller Bohrpositionen für das Leg 208, dessen Ziel die Untersuchung extremer klimatischer Ereignisse im Känozoikum war. Hauptziel hierfür war die Gewinnung vollständiger ungestörter Sedimentsequenzen über einen größeren Tiefenbereich, die klimatischen Ereignisse, wie die E/O Grenze (Eozän-Oligozän Grenze), das ELMO Ereignis (Chron C24n ELMO event), das PETM (*Paleocene Eocene thermal maximum*), das ELPE Ereignis (Mid-paleocene biotic event) und die K/T-Grenze (Kreide-Tertiär-Grenze) beinhalten.

Für eine bestmögliche vertikale Auflösung und Eindringung der seismischen Signale in die Sedimente, wurde für die Datenerhebung der Meteor Ausfahrt M49/1 ein Mehrfrequenzansatz mit zwei unterschiedlichen seismischen Quellen gewählt.

Der Walfisch Rücken teilt den südöstlichen Atlantik in das nördlich liegende Angola Becken und das südlich gelegene Kap Becken. Er gilt als Barriere für die Tiefenwässer der beiden Becken, wobei sich das Tiefenwasser des Angola Beckens aus Nordatlantischem Tiefenwasser (NADW) und das des Kap Beckens aus Antarktischem Bodenwasser (AABW) zusammensetzt.

Die Sedimente des Walfisch Rücken bestehen hauptsächlich aus ungestörten känozoischen Sequenzen, deren Mächtigkeit zwischen ~150 m am Kontakt zum Angola Becken und ~450 m auf der Rückenachse variieren. Mit Hilfe einer Berechnung synthetischer Seismogramme aus den Dichte- und Geschwindigkeitsmessungen der Bohrlochdaten wurden die seismischen Daten mit den Bohrdaten korreliert. Die Ergebnisse dieser simplen Modellierung ermöglichen das Zuordnen der klimatischen Ereignisse, wie z.B. der E/O-Grenze oder des ELMO Ereignisses, zu bestimmten seismischen Reflektoren. Die kontinuierlichen Reflektoren der einzelnen Ereignisse zeichnen sich dabei durch gleiche seismische Attribute an den unterschiedlichen Bohrlokationen sowie durch eine regionale Verbreitung aus.

Eine neu entwickelte, zusätzlich zu den Standardprozessingschritten durchgeführte statische Korrektur der Watergun Daten liefert hochauflösende seismische Abbildungen, mit einer wesentlich genaueren Stratigraphie als die der GI-Gun. Ein Abgleich mit den magnetischen Bohrlochmessungen zeigt, dass es mit Hilfe dieser hochauflösenden

Tiefseeseismik erstmalig möglich ist, die Meter bis Submeter mächtigen tonhaltigen Klimahorizonte wie das PETM, das ELMO Ereignis und das ELPE Ereignis in der Seismik abzubilden. Anders als in den GI-Gun Daten, welche durch ihre größere Wellenlänge limitiert werden, bilden sich die Horizonte in der Seismik als einzelne deutlich voneinander getrennte Reflektoren oder Reflektorenpakete ab.

Unter Vernachlässigung tektonischer Ereignisse, welche für das Arbeitsgebiet während der letzten 60 Mio Jahre auch nicht bekannt sind, repräsentieren die mit Hilfe der Stratigraphie des Legs 208 datierten seismischen Reflektoren unter Berücksichtigung der Subsidenz der ozeanischen Kruste den Paläo-Meeressboden des Arbeitsgebietes. Mit Hilfe eines Gridding-Algorithmuses wurde somit ein Modell des Paläomeeresbodens während des Känozoikums erstellt. Die Ergebnisse des Modells zeigen, dass die Subsidenz Raten in etwa den Sedimentationsraten des Arbeitsgebietes entsprachen. Zusätzlich wird die Entstehung einer Kanalstruktur über den Walfisch Rücken im süd-östlichen Teil des Arbeitsgebietes zwischen 28°S und 30°S hervorgehoben, welche möglicherweise mit einem Austausch von Tiefenwässern zwischen dem Kap Becken und dem Angola Becken zusammenhängt. Mit Hilfe eines auf der Stratigraphie des Legs 208 basierenden Altersmodells, lässt sich das Einsetzen der Strömung über den Walfisch Rücken auf das mittlere Miozän datieren.

Bereits bekannte Messungen der Wassertemperatur und des Salzgehalts weisen den Walfisch Kom am südwestlichen Teil des Walfisch Rückens als einen weiteren möglichen Durchflussspunkt über den Rücken aus. Die Ergebnisse der bathymetrischen und seismischen Profile entlang des Walfisch Kom zeigen, dass die Blöcke des Walfisch Rückens einen möglichen Durchfluss bilden, der das AABW, welches vom Kapbecken aus durch die Coriolis Kraft in den Durchfluss gedrückt wird, in Richtung des Angola Becken leitet könnte. Mehrere Toplap Strukturen, strömungsinduzierte Driftkörper and Sedimentwellen entlang des Durchflusses weisen auf rezente Strömungsaktivitäten im Walvis Kom hin. Zusätzlich zeigen die Daten eine Abnahme des Strömungsquerschnittes, welches zu einer Abnahme der Sedimentmächtigkeiten entlang des Durchflusses in Richtung des Angola Beckens führt. Mit Hilfe eines einfachen Altersmodells lässt sich das Einsetzen einer Strömung auf das Untere Miozän datieren.

Anders als bei der klassischen Annahme, dass der Walfisch Rücken eine unüberwindbare Barriere für Tiefenwasser mit nur zwei Durchflussspunkten (Walfisch Passage und Namib Col) ist, zeigen die Ergebnisse der Untersuchungen der Tiefenwasserströmungen, dass weitere rezente Durchflussspunkte entlang des Rückens auftreten bei denen es zu einem Austausch von Tiefenwässern kommen kann. Zeitlich setzt

---

die Strömungsaktivität in beiden Regionen während des Miozäns ein, welches für den Süd-Atlantik eine besonders dynamische Periode war, in der sich u.a. der Zentral Amerikanische Seeweg schloss und sich die heutige Tiefenzirkulationzelle des Atlantiks bildete.

## Summary

The history of sedimentation and current activities at the northeastern flank of Walvis Ridge is investigated by a correlation of multichannel seismic data collected during R/V Meteor Cruise M49/1 in early 2001 with borehole measurements of Ocean Drilling Project (ODP) Leg 208, which was realized in 2003. Meteor Cruise M49/1 was the main seismic pre-site survey for ODP Leg 208 'Early Cenozoic Extreme Climates: The Walvis Transect', whose main objectives were to recover intact composite sequences from climatic transitions like the Eocene/Oligocene (E/O) boundary, the Chron C24n ELMO event, the Paleocene Eocene Thermal Maximum (PETM), the Mid-Paleocene biotic event (ELPE Event) and the Cretaceous/Tertiary (K/T) boundary. During Meteor Cruise M 49/1 multi-frequency seismic data were collected using three seismic sources, two Generator Injector (GI) Guns (0.4 l; 100 Hz -500 Hz and 1.7 l; 30 Hz - 200 Hz) and one Watergun (0.16 l; 200 Hz - 1600 Hz), in a quasi simultaneous mode in order to get best possible penetration and resolution of the sub-surface structures.

Walvis Ridge divides the southeastern Atlantic Ocean into two basins, the Angola Basin to the north and the Cape Basin to the south. It is well known as an impassable barrier for bottom waters which separates Antarctic Bottom Waters (AABW) widely distributed in the Cape Basin from North Atlantic Depth Waters (NADW) in the Angola Basin. The sediments of the northeastern flank of Walvis Ridge are characterized by mostly undisturbed sequences of Cenozoic sediments, with varying thickness of ~150 m at the edge of the Angola Basin and ~450 m at the axis of the ridge.

A correlation of seismic data with borehole data was accomplished by calculating synthetic seismograms using GRA density measurements of the cores and an averaged velocity model. This "simple" event modeling allows to assign ages to the seismic reflectors and to identify key horizons/boundaries like the E/O and the K/T boundaries as well as the ELMO event and deposits of the PETM, representing Cenozoic climatic events. The seismic pattern of these target horizons shows similar properties at the different sites indicating their regional distribution.

A special static correction in addition to standard seismic processing steps resulted in high quality high resolution deep sea Watergun images. A comparison between the seismic images and the magnetic core measurements of Leg 208 proves that Watergun data allows imaging of sub-meter sediment layers like the PETM or the ELMO event. In contrast to the

lower resolution GI-Gun data, the critical transitions occur as single horizons, separated from each other by continuous lower amplitude reflector packages on the Watergun data.

Several significant seismic reflectors, whose ages were determined using the stratigraphy of Leg 208, can be traced across the entire survey area. The reflectors represent the paleoseafloor of the study area under consideration of the subsidence though neglecting possible tectonic events as they are unknown for this region in the last 60 Ma. Gridding of these horizons leads to a model of the paleoseafloor, which shows that the rate of subsidence of the Angola Basin almost equals the increasing thickness of the sediment column. In addition the model indicates the development of a channel structure across the ridge in the southeast of the study area between 28°S and 30°S, which is possibly connected to an exchange of AABW and NADW between Cape Basin and Angola Basin. Determining the age of this channel by using Leg 208 stratigraphy suggests that current activities have increased since the Middle Miocene.

Southwest of the area drilled during ODP-Leg 208, the seismic profiles of Meteor Cruise M 49/1 cross a suggested flow path of AABW between Cape Basin and Angola Basin in a region called Walvis Kom. Walvis Kom is suitable for a bottom water transfer due to its channel like structure. AABW in the Cape Basin might be pushed into the flow path by the Coriolis Force and continues to flow into the Angola Basin. Several toplap structures, contourite-sheeted drifts and sedimentary waves indicate recent bottom water activities in the channel. A combination of bathymetry data and seismic data shows a reduction of the current cross-section along the flow path, which must result in an increasing current velocity explaining less deposition along the path way in direction to the Angola Basin. A simple age model, based on the stratigraphy of Leg 208 at the 28°S, determines the initiation of current activities during the Lower Miocene at ~16 Ma.

In addition to the assumption that Walvis Ridge builds an impassable barrier for bottom waters with at least two leakages (Walvis Passage and Namib Col), our results suggest two more leakages across the ridge. The initiation of bottom water exchange through these pathways started during the Miocene. The Miocene is known as an oceanographic dynamic period for the South Atlantic, where for example the Central American Seaway was closed and the recent thermohaline circulation of the South Atlantic developed.

## 1. Introduction

### 1.1 General introduction

In order to find an accurate location for a drill site in the ocean, it is important to have a good knowledge about the geological situation below the sea bottom. Normally, for this task, seismic data, which illustrates an overview of the sea bottom and the sedimentary features, can be used. In early 2001 R/V Meteor Cruise M49/1 carried out an expedition into the South Atlantic to identify drilling positions for Ocean Drilling Program (ODP) ‘Early Cenozoic Extreme Climates: The Walvis Ridge Transect’. The subsequent ODP Leg 208 took place in Spring 2003 at the northeastern part of Walvis Ridge, where, based on the seismic pre-site survey data, six sites were drilled with success (Fig. 1.1) As most of previous studies of deep sea drilling projects are based on interpretation which refer to the location of the borehole, in this work a correlation of the borehole data of Leg 208 with the seismic data of the Cruise M49/1 offers the possibility to study the spacial distribution of features reached in the borehole.

Suspan (1899) was the first to advocate that a temperature contrast of 1.5 °C between the bottom waters of the Angola Basin and the Cape Basin can be explained by a ridge that divides the basins and stretches from the Mid-Atlantic ridge to the African continent. He proposed the name ‘Walfisch Ridge’ for it, because he believed that the postulated ridge joined Africa near Walvis Bay (Suspan, 1899). Later expeditions to the South Atlantic confirmed the existence of such a ridge and the presented data suggested that the ridge prevents Antarctic Bottom Waters (AABW) in the Cape Basin from entering the Angola Basin (Wüst, 1936). Today, the ridge is still known as a nearly impassable barrier for bottom waters currents (Arhan et al., 2003).

The Paleogene, which is focus of this study, represents a climatically dynamic period in Earth history, where stable isotopes and other temperature proxies reveal a complex history of warming and cooling, characterized by periods of both gradual and rapid change (Miller et al., 1987, Miller and Katz, 1987, Stott et al., 1990, Zachos et al., 2001, 1994). The most prominent climatic event of the Paleogene is a transient, but extreme ‘greenhouse’ interval known as the Paleocene Eocene Thermal Maximum (PETM), at ~55.0 Ma, where isotope records suggest that deep ocean and high-latitude surface waters warmed by 4°C and 8°C (e.g. Kaiho et al. 1996). Progress in characterizing Paleogene oceanography and climate history, in particular events like the PETM, depends on the quality of the multicored sequences of the

drill sites. The ODP extreme climate advisory panel, Program Planning Group (PPG) recognized the dearth of high resolution records across climate transients and hence formulated new questions concerning extreme climates (Zachos, Kroon, Blum et al., 2004) as well as potential drilling targets among which was Walvis Ridge. The major goal of Leg 208 was the acquisition of sediments which can be used for characterization of short-term changes in the ocean chemistry and circulation that theoretically should have accompanied climatic extremes, as well as their effects on the oceanic biota (Zachos, Kroon, Blum et al., 2004).

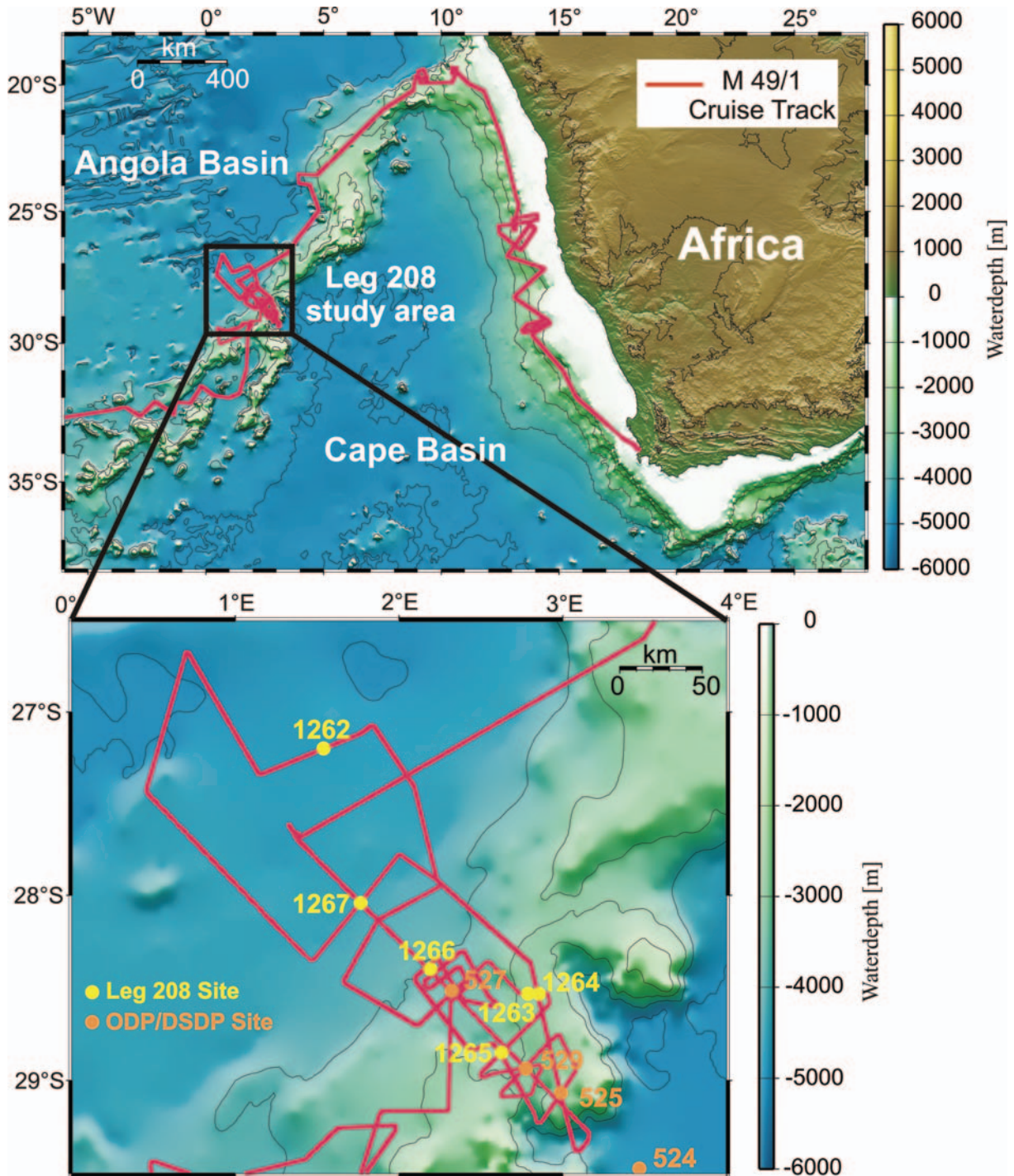


**Figure 1.1:** Cruise Track of R/V Meteor Cruise M49/1 with ODP and DSDP drill sites



Walvis Ridge, located in the eastern South Atlantic Ocean is one of the few known locations where it is possible to recover undisturbed Paleogene sediments over a broad range of depths, including depths exceeding 4.5 km. The ridge was also the target of Deep Sea Drilling Project (DSDP) Leg 74, which occupied five drill sites on the northern flank of the ridge between 2.5 km and 4.2 km water depth (Moore et al., 1984). The sediments can be characterized by pelagic sediments with moderate sedimentation rates (~6-15 m/my) and good magnetic stratigraphy. For proposing new drill positions for Leg 208, where it is possible to recover undisturbed sequences of Paleogene sediments in different water depth, the seismic survey M49/1 from Cape Town to Montevideo was undertaken in early 2001 (Spieß et al., 2003). The six drill sites drilled during Leg 208 in Spring 2003 on outer Walvis Ridge, cover a paleodepth range of 2.2 km, sufficient to constrain large, as well as subtle, changes in the chemistry of deep and intermediate waters. The six sites were drilled at different water depths between 2500 m and 4770 m and cover intact composite sequences of Lower Cenozoic sediments from a wide range of depth (Fig. 1.2). Advances in coring technology and drilling strategies allowed a 100% recovery of the sequences, which, in contrast, were only partly recovered during Leg 74 (Zachos, Kroon, Blum et al., 2004). A major achievement of Leg 208 was the recovery of continuous undisturbed cores spanning over a half-dozen “critical” intervals or events including the Eocene/Oligocene (E/O) boundary, the Cretaceous/Tertiary (K/T) boundary, the Chron C24N Eocene layer also called ELMO horizon (Lourens et al., 2005), the Mid Paleocene Biotic event (Zachos, Kroon, Blum et al., 2004) also called ELPE event (U.Röhl, University Bremen, pers.com.) and the PETM (Zachos, Kroon, Blum et al., 2004). The surrounding Lower Eocene and Upper Paleocene sediments of these events at Walvis Ridge lie within the longest, most stratigraphically continuous and astronomically tuned sequence of marine sediments of the deep sea (Röhl et al., 2007).

The resolution and penetration of the seismic signal depend on the frequency of the seismic source. Higher source frequencies image the sediment structures in higher details, but with a decreasing penetration. For this reason in this study a multi-frequency approach is used, which provides maximum resolution of sediment features in different water depths. To meet these requirements during R/V Meteor Cruise M 49/1, three different seismic sources, i.e. two Generator Injector gun sources (GI-Gun, Soderia Inc.) and one S15 Watergun (Soderia Inc.), were used operating in an alternating mode. Whereas the GI-Guns are able to image the whole sediment column down to the crystalline basement, the higher resolution Watergun is used to image the first 200 m to 300 m of the sediment column in a higher detail.

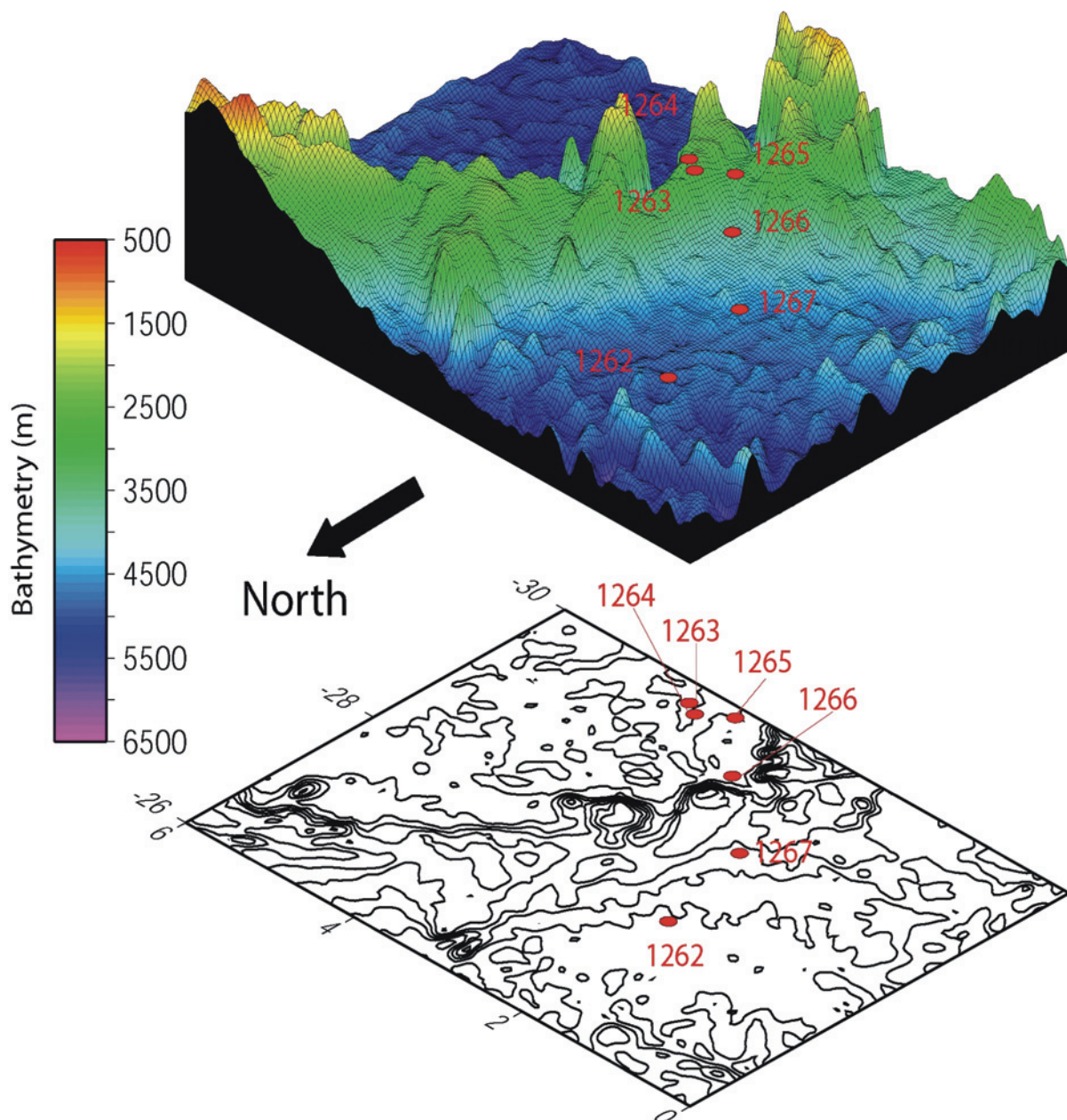


**Figure 1.2:** Three-dimensional diagram of ODP Leg 208 drill site locations in different water depth (adapted from Zachos, Kroon, Blum et al., 2004).

The objectives of this study are:

- The correlation of the seismic data with the borehole data of ODP Leg 208 to map the spatial distribution of climatic events (e.g. PETM, ELMO horizon) reached in the borehole
- The optimization of processing procedures of Watergun data to increase the quality of the stacked and migrated data
- To look for indicators in the seismic data which allude on bottom water activities along or across Walvis Ridge.

## 1.2 Data

The seismic data presented in this study were collected with the German research vessel RV Meteor during the Cruise M 49/1 from Cape Town to Montevideo in early 2001. For acquisition of the data the GeoB marine multi-channel seismic system was used. In total ~2400 km of seismic profiles were processed and analysed for this study.

The borehole data used for the correlation with the seismic data were collected during ODP Leg 208 'Early Cenozoic Extreme Climates: The Walvis Ridge Transect' in Spring 2003. During that cruise six sites were drilled at different water depths between 2500 m and 4770 m (Zachos, Kroon, Blum et al., 2004).

### 1.2.1 Seismic data / Data acquisition

During the R/V Meteor Cruise M49/1 the GeoB marine multi-channel seismic system was used including three different seismic sources, a seismic streamer with programmable hydrophone arrays, a streamer control unit, a recording unit and a trigger unit (Spieß et al., 2003) (Fig. 1.3). The navigation data were provided by the ship's Global Positioning System (GPS).

As seismic sources two GI-Guns, (normal chamber, 1.7 l; 30 Hz – 200 Hz and reduced chamber 0.4 l; 100 Hz – 500 Hz) and one Watergun (0.16 l; 200 Hz – 1600 Hz) were used. The shot interval was 9 sec resulting in a shot distance of ~25 m when sailing with an average speed of 6 knots. For recording a 96-channel oil-filled Syntron streamer of 600 m length equipped with separately programmable hydrophone-groups was used. 48 channels consisting of 13 hydrophones each, a group length of 6.25 m long and a group distance of 12.5 m were used for recording GI-Gun data, while 48 groups consisting of 9 hydrophones and a group length of ~2 m were used for the recording of Watergun data. 10 birds kept the streamer at a constant water depth within a range of 1 m. Recording and management of the data were controlled by the data acquisition unit (Bison Spectra). GI-Gun data were sampled at 250  $\mu$ s, the higher resolution Watergun data were recorded with a sampling rate of 125  $\mu$ s. The data were saved in standard SEG-Y format.

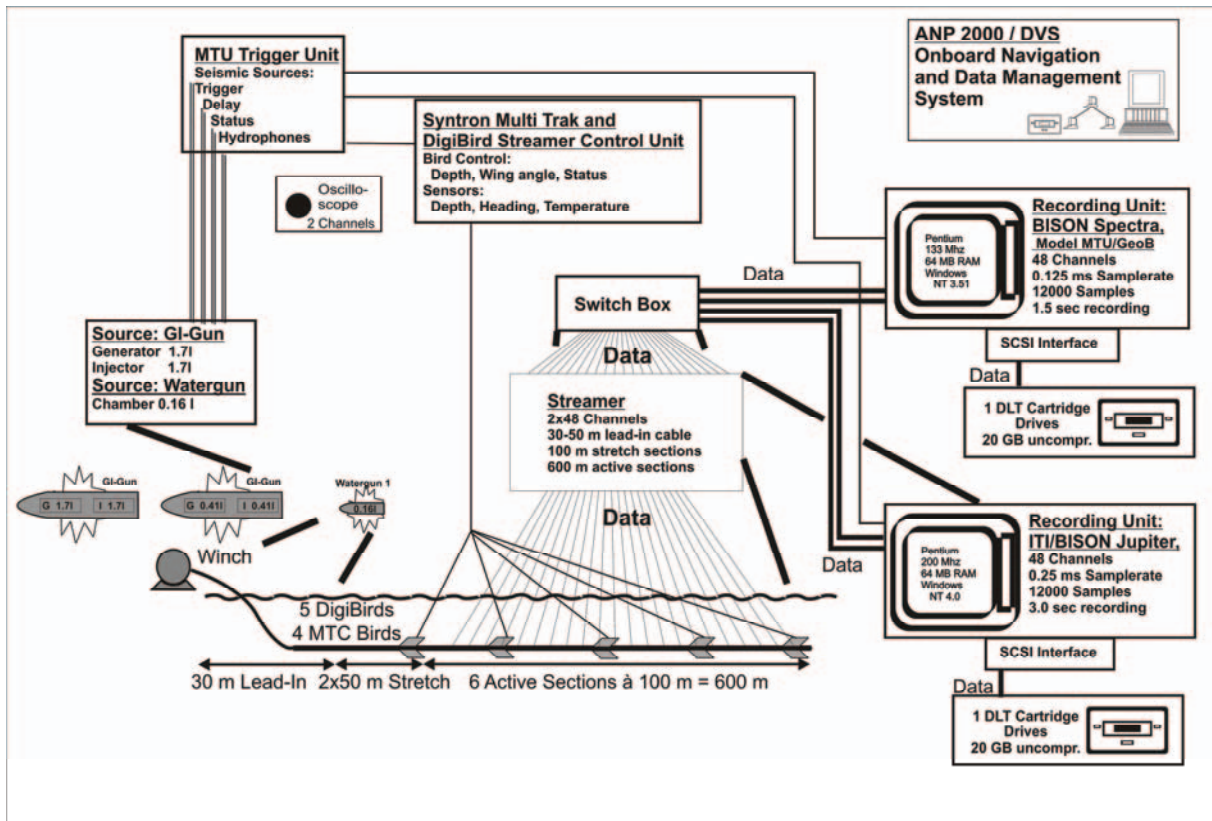


Figure 1.3: Outline of the Bremen high resolution reflection seismic system (adapted from Spieß et al., 2003).

### 1.2.1.1 Processing of the multichannel GI-Gun data

For standard processing steps of GI-Gun data, the commercial ‘Vista’ software (Seismic Image Software LTD.) was used. Standard seismic processing procedures included trace editing, static and delay corrections, velocity analysis, Normal-Move-Out corrections (NMO-corrections), bandpass frequency filtering, stack and time-migration. For Common Mid Point (CMP) sorting and static corrections, which are needed for setting up the geometry of the GI-Gun data, an ‘in-house’ software package called ‘Geoapp’ (Zühlsdorff, pers.com.) was used. This program utilized 1) shot number and time information, 2) navigation information, 3) depth and heading information of the birds. First, a time interpolation was carried out to resample the information of the data to the same time interval, then, based on the navigation data of the ship and the heading and depth data of the birds, the reflection midpoints between the sources and the hydrophones were calculated for each trace. The midpoints were sorted into CMPs. A CMP distance of 10 m was chosen for the processing of all profiles of this study. In the end, a static correction was calculated out of the heading and depth values of the birds. All calculated values were added to the headers of the seismic data, which could be processed using the standard tools of the Vista software package. The

interpretation of the data was carried out with the commercial software package Kingdom Suite 7.4 (Seismic Micro Technologies, Inc.).

### 1.2.1.2 Processing of the multichannel Watergun data

Due to wave motions during the acquisition of the seismic data, the source and the receivers move vertically in the range of the wavelength of the signal of the Watergun ( $\sim 400$  Hz,  $\lambda = \sim 3$  m). For this reason the Watergun data need to be carefully corrected in depth, before it is possible to stack and migrate the data using the standard processing steps as described above for GI-Gun data (Chapter 1.2.1.1). Standard processing steps and stacking using the statics of the bird controlled streamer mostly lead to a lack of coherency and a significant reduction in data quality (Fig. 1.4a). The added static correction is based on flattening the whole data set on the time level and to re-import the topography. It consists out of four steps and starts in a NMO-corrected CMP gather after standard processing steps like trace editing, setup of the geometry, static correction based on the bird data, velocity analysis and a NMO-correction.

1. The first-arrivals of the NMO-corrected CMP-gather are picked using an automatic algorithm. To get optimal picking results of the first arrivals, the negative values of the traces are deleted and the resulting traces are squared. These modified traces are used as an input for our custom-picking algorithm, which uses a moving window of length of 2.5 ms for identifying the maximum peaks of each trace. To ensure that the algorithm picks in the right depth, manual picks of seafloor, picked in a brutestack or in a one channel record of the Watergun, are used.
2. The picks of each trace are used to flatten the NMO-corrected CMP-gather on the same time level (Fig. 1.5a, 1.5b).
3. This flattened NMO corrected CMP-gather is stacked using a standard CMP-stacking tool (Fig. 1.5c), whereas the geometry for the CMP sorting, which was done by using the ‘in-house’ software package Geoapp’ (Zühlsdorff, per. com), still can be used.
4. The morphology of the seafloor, which is lost during the flattening of the CMP-gather is superimposed by shifting the first arrivals of the Watergun data at the depth of the first arrivals of the GI-Gun data. They are characterized by a pronounced peak and can be easily manually picked using a standard picking tool of the commercial seismic software package ‘Vista’ (Seismic Image Software LTD.).



The imprecision resulting out of the differences in the source frequency of the GI-Gun and the Watergun amounts a few meter which is neglectable in water depth which a grater than 2000 m.

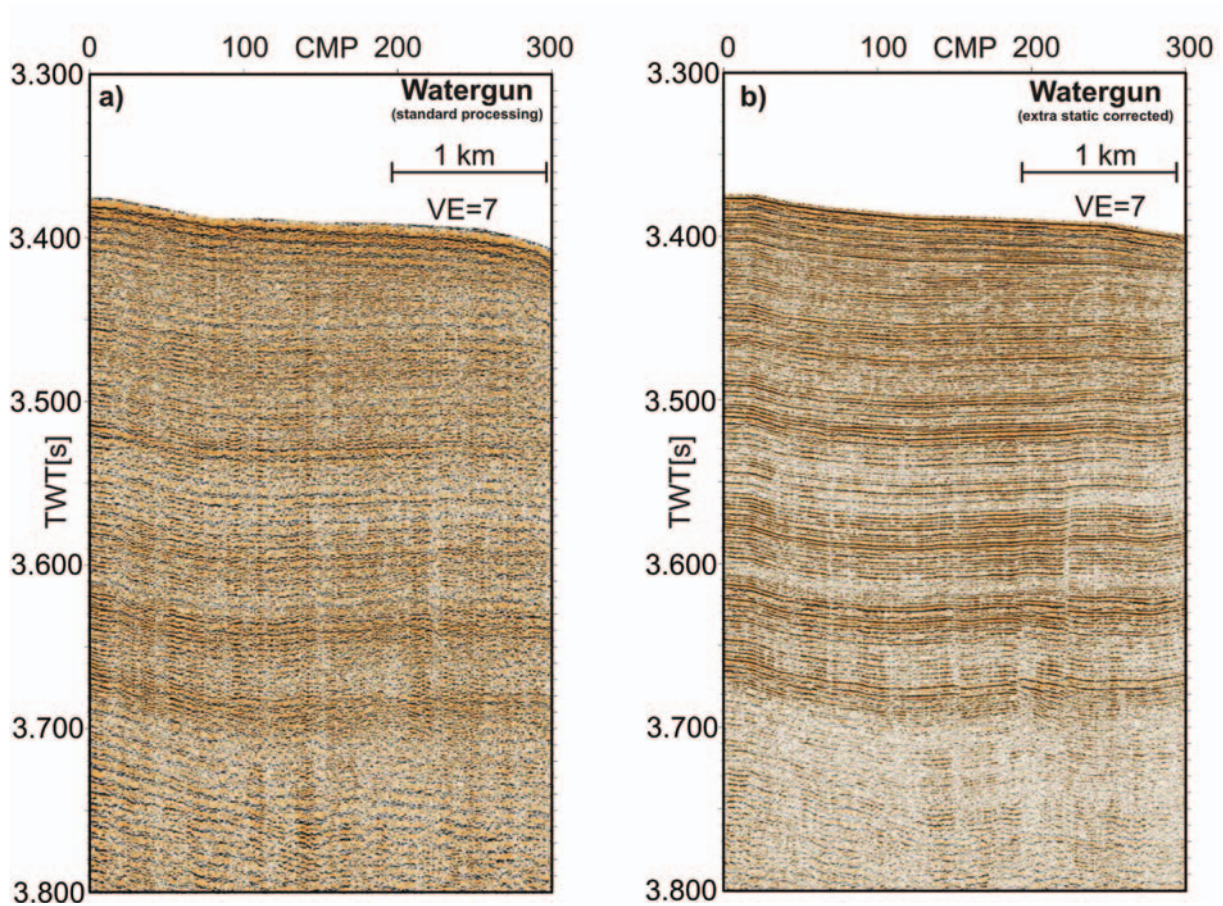


**Figure 1.4:** High resolution Watergun data (part of Profile GeoB01-046 at the flank of Walvis Ridge).

**a):** Stack of high resolution Watergun data processed using standard processing steps.

**b):** Same stack like in A) including special processing step of NMO-leveling.

All processing steps, including the optimized static corrections, were done using the commercial seismic software package 'Vista'. Due the correction of the Watergun statics are not standard processing tools of the 'Vista' software package, specific tools were programmed using FORTRAN and implemented into the 'Vista' software package using C++. The described procedure results in high-quality Watergun images (Fig. 1.4b), which can also be loaded and interpreted with the commercial software package Kingdom Suite 7.4.



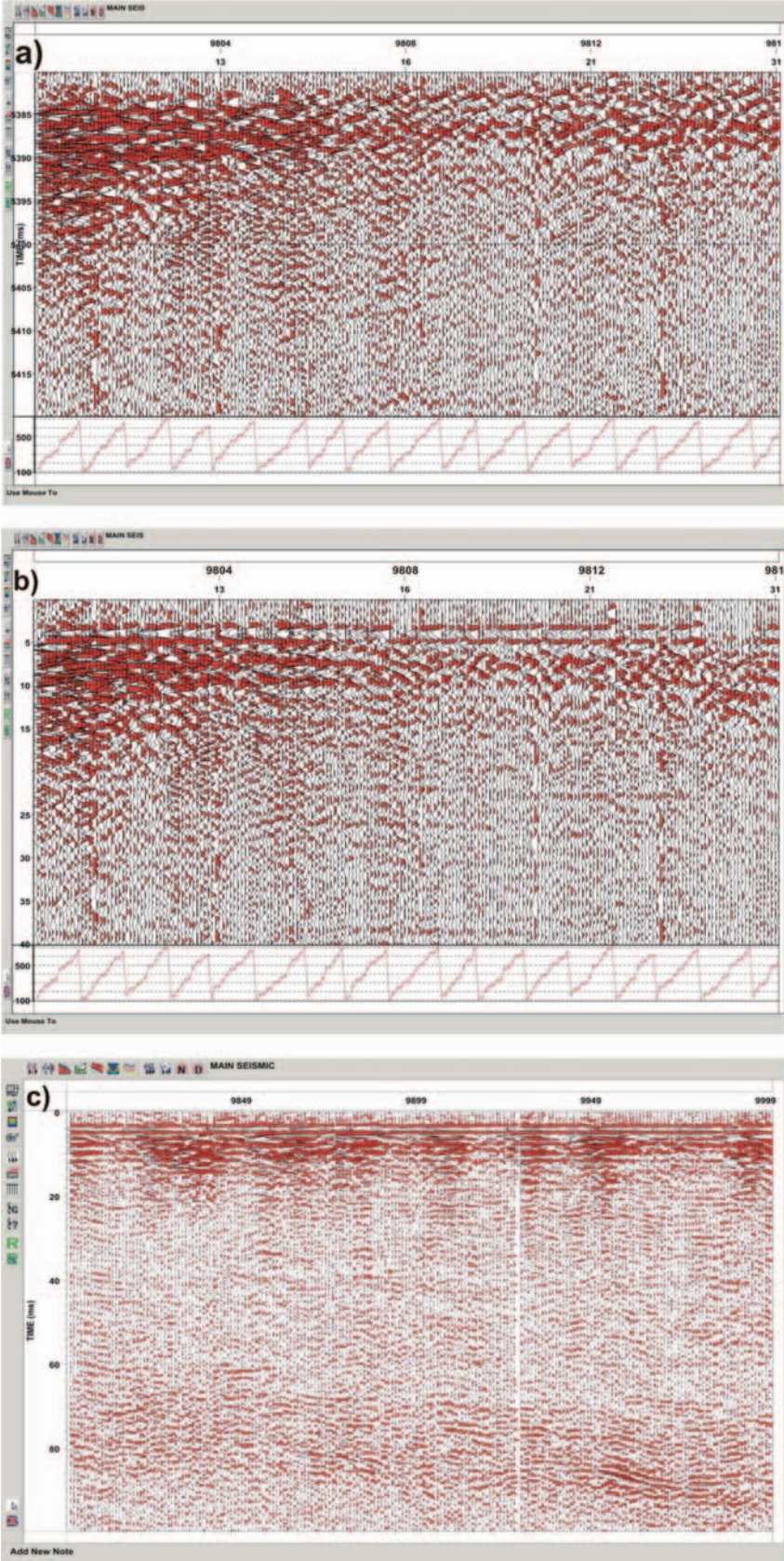


**Figure 1.5:** Screenshots of processing steps of Watergun data  
a) CMP sorted NMO-gather including standard static corrections of the streamer using bird data.  
b) CMP sorted NMO-gather after leveling using the automatic picking algorithm.  
c) CMP stack of leveled NMO-gather. Morphology is lost during the leveling.

### 1.2.3 Sediment Echo-sounder (Parasound) data

The Parasound system (Grant and Schreiber, 1990) is a hull-mounted high frequency sediment echo-sounder which is permanently installed on the R/V Meteor. The system utilizes the parametric effect by emitting two high amplitude, high frequency sound waves in order to generate a secondary sound wave with a difference frequency between 2.5 kHz – 5.5 kHz. This secondary sound wave is focused within an emission cone of 4° opening angle and results in a footprint diameter of  $\sim 7\%$  of the water depth. The vertical resolution of the system is on the order of a few decimeters. Depending on the type of the sediments the penetration of the signal varies between 10 m and 200 m. The system is compensated for roll, pitch and heave as a means of ensuring vertical sound emission. For the digital recording the ParaDigMa acquisition system (Spieß, pers com.) was used. The data were stored in a compressed SEG-Y format. Before display a band pass frequency filter of 2.0 kHz – 6.0 kHz was applied during processing.

### 1.2.4 Bathymetry (Hydrosweep) data

The Hydrosweep swath bathymetric system, like the Parasound system, is a hull mounted system which is also permanently installed on the R/V Meteor. The echosounder generates 59 pre-formed beams over an angle of 90° for sampling the seafloor at a frequency of 15.5 kHz. Thus, it is possible to map a seabed swath of width equal to two times the water depth (Grant and Schreiber, 1990). To avoid depth errors of the outer beams due to refraction, a patented calibration process was used, which compares depth values of the central and the outer beams in order to calculate a mean sound velocity from the best fit between the two values. This configuration ensures that residual depth errors are less than 0.5% of the water depth (Grant and Schreiber, 1990).

For processing, the public domain software Multibeam System (Caress and Chayes, 1996) was used which has an automatic and an interactive editing tool for the correction of navigation and depth values. The automatic tools were used to delete bad outer beams values, abnormal depth values and erroneous navigation data, before an interactive editing was carried out. The processing steps had to be carried out carefully, because artifacts and structures of the seafloor can occur on the same scales. After processing the data were gridded and displayed using the public domain software package GMT (Wessel and Smith, 1998).



### 1.2.5 Borehole data

Main objectives of Leg 208 were to recover intact composite sequences of “critical” transitions like the K/T boundary, the E/O boundary and the PETM, whereas the PETM interval was the main focus. It was recovered at five of the six sites along a depth transect of 2.2 km. The sediment is marked by a red clay layer, which varies in thickness from 0.3 m to 0.5 m (Fig. 1.6). The carbonate content drops to 0 %wt at all Sites except Site 1265 (Zachos, Kroon, Blum et al., 2004).

During DSDP Leg 74 drilling in the Walvis Ridge area, the PETM and other “critical” intervals were not recovered at all sites in part of low recovery and in part because of local unconformities (Zachos, Kroon, Blum et al., 2004). Based on the seismic data of R/V Meteor Cruise M 49/1 (Spieß et al., 2003) areas to the east of the existing sites appeared to provide more continuous sequences, which have a high potential to recover “critical” events. A depth transect with 5 primary and 11 alternate sites was designed using the high resolution seismic data set of R/V Meteor Cruise M 49/1. The potential to recover the PETM boundary and other “critical” events was maximized by selecting locations for the drill sites that had relatively thick Paleogene sequences and thin Neogene cover (Zachos, Kroon, Blum et al., 2004).

In Spring 2003, during Leg 208 six drill sites (1262-1267) were drilled on a depth transect with water depths between 2500 m and 4470 m (compare Fig. 1.1 and 1.2). The Upper Palaeocene sediments were drilled at five sites (Sites 1262, 1263, and 1265-1267), the Upper Maastrichtian and Lower Paleocene at two sites (1262 and 1267), and the Neogene at all six sites including Site 1264 from which the Lower Oligocene through Pleistocene was recovered. At least two APC (Advanced Piston Corer) and /or XCB (Extended Core Barrel) drilled holes were taken at each site to ensure recovery of a complete sequence, and cores were overlapped to facilitate compilation of composite sections. The core log data (magnetic susceptibility, natural gamma radiation, and color reflectance) were assembled during the drilling for correlation. In some cases a third or fourth hole was cored to ensure the recovery of at least two “critical” intervals (Zachos, Kroon, Blum et al., 2004).

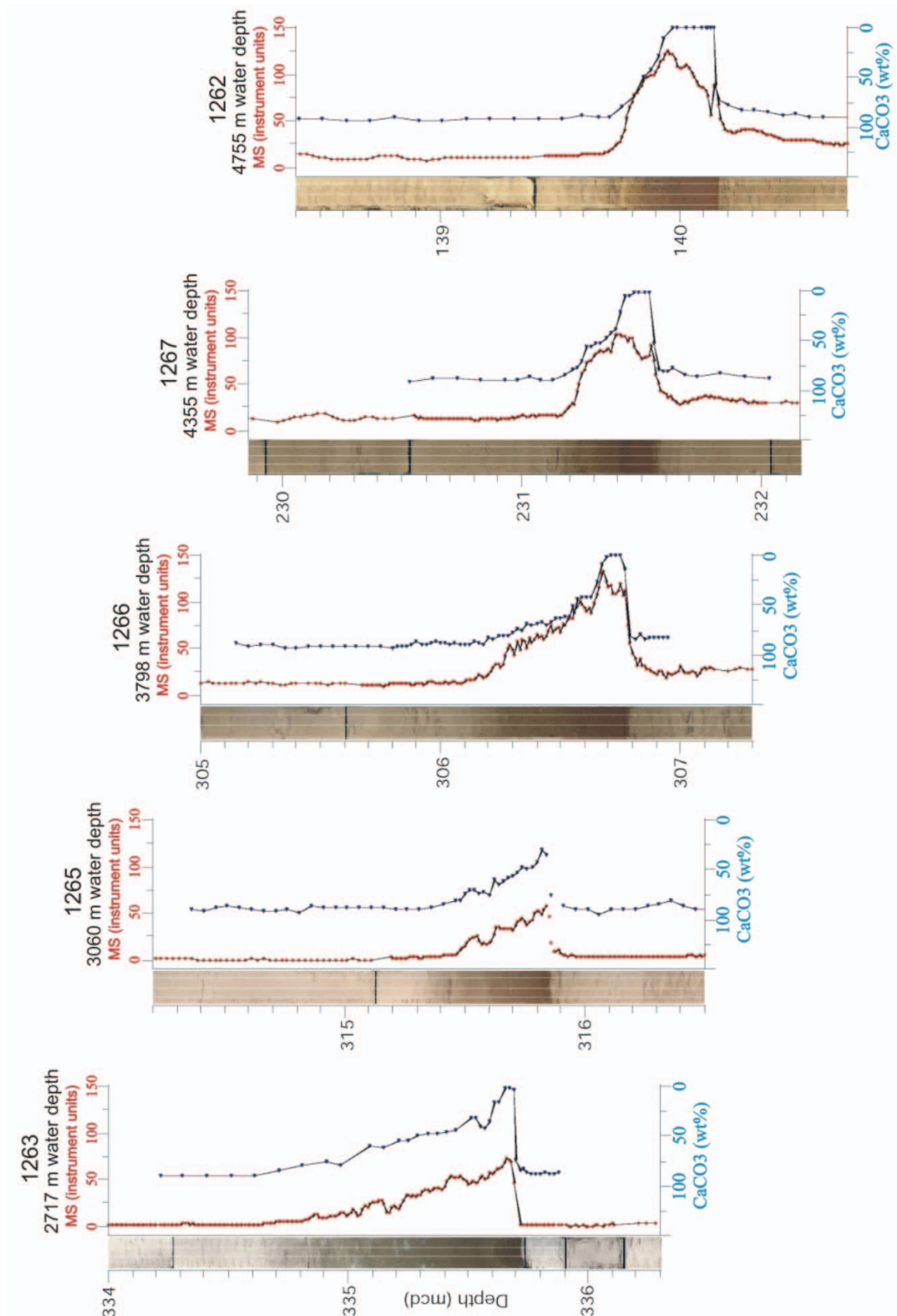


**Figure 1.6:** Composite digital images, magnetic susceptibility (MS), and CaCO<sub>3</sub> through the Paleocene-Eocene Thermal Maximum (PETM) at five ODP Leg 208 sites (from Zachos, Kroon, Blum et al., 2004).

### 1.3 The paleoclimate (a general overview)

Successful prediction of future global climate is critically dependent on understanding its complex history, some of which is documented in paleoclimate time series extracted from the deep-sea sediment and ice cores. These recordings exhibit frequent episodes of abrupt climate change believed to be the result of nonlinear response of the climate system to internal or external forcing (Rial, 2003). During the last 65 million years and beyond, Earth's climate system has experienced continuous change, drifting from extremes of expansive warmth with ice-free poles, to extremes of cold with massive continental ice-sheets and polar ice caps. It is possible to distinguish the climate changes into three groups 1) long term trends, 2) rhythms or short term trends and 3) aberrations or events. Most of the progress in resolving the rates and the scales of Cenozoic climate change can be attributed to the development of high resolution deep-sea oxygen ( $\delta^{18}\text{O}$ ) and carbon ( $\delta^{13}\text{C}$ ) isotope records, whereas the  $\delta^{18}\text{O}$  data have served as the principal means of reconstructing global and regional climate change on the variety of geologic time-scales. Figure 1.7 illustrates global deep-sea oxygen and carbon isotope records based on data compiled from more than 40 DSDP and ODP sites. Long term trends ( $\sim 10^6$ - $10^7$  years) are reflected in the general trends of the  $\delta^{18}\text{O}$  curve e.g. a warming trend expressed by a decrease in  $\delta^{18}\text{O}$  occurring early in the Cenozoic, from mid Paleocene (59 Ma) to early Eocene (52 Ma), peaked with the early Eocene Climatic Optimum (EECO, 52 to 50 Ma) which is followed by 17 m.y.-long trend in cooling. Rhythms or short-term trends ( $\sim 10^4$ - $10^5$  years, not resolved in Figure 1.7) have orbital scales and depend on changes of the eccentricity, obliquity and the axial precession of the Earth. They vary the climate in a quasi-periodic fashion during all intervals. The most interesting and unexpected variations of Earth climate are aberrations or events ( $\sim 10^3$  - $10^5$  years). They are characterized by brief anomalies that stand out well above the "normal" background variability and usually they are accompanied by a major perturbation in the global carbon cycle (Zachos et al., 2001).

This study is mainly focused on "critical" climatic events and transitions occurring during the Paleogene. It represents a climatically dynamic period in Earth history, where stable isotopes and other temperature proxies reveal a complex history of warming and cooling characterized by periods of both gradual and rapid change (Miller and Katz, 1987; Stott et al, 1990; Zachos et al., 1994, 2001). The most prominent event of the Paleogene climate is the transient but extreme greenhouse interval known as the PETM at  $\sim 55$  Ma, which is characterized by a dramatic reorganisation within the marine and terrestrial ecosystem coincident with one of the most abrupt global warming episodes in Earth history

(e.g. Kennett and Stott, 1991; Thomas and Shackleton, 1996, Zachos et al., 2003, Gibbs et al., 2006). Unlike to other smaller events, the PETM, which occurs as a carbonate-poor red clay layer in the sediments of the deep sea, is clearly resolved in the global oxygen ( $\delta^{18}\text{O}$ ) and carbon ( $\delta^{13}\text{C}$ ) records of Figure 1.7. Major changes in ocean chemistry, as inferred from shifts in the carbon isotope patterns and distribution and preservation patterns of terrigenous and biogenic sediments on the seafloor (e.g. Kennett and Stott, 1990; Robert and Kennett, 1997), characterize the PETM. Global Isotope records suggest that the deep waters warmed by  $\sim 4^\circ\text{C}$  (Fig. 1.8) (Tripathi and Elderfield, 2005). The surface waters at the high latitudes even warmed by  $8^\circ\text{C}$  which resulted in the deglaciation of the ice-sheets (Kaiho et al., 1996). Possible triggering mechanisms for the PETM include crossing a threshold temperature as the Earth warmed gradually (Thomas and Shackleton, 1996), comet impact (Kent et al., 2003), explosive volcanism (Bralower et al., 1997) or ocean current reorganization and erosion at continental slopes (Katz et al., 2001), whereas orbital forcing has been excluded (Cramer et al., 2003).

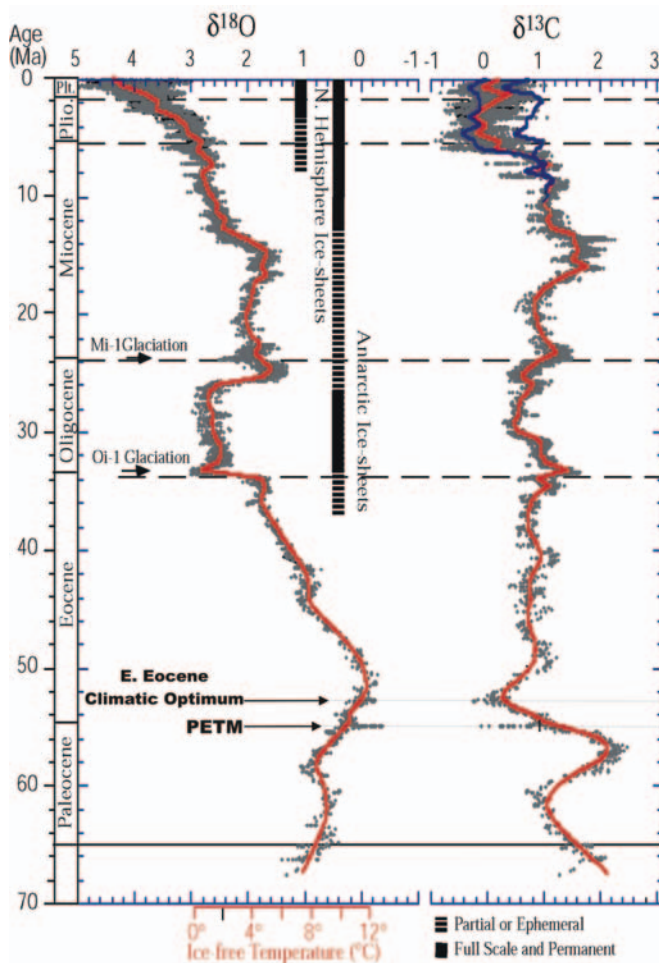


**Figure 1.7:** Global deep-sea oxygen and carbon isotope records based on data compiled from more than 40 DSDP (Deep Sea Drilling Project) and ODP (Ocean Drilling Program) (modified after Zachos et al., 2001).

As mentioned before (compare Chapter 1.1 and Chapter 1.2.5), the red clay layer representing the PETM was fully recovered at five of the six drill sites of ODP Leg 208. As to be seen in the Figure 1.6 the carbonate content of the 0.5 m to 0.6 m thick layer drops down to 0 wt% at all sites. About 2 million years later a second global thermal maximum, characterized by the same biotic and geochemical characteristics, but of smaller magnitude, was deposited. The carbonate red clay layer found in deep sea cores of Walvis Ridge was termed the ELMO horizon (Lourens et al. 2005). Same as at the PETM, the ELMO horizon was recovered at five of the six sites of ODP Leg 208. The 0.2 m – 0.4 m thick clay layer can also be characterized by dropping carbonate content on 0 wt% (Fig. 1.9). Additionally, this study investigates on a third event, the Mid-Paleocene biotic event (~ 58.8 Ma) also called ELPE event (Ursula Röhl, University Bremen, pers. com.) which is characterized by an decrease in clay content and also represents a global climatic event (Zachos, Kroon, Blum et al., 2004).

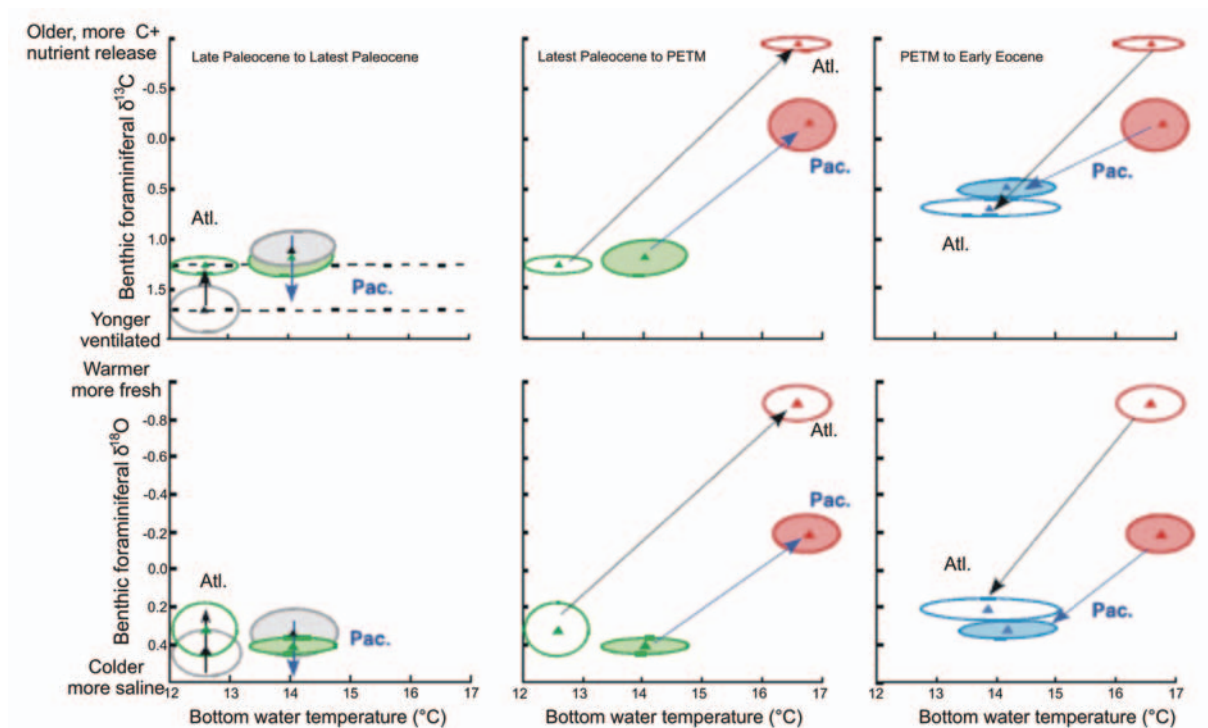


**Figure 1.8:** Cross-plot for bottom water temperature versus benthic foraminiferal  $\delta^{13}\text{C}$  and  $\delta^{18}\text{O}$  across the PETM, illustrating the evolution of deep-water gradients between North Pacific (Shatsky Rise, shaded ellipses) and South Atlantic (Walvis Ridge, open ellipses). Range (ellipses) and average values (triangle) are shown for specific time slices (gray: Late Paleocene, green: Latest Paleocene, red: PETM, blue: Earliest Eocene; adapted from Tripathi and Elderfield, 2005).

There are multiple hypotheses to explain such large-scale, short-term changes in the Paleogene climate, although none have gained universal acceptance. In general, the role of ocean gateways and the greenhouse gas levels, among many other factors, are considered as

the key variables (Zachos, Kroon, Blum et al., 2004). Theoretical models have invoked either the absence of a circum-Antarctic current or higher greenhouse levels, or a combination of both during the climatic changes in the Paleogene (e.g. Bice et al., 2000, Sloan and Barron, 1992).

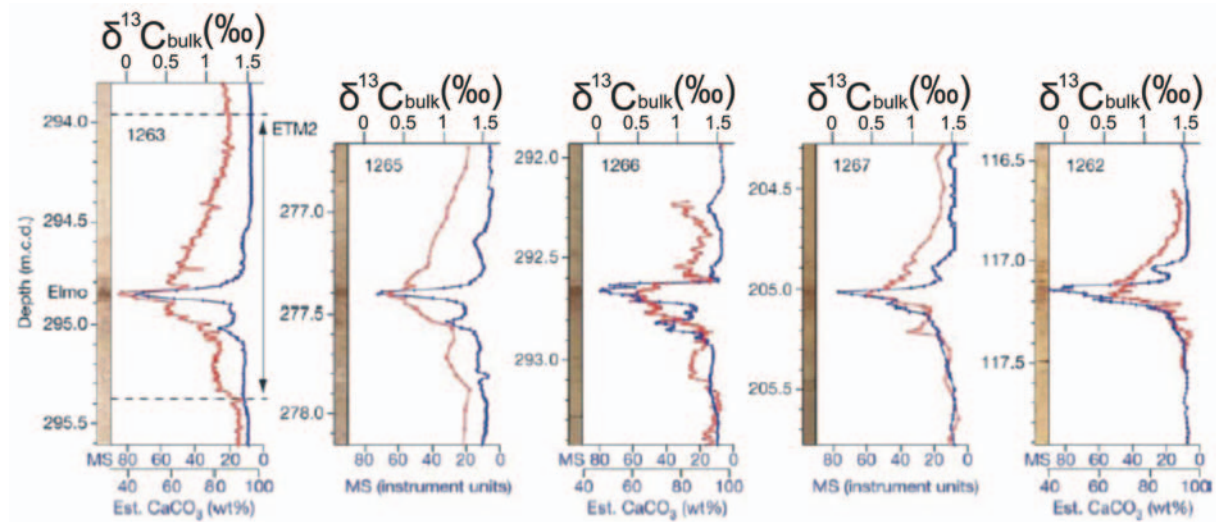


**Figure 1.9:** Composite digital images, bulk carbonate ( $\delta^{13}\text{C}$ ) and magnetic susceptibility (MS) records across the ELMO horizon at five ODP Leg 208 sites (adapted from Lourens et al., 2005).

#### 1.4 The thermohaline circulation (a general overview)

The world ocean is an important part of the Earth climate system because of its property to carry and store huge amounts of heat. It interacts with the atmosphere, exchanging heat and moisture. The ocean currents and the large-scale circulation redistribute the water masses over a broad area, thus making the interaction between both the ocean and the atmosphere non-local (e.g. Brydon and Imawaki, 2001, Brown et al., 1989). Additionally, the oceans are the biggest reservoir for greenhouse gases like carbon dioxide ( $\text{CO}_2$ ) of the Earth, which affects the thermal radiation from Earth into space. By the absorption at the sea surface and the creation of deep waters, the greenhouse gases are transported and partly stored in the ocean (Huhn, 2005). Therefore, the knowledge of large-scale ocean currents and their variability is required to improve our understanding of the Earth climate system.

The vast water masses of the ocean lies below a kilometer extending to depths of 4 km to 5 km. The water, which is everywhere cold with a potential temperature less than  $4^\circ\text{C}$ , is formed when cold, dense water sinks from the surface to great depths at high latitudes. It spreads out from the north and the south to fill the ocean basins (Brown et al., 1989, compare Fig 1.10). The densest water at the sea surface, which is dense enough to sink to the ground, is formed, when frigid air blows across the ocean at high latitudes in winter (Steward, 2003).



Present-day, bottom reaching water masses are only built in the North Atlantic and in the Southern Ocean: In the north the North Atlantic Depth Water (NADW) is formed in the Atlantic between Norway and Greenland and in the south the Antarctic Bottom Water (AABW) is formed near Antarctica (e.g. Gordon, 1996; Brix, 2001). At mid and low latitudes, the density of the water, even in winter, is sufficiently low that the water cannot sink more than a few hundred meters into the ocean. The circulation of the deep waters, also called thermohaline circulation, is mostly wind driven, but tidal mixing is also important. The wind enters through several ways. It cools the surface and evaporates water, which determines where deep convection occurs. Additionally, it produces turbulences in the deep ocean which mixes cold water upward (Steward, 2003).

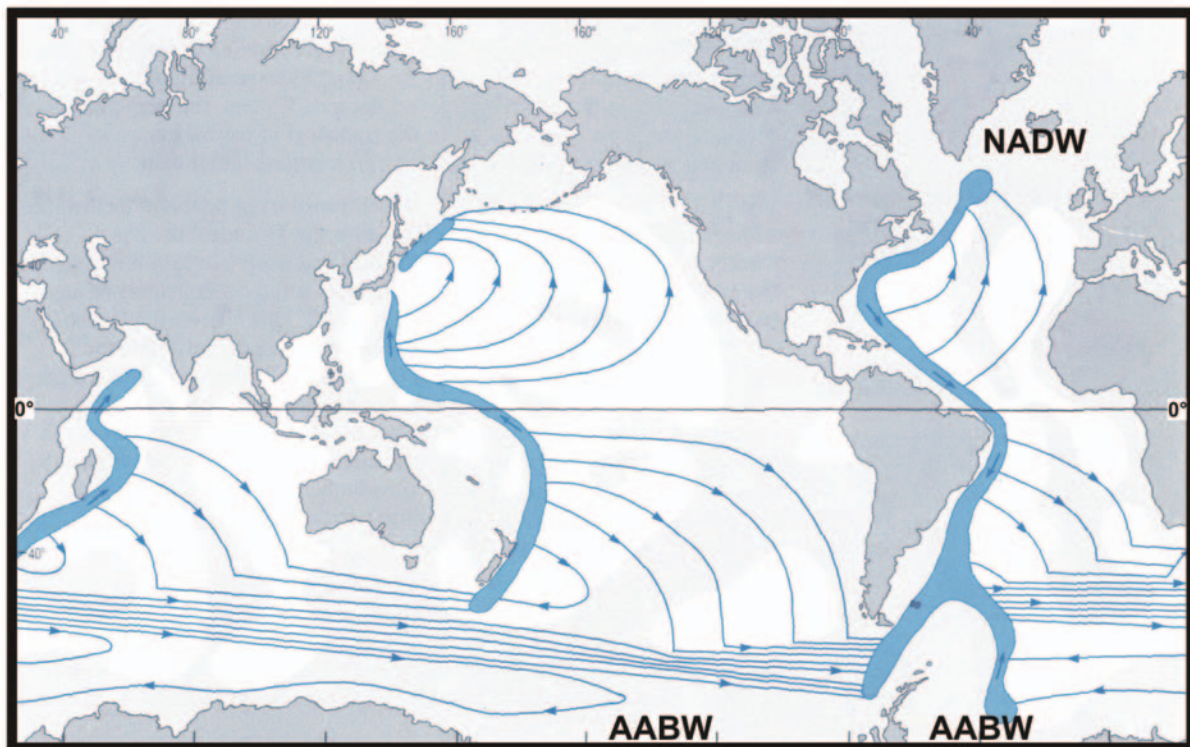


**Figure 1.10:** A model of the thermohaline circulation after Stommel (Stommel and Arons, 1960) with source regions of NADW (North Atlantic Depth Water) in the north and AABW (Antarctic Bottom Water) in the south (modified after Brown et al., 1989).

The volume of the deep water is far larger than the volume of the surface water. Although currents in the deep ocean are relatively weak, their mass transports are comparable to the mass transports of surface currents. The contrast between the cold deep water and the warm surface water determines the stratification of the oceans and the fluxes of heat and other variables e.g. salinity, carried by the deep circulation and influences Earth's heat budget and climate. The fluxes vary from decades to centuries to millennia, and this variability is thought

to model the Earth's climate over such time intervals. Two aspects of the deep circulation are especially important for the Earth's climate and its possible response to increased CO<sub>2</sub> absorbed from the atmosphere: 1) the ability of cold water to store CO<sub>2</sub> absorbed from the atmosphere, and 2) the ability of the deep currents to modulate the heat transported from the tropics to high latitudes. The oceans are the primary reservoir of readily available CO<sub>2</sub>, an important greenhouse gas (Steward, 2003).

Walvis Ridge, which is the main objective of this thesis, is located in the South Atlantic, which oceanography and paleoceanography is characterized by the exchange of heat between the North and the South Atlantic. Without this heat transfer, northern Europe would have entirely less clement climate (Berger and Wefer, 1996). A central problem in oceanography concerns the efficiency and stability of the heat transfer from South to North Atlantic, within the general framework of global thermohaline circulation (Gordon, 1986). Today circulation in the deep western South Atlantic, the main flow path of the deep waters, is dominated by interactions between NADW flowing towards the south and Circumpolar Deep Water (CDW) flowing to the north. The density characteristics of these water masses are such that NADW divides the southern water mass into an upper and a lower branch (Reid, 1989). Consequently the relatively warm and saline NADW occupies the depth interval between 2000 m and 4000 m, while below 4000 m lower AABW are encountered. The mixing zone between NADW and AABW is marked by gradients in temperature, salinity nutrient concentrations, and in the corrosiveness of the water with respect to calcium carbonate (CaCO<sub>3</sub>). For the eastern basins of the South Atlantic, i.e. the Guinea Basin and the Angola Basin, the inflow of AABW is restricted by the Mid-Atlantic Ridge in the west and the Walvis Ridge in the south (Bickert and Wefer, 1996). Especially for the deepest parts of Angola Basin and Cape Basin, Walvis Ridge is known as an impassable barrier for the AABW (Arhan et al., 2003), wherefore the deepest parts of Angola Basin are filled almost exclusively by NADW and the deepest parts of Cape Basin, although located eastwards of the Mid-Atlantic Ridge are dominated by AABW below 4000 m (Bickert and Wefer, 1996). An exchange between the two water masses in the eastern part of the South Atlantic occurs mostly in a vertical direction. Figure 1.11 illustrates a west-east profile of salinity and potential temperature measurements across the South Atlantic (Siedler et al., 1996), where the separation of the AABW (potential temperature < 1.4°C, salinity < 34.82 ppt) in the Cape Basin is clearly visible. Until now, only the Walvis Passage, near 37° S-7° W, in excess of 4000 m water depth, is known and verified as a gateway, where an exchange and a mixture of



depth waters occur between the Cape Basin and the Angola Basin (Connary and Ewing, 1974).

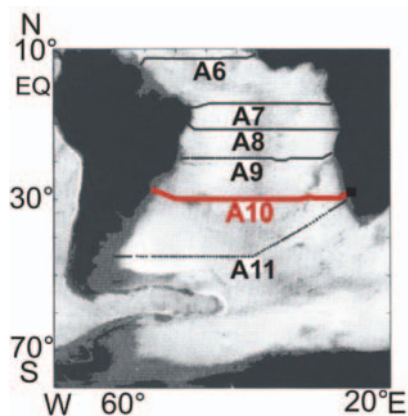
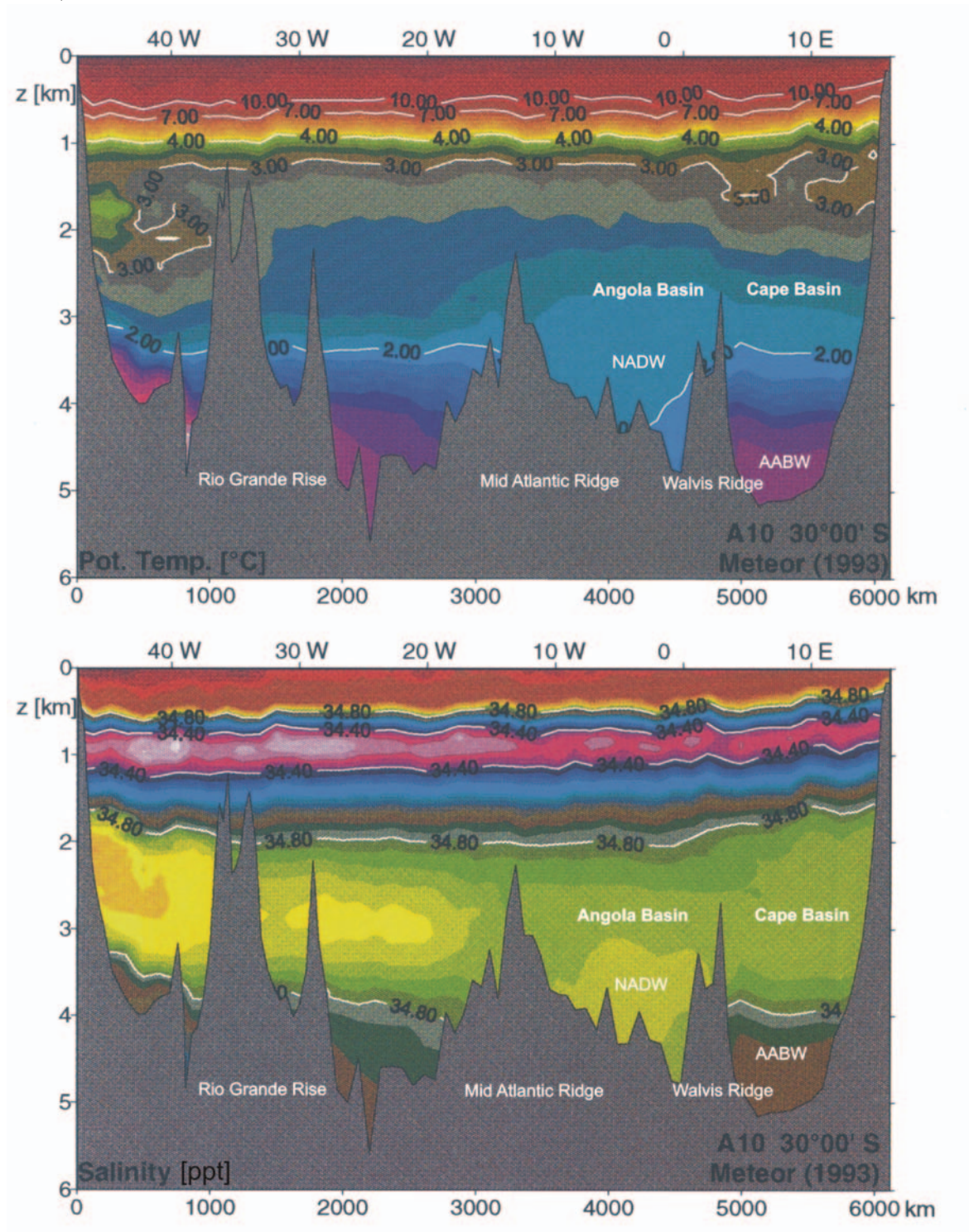


**Figure 1.11:** Zonal section of potential temperature (referenced to the surface) and salinity along the A10 Meteor Profile of the WOCE (World Ocean Circulation Experiment in the South Atlantic), (modified after Siedler et al., 1996).

## 1.5 Role of candidate

The ~2400 km of seismic data presented in this thesis were recorded during R/V Meteor Cruise M49/1 in early 2001. Prof. Dr. Volkhard Spiess (University of Bremen) as the chief scientist was responsible for the technical acquisition system and the design of the seismic survey. Dr. Sebastian Krastel (University of Bremen), as a member of the scientific crew of this cruise, processed several GI-Gun profiles, which were used as the pre-site survey for ODP Leg 208. They proposed in cooperation with Prof. Dr. James Zachos (University of California, Santa Cruz) the drill site positions of ODP Sites 1262 – 1267, which were drilled in spring 2003 with success (Zachos, Kroon, Blum et al., 2004).

I programmed the optimization of the processing of the Watergun data, calculated all synthetic models of the manuscripts, and processed the remaining GI-Gun and all Watergun profiles presented in this study. All four manuscripts of the thesis were written by myself.

## 1.6 References:

Arhan M., Mercier H., Park Y.H., 2003. On the deep water circulation of the eastern South Atlantic Ocean, *Deep-Sea Research I* 50, 889-916.

Berger W.H., Wefer, G., 1996. Central Themes of South Atlantic Circulation. From Wefer G., Berger W.H., Siedler G., Webb D.J., (eds) 1996. *The South Atlantic: Present and Past Circulation*. Springer-Verlag Berlin Heidelberg, pp 1-11.

Bice K.L., Scotese C.R., Seidov D., Barron E.J., 2000. Quantifying the role of the geographic change in Cenozoic ocean heat transport using uncoupled atmosphere and ocean models. *Palaeogeogr., Palaeoclimatol., Palaeoecol.*, 161, 295-310.

Bickert T., Wefer G., 1996. Late Quaternary Deep Water Circulation in the South Atlantic: Reconstruction from Carbonate Dissolution and Benthic Stable Isotopes. From Wefer G., Berger W.H., Siedler G., Webb D.J., (eds) 1996. *The South Atlantic: Present and Past Circulation*. Springer-Verlag Berlin Heidelberg, pp 599 – 620.

Bralower T.J., Thomas D. J., Hirschmann M.M., Whitney D.L., Zachos J.C., Röhl U., Sigurdsson H., Thomas E., 1997. High-resolution records of the late Paleocene thermal

maximum and circum-Caribbean volcanism: Is there a causal link? *Geology*, 25, No. 11, pp. 963–966.

Brown J., Colling A., Park D., Phillips J., Rothery D., Wright J., 1989. Book: *Ocean Circulation*. The Open University, Walton Hall, and Butterworth-Heinemann.

Brix H., 2001. North Atlantic Deep Water and Antarctic Bottom Water: Their Interaction and Influence on Modes of the Global Ocean Circulation. PhD dissertation Dept. of Physics and Electrotechnology, University of Bremen, available on the web:

[http://elib.suub.uni-bremen.de/diss/docs/E-Diss164\\_diss\\_hbrix\\_2.pdf](http://elib.suub.uni-bremen.de/diss/docs/E-Diss164_diss_hbrix_2.pdf)

Brydon, H.L., Imawaki, S., 2001. Ocean heat transport . From: Siedler G., Church J., Guold J., (eds) 2001. *Ocean Circulation and Climate*. Academic Press, pp. 455-474.

Caress D.W., Chayes D.N., 1996. Improved processing of Hydrosweep DS Multibeam data on the R/V Maurice Ewing. *Marine Geophysical Researches*, 18, 631-650.

Connary S.D., Ewing M., 1974. Penetration of Antarctic Bottom Water from the Cape Basin into the Angola Basin. *Journal of Geophysical Research*, 79, 463-469.

Cramer B.S., Wright J.D., Kent D.V., Aubry M.-P., 2003. Orbital climate forcing of  $\delta^{13}\text{C}$  excursions in the late Paleocene-early Eocene (chrons C24n-C25n). *Paleoceanography* 18 (4), pp 1094.

Gibbs S.J., Bralower T.J., Bown P.R., Zachos J.C., Bybell L.M., 2006. Shelf and open-ocean calcareous phytoplankton assemblages across the Paleocene Eocene Thermal Maximum: Implications for global productivity gradients. *Geology*, 34, no.4, 233-236.

Gordon A.L., 1986. Inter-ocean exchange of thermohaline water. *Journal Geophysical Research* 91: 5037-5046.

Gordon A.L., 1996. Comment on the South Atlantic's Role in the Global Circulation. From Wefer G., Berger W.H., Siedler G., Webb, D.J., (eds) 1996, *The South Atlantic: Present and Past Circulation*. Springer-Verlag Berlin Heidelberg, pp 599 – 620.

Grant J.A., Schreiber R., 1990. Modern Swath Sounding and Sub-Bottom Profiling Technology for Research Applications: The Atlas Hydrosweep and Parasound Systems. *Marine Geophysical Researches* 12, 9-19.

Huhn O., 2005. Transfer von Nordatlantischem Tiefenwasser durch den Südatlantik mit Tracer-Verteilungen und Transitzeit-Verteilungen. . PhD dissertation Dept. of Physics and Electrotechnology, University of Bremen, available on the web:

[http://elib.suub.uni-bremen.de/diss/docs/E-Diss1206\\_ohuhn\\_thesis.pdf](http://elib.suub.uni-bremen.de/diss/docs/E-Diss1206_ohuhn_thesis.pdf)

Kaiho K., Arinobu T., Isishwatar R., Morgans H.E.G., Okada H., Takeda N., Tazaki K., Zhou G., Kajiwaru Y., Matsumoto R., Hirai A., Niitsuma N., Wada H., 1996. Latest Paleocene benthic foraminiferal extinction and environmental changes at Tawanui, New Zealand, *Paleoceanography*, 11:447-465.

Katz M.E., Cramer B.S., Mountain G.S., Katz S., Miller K.G., 2001. Uncorking the bottle: What triggered the Paleocene/Eocene thermal maximum methane release? *Paleoceanography* 16, 1-14.

Kennett J.P., Stott L.D., 1990. Proteus and Proto-oceanus: ancestral Paleogene oceans as revealed from Antarctic stable isotopic results: ODP Leg 113. In Barker, P.F., Kennett, J.P., et al., *Proc. ODP Sci. Results*, 113: College Station, TX (Ocean Drilling Program) 865-880.

Kennett J.P., Stott L.D., 1991. Abrupt deep-sea warming, palaeoceanographic changes and benthic extinctions at the end of the Palaeocene. *Nature*, 353, 225-229.

Kent D.V., Cramer B.S., Lanci L., Wang D., Wright J.D., Van der Voo R., 2003. A case for a comet impact trigger for the Paleocene/Eocene thermal maximum and carbon isotope excursion. *Earth and Planetary Science Letters*, 211, 1-2, 13-26.

Lourens J., Sluijs A., Kroon D., Zachos J.C., Thomas E., Röhl U., Bowles J., Raffi I., 2005. Astronomical pacing of late Paleocene to early Eocene global warming. *Nature*, 435, 1083-1087.

Miller K.G., Janecek T.R., Katz M.E., Keil D.J., (1987) Abyssal circulation and benthic foraminiferal changes near the Paleocene/Eocene boundary. *Paleoceanography* 2, 741-761

Miller, K.G., Katz, M.E., 1987. Oligocene to Miocene benthic foraminiferal and abyssal circulation changes in the North Atlantic, *Micropaleontology*, 33, 97-149.

Moore T.C., Rabinowitz P.D., Shipboard Scientific Party, 1984. Initial reports of the Deep Sea Drilling Project, Leg 74, U.S. Govt. Printing Office, pp 1-894.

Reid J.L., 1989. On the total geostrophic circulation of the South Atlantic Ocean: Flow patterns, tracers, and transports. *Progress in Oceanography* 23, 149-244.

Rial J.A., 2003. Abrupt climate change: chaos and order at orbital and millennial scales. *Global and Planetary Change*, 41 (2004), 95-109.

Robert C., Kennett J.P., 1997. Antarctic continental weathering changes during the Eocene-Oligocene cryosphere expansion: clay mineral and oxygen isotopes evidence. *Geology*, 28, 927-930.

Röhl U., Westerhold T., Bralower T.J., Zachos J.C., 2007. On the duration of the Paleocene-Eocene thermal maximum (PETM). *Geochemistry, Geophysics, Geosystem* Volume 8, 12: 1-13 p.

Siedler G., Müller T.J., Onken R., Arhan M., Mercier H., King B.A., Saunders P.M., 1996. The Zonal WOCE Sections in the South Atlantic. From Wefer G., Berger W.H., Siedler G., Webb D.J., (eds) 1996, *The South Atlantic: Present and Past Circulation*. Springer-Verlag Berlin Heidelberg, pp 599 – 620.

Sloan L.C, Barron E.J., 1992. A comparison of Eocene climate models results to quantified paleoclimatic interpretations. *Palaeogeogr., Palaeoclimatol., Palaeoecol.*, 93: 183-202.

Spiess V., Cruise Participants, 2003. Report and preliminary results of Meteor Cruise M49/1, Capetown (South Africa) - Montevideo (Uruguay), 04.01.2000 - 10.02.2000. *Berichte Fachbereich Geowissenschaften, Universität Bremen*, No. 205: 1- 57.

Steward R.H., 2003. Introduction into physical oceanography. Book available on the web: <http://ioc.unesco.org/oceanteacher/OceanTeacher2/DigitalLibrary.htm>

Stommel H., Aarons, H.P., 1960. The abyssal circulation of the world ocean. Part I. Deep-Sea Research, 6, 140-145.

Stott L.D., Kennett J.P., Shackleton N.J., Corfield R.M., 1990. The evolution of Antarctic surface waters during the Paleogene: inferences from the stable isotopic composition of planktonic foraminifers, ODP Leg 113, In Barker P.F., Kenneth J.P., et al., Proc. ODP, Sci. Results, 113: College Station, TX (Ocean Drilling Program) 849-863.

Suspan A., 1899. Die Bodenformen des Weltmeeres, Petermanns Geogr. Mitt., 45, 117.

Thomas E., Shackleton N., 1996. The Paleocene-Eocene benthic foraminiferal extinction and stable isotopes anomalies. In Knox, R.W.O'B., Corfield, R.M., and Dunay, R.E. (Eds.), Correlation of the Early Paleogene in Northwest Europe. Spec.Publ.-Geol. Soc. London, 101: 401-441.

Tripati A., Elderfield H., 2005. Deep-Sea Temperature and Circulation Changes at the Paleocene-Eocene Thermal Maximum. Science, 308: 1894-1898.

Wessel P., Smith W.H.F., 1998. New, improved version of Generic Mapping Tools released. EOS Transaction, American Geophysical Union, 79(47), 579.

Wüst G., 1936. Das Bodenwasser und die Gliederung der Atlantischen Tiefsee. Wiss. Ergebnisse Deut. Atlantik Expeditionen Meteor, 6(1),3-107.

Zachos J.C., Stott L.D., Lohmann K.C., 1994. Evolution of early Cenozoic marine temperatures, Paleoceanography, 9:353-387.

Zachos J.C., Pagani M., Sloan L., Thomas E., Billups K., 2001. Trends, rhythms, and aberrations in global climate 65 Ma to present. Science, 292: 686-693.

---

Zachos J.C., Wara M.W., Bohaty S.M., Delaney M.L., Petrizzo M.R., Brill, A., Brawlower T.J., Premoli-Silva I., 2003. A transient rise in tropical sea surface temperature during the Paleocene Eocene Thermal Maximum. *Science*, 302, 1551-1554.

Zachos J.C., Kroon D., Blum P., Scientific Shipboard Party, 2004. Proceedings of the Ocean Drilling Program, Initial Reports Volume 208, available on the web:

[http://www-odp.tamu.edu/publications/208\\_IR/VOLUME/CHAPTERS/IR208\\_01.PDF](http://www-odp.tamu.edu/publications/208_IR/VOLUME/CHAPTERS/IR208_01.PDF)



## **2. Correlation of high-resolution seismic data with ODP Leg 208 borehole measurements**

Thomas Bartels\*, Sebastian Krastel, Volkhard Spiess

Manuscript published in ODP Leg 208 Scientific Results, Manuscript Number SR208-204

### **2.1 Abstract**

Walvis Ridge, located in the eastern South Atlantic Ocean, is one of the few known locations where it is possible to recover undisturbed, complete, and possibly expanded Paleogene sediments over a wide range of water depths. The main objective of Ocean Drilling Program (ODP) Leg 208 realized on outer Walvis Ridge in the summer of 2003 was recovery of intact composite sequences of “critical” transitions like the Cretaceous/Tertiary (K/T) boundary, Eocene/Oligocene (E/O) boundary, Paleocene/Eocene Thermal Maximum (PETM), and Eocene layer of mysterious origin (ELMO) event.

Meteor Cruise M49/1, in early 2001, was the main seismic pre-site survey for Leg 208. The high-resolution multichannel seismic system of the University of Bremen was used to identify drill sites at outer Walvis Ridge that promised recovery of undisturbed, complete, and possibly expanded Cenozoic sequences. Based on these new seismic data, six sites were drilled at water depths between 2500 m and 4755 m on the northeastern flank of Walvis Ridge during Leg 208.

To ground truth the seismic record, synthetic seismograms were calculated from closely spaced core logging density measurements of the Leg 208 cores. The high quality of both seismic and core logging data allows good correlation between synthetic seismograms and recorded seismic data. These results allow identification and characterization of target reflection horizons like E/O boundary, ELMO horizon, PETM and K/T boundary in seismic images and dating of individual reflectors.

Total sediment thickness in the survey area varies between 100 and 450 m, wherefore the study area can be separated into three zones which have different deposition conditions. In general the seismic data show a decrease in total sediment thickness with increasing distance from the ridge crest, but lateral variations in sedimentation rates were found across the entire survey area. Especially close to the crest of the ridge, these lateral variations in sedimentation



rates might indicate the influence bottom water currents on sedimentation at the outer Walvis Ridge.

## 2.2 Introduction

Walvis Ridge is a northeast-southwest-trending aseismic ridge that effectively divides the eastern South Atlantic Ocean into two basins, Angola Basin to the north and Cape Basin to the south (Fig. 2.1). The ridge consists of a series of interconnected crustal blocks that slope gradually toward the northwest and more steeply toward the southeast. Magnetic and gravity anomalies indicate that the ridge was formed by hotspot volcanism near the mid-ocean ridge as the basin gradually widened (Rabinowitz and Simpson, 1984). Walvis Ridge is well known as a nearly impassable barrier for bottom waters (Arhan et al., 2003). Pelagic sediments drape most of the ridge and generally increase in thickness toward the continental margin (Moore, Rabinowitz, et al., 1984). It is assumed that the ridge followed a simple thermal subsidence of ~1.1 km since the Maastrichtian (Moore, Rabinowitz, et al., 1984).

The thickness of pelagic sediments varies from ~200 m on the deep (>4.5 km) seafloor adjacent to the ridge to ~530 m near the summit (~2.5 km). These sediments are primarily calcareous oozes and chinks that range in age from Campanian to Holocene. In the Neogene section, nannofossil and foraminiferal nannofossil oozes with relatively high carbonate contents of as much as 90 wt% were found. The lower to middle Miocene sections are characterized by lower carbonate values between 0 and 20 wt%. Some intercalated slumps and turbidites were identified in Neogene deposits. Paleogene sediments are dominated by nannofossil- and foraminifer-bearing nannofossil oozes to chalk. The sediments have high carbonate contents, up to 80 wt%, through most of the Paleocene, Eocene, and Oligocene. Some smaller carbonate-poor intervals indicate episodes of carbonate compensation depth (CCD) shoaling (Zachos, Kroon, Blum, et al., 2004).

In spring 2003, six sites were drilled on outer Walvis Ridge during Ocean Drilling Program (ODP) Leg 208. The main objectives of Leg 208 were to analyze extreme climatic conditions in the Paleogene, date and utilize astronomical cycles, and the reconstruction of the eastern equatorial paleoceanographic development. Meteor Cruise M49/1 in early 2001 acted as main seismic pre-site survey for Leg 208 to optimize drill site locations.

To ground truth the seismic records and to construct a more precise seismic stratigraphy, it is possible to correlate the seismic records with well data from a nearby drill site by modeling reflection patterns. This was accomplished by visual correlation of seismic

traces with synthetic seismograms, calculated from drill site density and velocity measurements (e.g., Zühlsdorff and Spieß, 2001; White and Hu, 1998). The best results are commonly achieved when downhole logging data from near-vertical wells are available (White and Hu, 1998), but if, like in this study, no downhole velocity log exists, it is possible to estimate sonic data from density logs (e.g. Adcock, 1993, Zühlsdorff and Spieß, 2001). Therefore velocity and density profiles were constructed from measurements on rock samples or from core logging data as provided by the gamma ray attenuation (GRA) densitometer and the *P*-wave logger (PWL). Correlation of seismic data collected during Meteor Cruise M49/1 and core logging data measured during Leg 208 is a very promising approach due to the high quality of both data sets. In this paper we present seismic data from the pre-site survey collected during Meteor Cruise M49/1 and identify the target horizons of Leg 208 sites using synthetic seismograms. Using the stratigraphy of the cores of Leg 208 (Zachos, Kroon, Blum, et al., 2004) this method permits assignment of ages to individual reflectors and to characterize the seismic signature of target horizons. Seismic data will also be used for a first investigation of sedimentary features at outer Walvis Ridge.

## **2.3 Data and methods**

### **2.3.1 Seismic data**

Meteor Cruise M 49/1 in early 2000 from Cape Town (South Africa) to Montevideo (Uruguay) was the main pre-site survey for Leg 208. The main objectives were to collect high-resolution seismic reflection profiles to identify drill sites that promise recovery of undisturbed, complete, and possibly expanded Palaeogene sequences in different water depths. ~1800 line km of seismic profiles in the study area of Leg 208 were acquired on a water depth transect from ~2.5 to 4.5 km (Fig. 2.1).

The multichannel seismic system of the University of Bremen is specifically designed to collect seismic data with high lateral and vertical resolution. The alternating operation of a small-chamber Watergun (0.16 l; 200–1600 Hz), a Generator-Injector (GI) Gun (Sodera Inc.) with reduced chamber volume (0.4 l; 100–500 Hz), and a GI-Gun with normal chamber volume (1.7 l; 30–200 Hz) yielded three seismic data sets simultaneously. For recording of the GI-Gun and Watergun data, a 96-channel Syntron streamer of 600 m length equipped with separately programmable hydrophone groups was used. In this manuscript, we will only present GI-Gun data. 48 channels consisting of 13 hydrophones each, a group length of 6.25

m, and a group distance of 12.5 m were used for recording GI-Gun data. The shot interval was 9 s, resulting in a shot distance of ~25 m when sailing with an average speed of 6 kt. Ten birds kept the streamer at a constant water depth of ~3m below the sea surface within a range of 1 m. A magnetic compass at every bird allowed determination of hydrophone group position relative to the ship's course. GI-Gun data were digitally recorded at a sampling frequency of 4 kHz over a record length of 3000 ms. Positioning was based on Global Positioning System (GPS). For processing of seismic data a combination of in house and the commercial (Vista) software (Seismic Image Software LTD) was used. Standard seismic processing procedures employed included trace editing, setting up geometry, static and delay corrections, velocity analysis, normal move-out (NMO) corrections, band-pass frequency filtering, stacking, and time migration. A common midpoint (CMP) distance of 10 m was chosen for processing.

### 2.3.2 Calculation of synthetic seismograms

The reflection coefficient (R) between media of densities  $\rho_1$  and  $\rho_2$  and velocities  $v_1$  and  $v_2$  is given for vertical incidence waves by the Zoepritz equation:

$$R = (\rho_1 v_1) - (\rho_2 v_2) / (\rho_1 v_1) + (\rho_2 v_2)$$

The sequence of velocity and density changes with depth below the seafloor is referred to as the earth's reflection coefficient series. This series can be transformed into two-way traveltime (TWT) scale by using the velocity measurements. Synthetic seismogram can be calculated by mathematically convolving this series with the seismic wavelet. The impulse response function for the seismic modeling was computed using the state space approach (Mendel et al., 1979) which also takes all possible internal reflections into account. By comparing reflectors in the synthetic seismogram with density measurements of the core, it is possible to assign reflectors to geologic events. The detailed procedure for calculating the synthetic seismogram is described below.

### 2.3.3 Editing of GRA Density Data

GRA density measurements with a sampling interval of 2 to 3 cm are available for all sites of Leg 208. All sites consist of two to four holes. As individual holes usually do not

recover the entire stratigraphy of a site, it is necessary to merge and edit the density data to create composite data sets for each site (Fig. 2.2.1-2.2.4). This was done using stratigraphic tie points determined during the cruise (Zachos, Kroon, Blum, et al., 2004).

After creating a composite data set for each site, a moving window with a length of 50 measured values was used to calculate a local average density and to detect spurious density values, likely caused by voids, cracks, or gas bubbles within the cores and at the ends of the

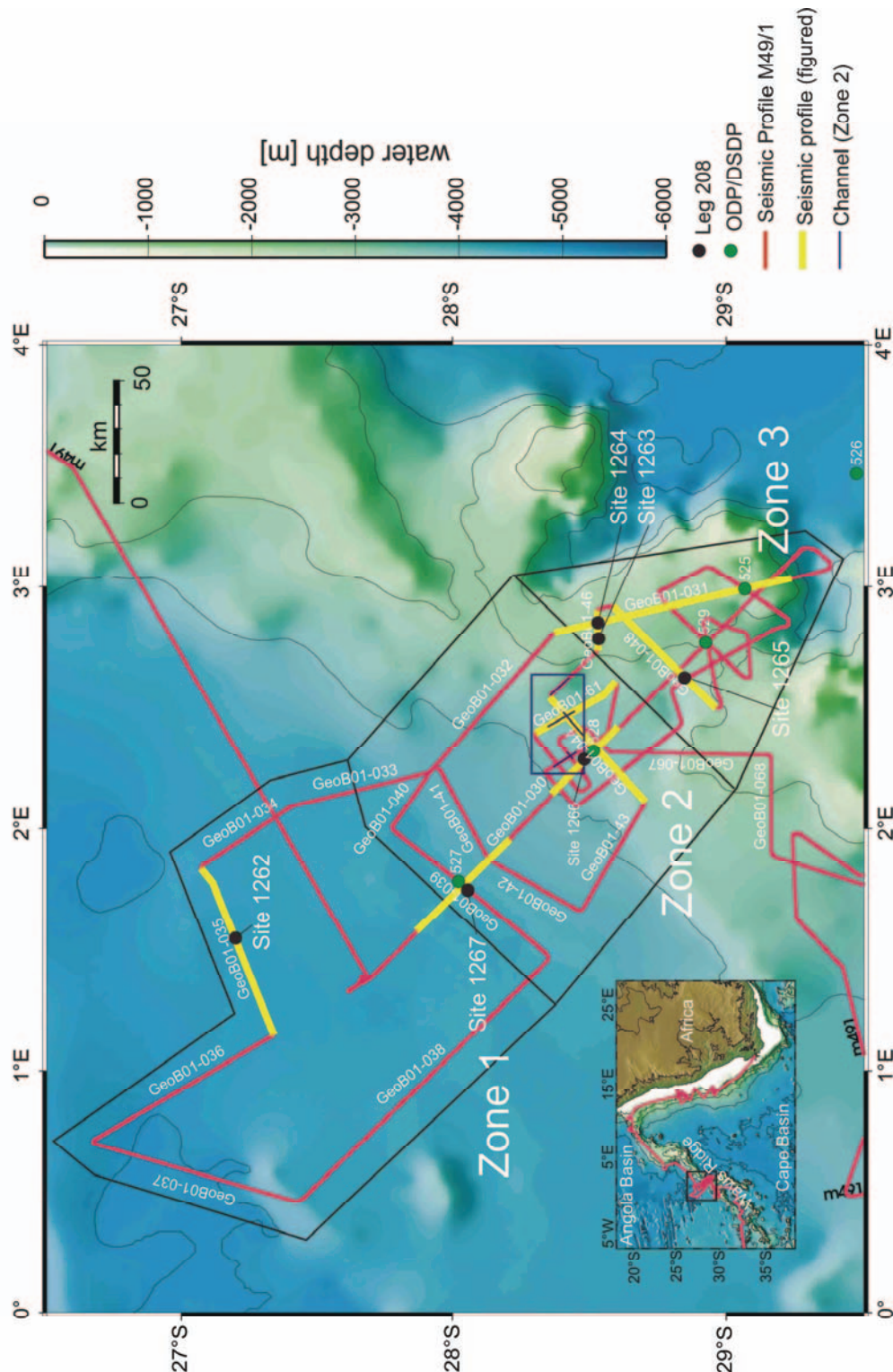


Figure 2.1: Seismic pre-site survey ODP Leg 208

core sections. These artifacts cause unrealistic values for reflection coefficients and thus are replaced by the last density value which was accepted by the moving window. The criterion to replace was that a value should not differ more than four times of the root means square deviation of the window. Furthermore, data gaps which cannot be filled were linearly interpolated to avoid unnatural reflection coefficients caused by small data gaps. A correction of the GRA density values to in-situ conditions, which accounts for decrease in hydrostatic pressure, temperature change, and porosity rebound during core recovery (Hamilton, 1976) was not carried out because relative density variations especially for the upper 150 m of the sediment column will not be significantly changed (e.g., Mosher et al., 1993; Rohr and Gröschel-Becker, 1994).

#### **2.3.4 P-Wave velocity models**

The sampling intervals of the whole-core velocity data sets are ~25 cm and more, which is much larger than the sampling intervals of the GRA density measurements of the Leg 208 cores (Zachos, Kroon, Blum, et al., 2004). This discrepancy makes it impossible to calculate reflection coefficients with a detailed velocity model. Additionally detailed velocity measurements were not done at all depths of each site. Adventitious velocity data are less important for the calculation of reflection coefficients since values scatter around a mean trend and variations in marine surface sediments do not exceed 5% (e.g. Weber et al., 1997; Breitzke, 1999). In contrast, the associated density variations within the marine surface sediments are usually > 20% (e.g. Weber et al., 1997; Breitzke, 1999). Additionally, a careful analysis of the velocity and GRA density measurements shows a positive correlation, of smaller velocity excursions and density variations. Therefore, the effect of the velocity data on the reflection coefficient is small. We estimate the overall error, which is introduced by assuming a smooth velocity depth profile and ignoring the velocity contribution to variations in reflection coefficients, to be only 10%-20%. Zühlsdorff and Spieß (2001) estimated similar errors using the same methods for data from ODP Leg 168 at the eastern flank of Juan de Fuca Ridge.

In addition, close inspection of the velocity data also shows a large number of spurious data points. These facts support the use of a simple velocity model that is still sufficient to identify our target reflectors, but with obvious restrictions. For example interpretation of waveforms, as well as interpretation of amplitudes of individual reflectors, is of limited quality since effects such as interference definitely cause discrepancies between recorded and

modeled data. The velocity model is, of course, needed for conversion of the mbsf scale to a timescale, too.

### 2.3.5 Correlation of the synthetic seismograms with the seismic record

After creating whole continuous GRA density data sets for each site, it is necessary to convert the mbsf scale to a timescale and to calculate the series of reflection coefficients. In the first step, a constant velocity of 1500 m/s was used. A sampling interval of 250  $\mu$  s, which is the same as for the seismic data, was used to preserve the complete information of the GRA density measurements. To create a seismic trace the density data must be convolved using a seismic wavelet. Although it is possible to pick seafloor reflections, a synthetic wavelet is used. Synthetic wavelets are smoother than recorded wavelets and appear to me more useful for visual correlation of reflection patterns. Differences in the vertical energy distribution between synthetic wavelets and recorded wavelets do not appear (Zühlsdorff and Spieß, 2001). In this study, for convolving the reflection coefficients, a Ricker wavelet (Ricker, 1953) with a frequency of 150 Hz, which is the main frequency of the GI Gun, was used (Fig. 2.2.1-2.2.4). Synthetic data were then compared with seismic data at the CMP of the drill site location. In the next step the velocity model was fine tuned using velocity information from whole-core analysis to improve the depth to time conversion for better synthetic to seismic matching. It turned out that the best-fit velocity models usually correspond to linear regressions of the velocity measurements, which take the general velocity trend into account, namely the increase of the velocity with depth, but neglects all small-scale velocity variations (2.2.1-2.2.4).

For Site 1267 no velocity measurements or information exist. Therefore a velocity model of a nearby drill site is used. In this case, the velocity model of Site 1266 is used, which is located on the same seismic profile GeoB01-030 which is characterized by only few changes in the sedimentation pattern.



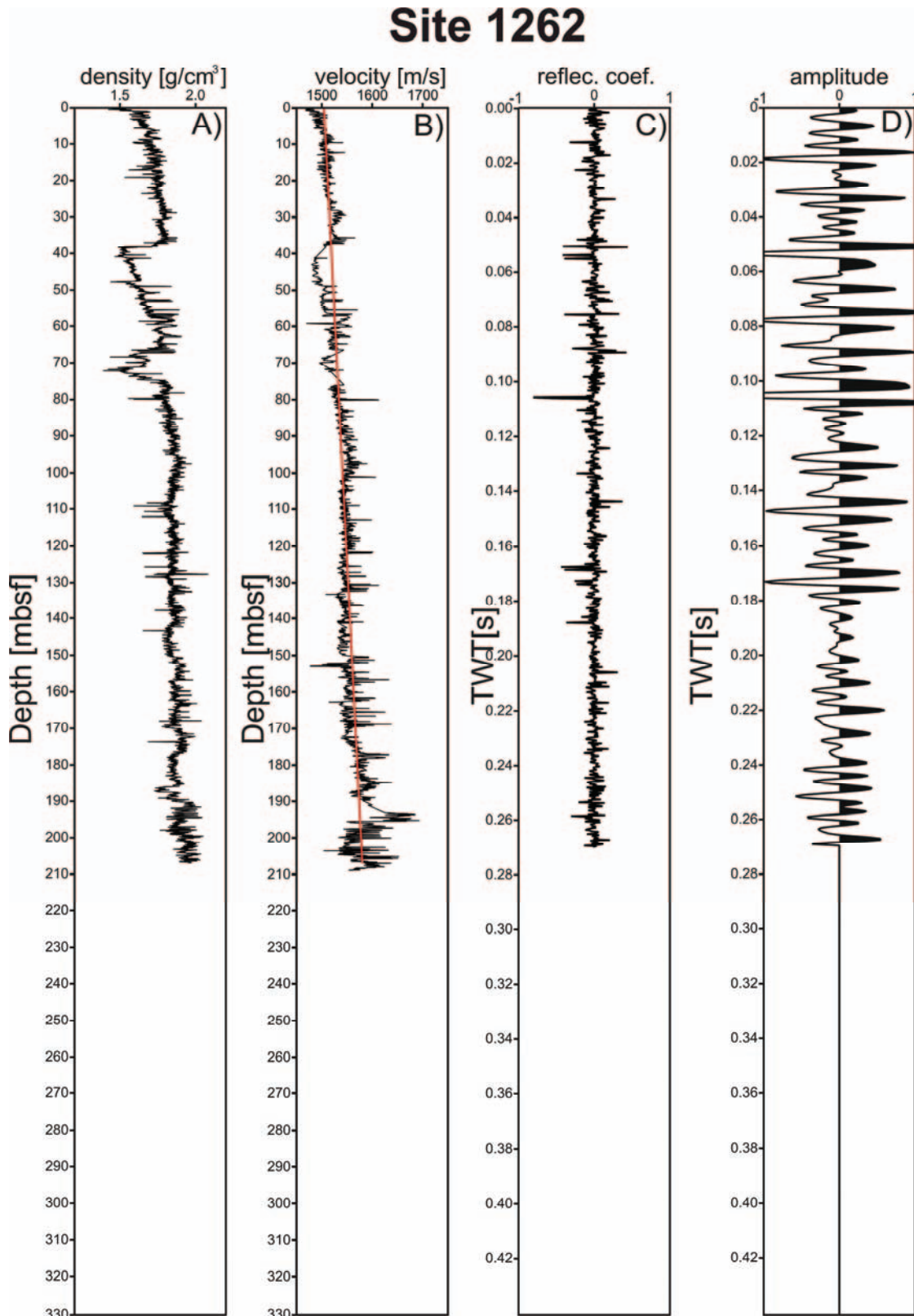


**Figure 2.2.1:** Core Data Site1262:

- A) GRA density constructed from Holes 1262A, 1262B, 1262C, and 1262D using Splice Tables
- B) Velocity measurements from Site 1262 with regression line (red) used for the conversion from a depth scale to a timescale
- C) Resulting reflection coefficient
- D) Resulting synthetic seismogram using a Ricker wavelet with 150 Hz

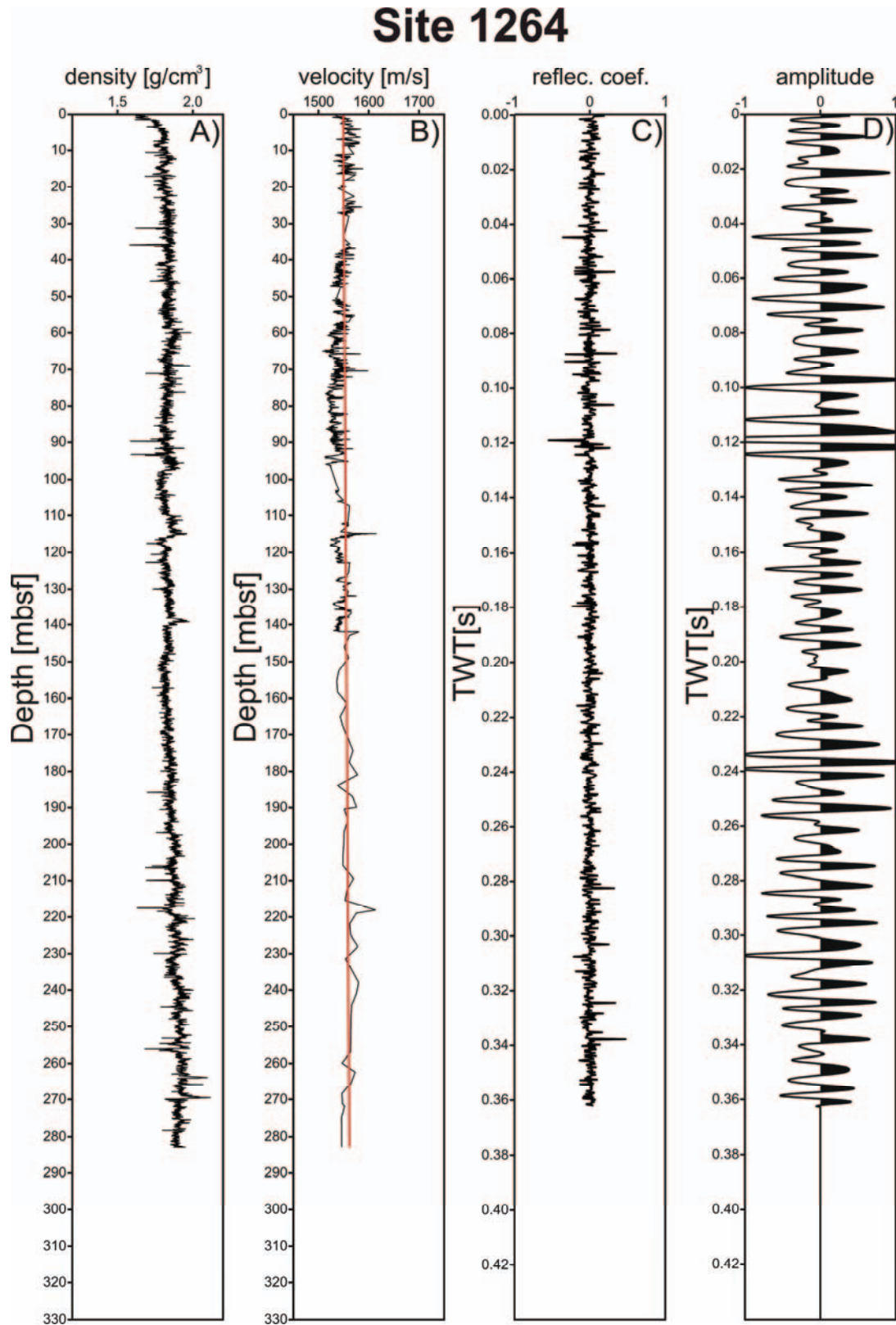


**Figure 2.2.2:** Core Data Site1264:

- A) GRA density constructed from Holes 1264A, 1264B, and 1264C using Splice Tables
- B) Velocity measurements from Site 1264 with regression line (red) used for the conversion from a depth scale to a timescale
- C) Resulting reflection coefficient
- D) Resulting synthetic seismogram using a Ricker wavelet with 150 Hz

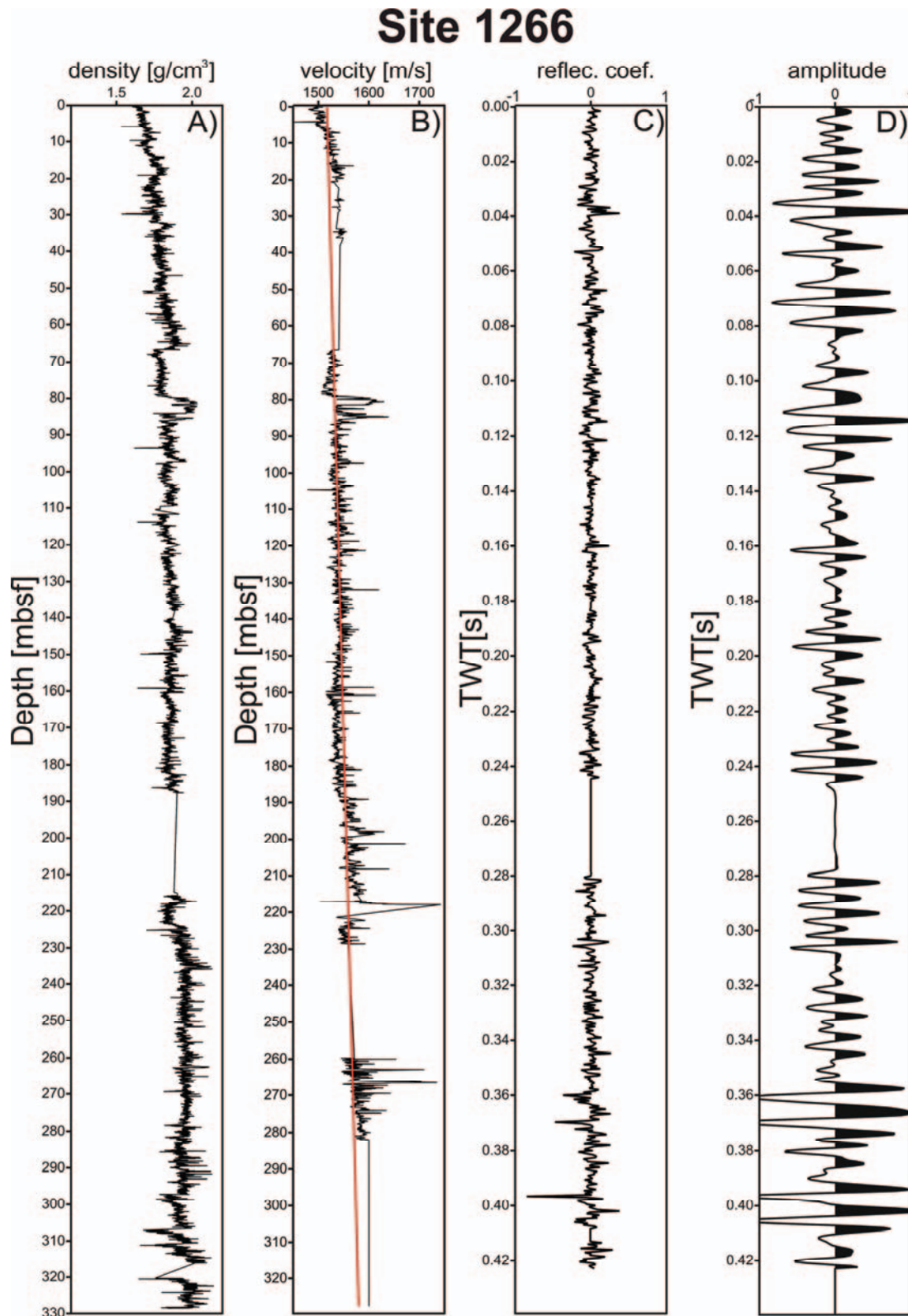


**Figure 2.2.3:** Core Data Site1266:

- A) GRA density constructed from Holes 1266A, 1266B and 1266C using Splice Tables
- B) Velocity measurements from Site 1266 with regression line (red) used for the conversion from a depth scale to a timescale
- C) Resulting reflection coefficient
- D) Resulting synthetic seismogram using a Ricker wavelet with 150 Hz

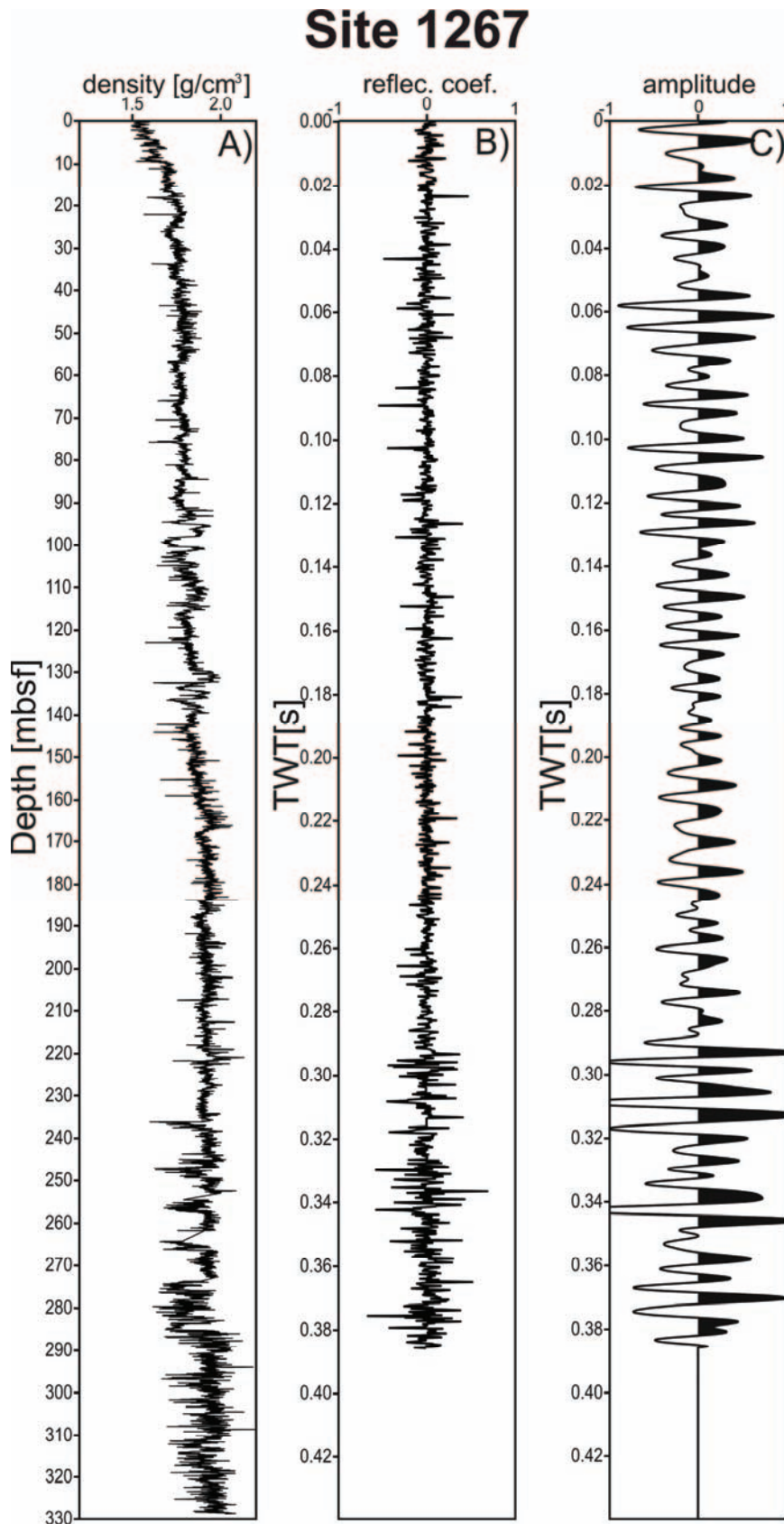


**Figure 2.2.4:** Core Data Site1267:

- A) GRA density constructed from Holes 1267A and 1267B using Splice Tables
- B) Resulting reflection coefficient
- C) Resulting synthetic seismogram using a Ricker wavelet with 150 Hz



## 2.4 Description of the Sites

Six sites were drilled at water depths between 2500 and 4770 m on the northeastern flank of Walvis Ridge during Leg 208 (Fig. 2.1). The main objective of Leg 208 was to recover intact composite sequences of “critical” transitions in the Paleogene (Zachos, Kroon, Blum, et al., 2004). This paper concentrates on these transitions, namely the following:

- Eocene/Oligocene (E/O) boundary (35.7 Ma): this sharp transition is marked by a step increase in magnetic measurements and a step decrease in color lightness (Zachos, Kroon, Blum, et al., 2004).
- Chron C24n ELMO event (53.2 Ma): this event is characterized by a drop in calcium carbonate content in the sediment (Zachos, Kroon, Blum, et al., 2004) and is characterized by density contrast of  $\sim 10\%$  in comparison to the surrounding sediments. The layer was reached at five of the six sites and has a thickness of  $\sim 30$  cm (Zachos, Kroon, Blum, et al., 2004).
- Paleocene/Eocene Thermal Maximum (PETM, 55 Ma): isotope records suggest that at  $\sim 55$  Ma the deep ocean and high-latitude surface waters warmed by  $4^\circ\text{C}$  and  $8^\circ\text{C}$ , respectively (e.g., Kaiho et al., 1996). The PETM at the Leg 208 sites is a clay layer without carbonate content. The thickness of the layer varies from 50 cm at the deepest site to 80 cm at the shallower sites same as the ELMO horizon the density of the PETM increases about  $\sim 10\%$  (Zachos, Kroon, Blum, et al., 2004).

Additionally, it is possible to identify the Miocene *Bolivina* Acme event (18 Ma), which represents a foraminiferal assemblage dominated by small, smooth, thin-walled bolivinids (Smart and Murray, 1994) at all sites and the Cretaceous/Tertiary (K/T) boundary (66.4 Ma) at the two deepest Sites 1262 and 1267.

Identification of the critical transitions on the seismic data was done by means of correlation the synthetic seismograms. Figure 2.3 shows data examples for Sites 1262, 1264, 1266, and 1267. Because of the high quality of both data sets, the reflection patterns of the synthetic seismograms fit well with the seismic traces. This “event modeling” offers the possibility to assign the characteristic layers of the drill sites to the seismic reflectors. The depths values of the target horizons described below are calculated from seismic traveltime including the simplified linear velocity model used for calculation of the synthetic

seismograms. The resolution of the top and base of the target horizons like PETM and ELMO horizon scaling on meter to sub-meter scale is not possible with a GI-Gun ( $\sim 150$  Hz) as a

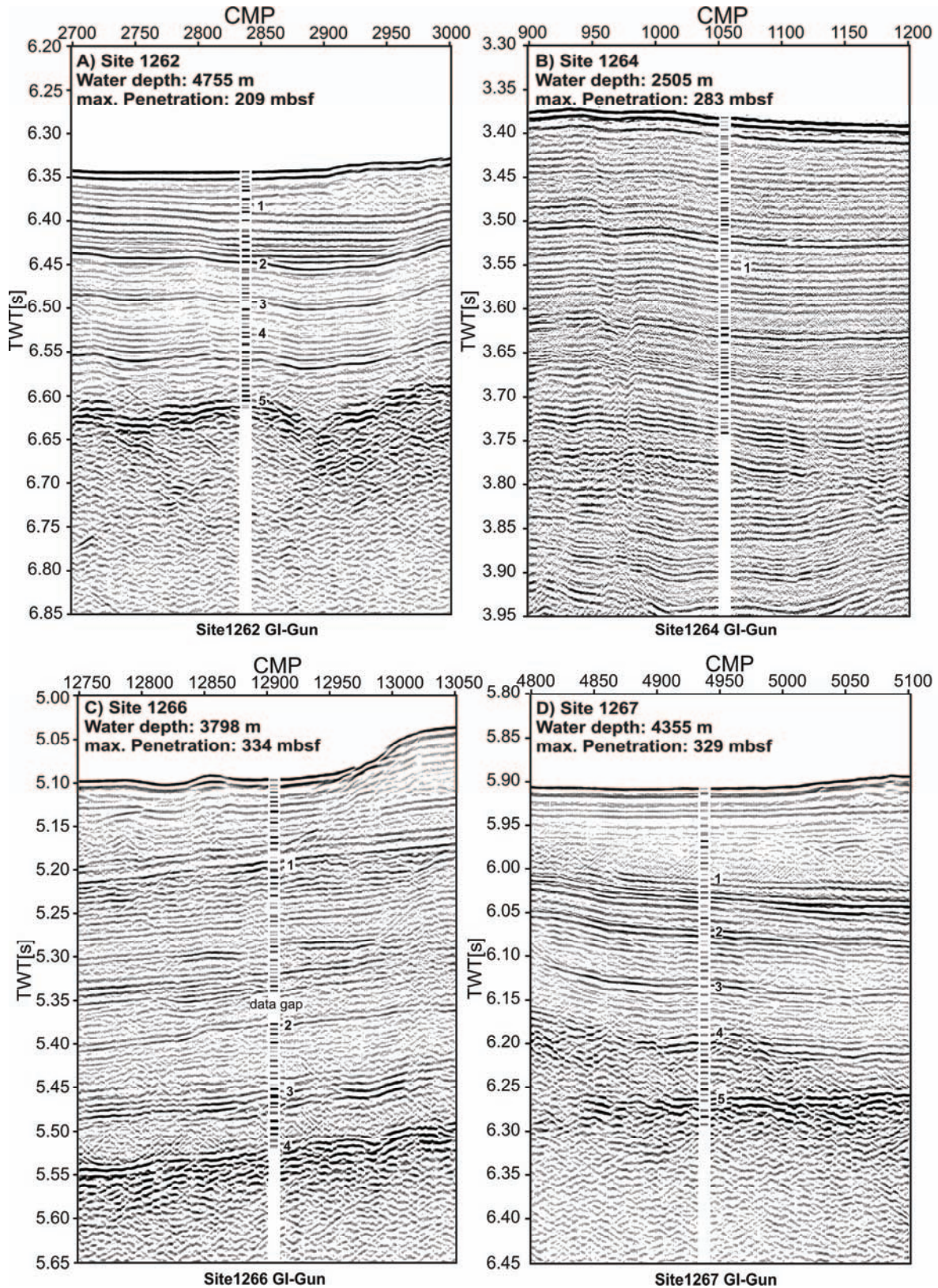


**Figure 2.3:** Correlation of synthetic seismograms with the seismic data Sites: (A) 1262, (B) 1264, (C) 1266, and (D) 1267. Horizons: (1) Miocene Bolivina Acme, (2) E/O boundary, (3) ELMO horizon, (4) PETM, (5) K/T boundary. CMP = common midpoint. GI = generator injector

seismic source. For this task a wavelet with a length which is not smaller than two times the thickness of the layer is needed (Badley, 1985). However, the fit of the reflection pattern together with the knowledge of the physical properties of each event (Zachos, Kroon, Blum, et al., 2004) allows identifying the seismic reflectors in which each event must be included. Because of changing density values, e.g. the increase of 10% for the ELMO horizon and the PETM, those reflectors are mostly characterised by stronger amplitudes.

The synthetic seismograms of Sites 1263 and 1265 are missing because of spurious data values in the GRA density values, wherefore synthetic seismograms do not fit with the seismic data. Hence, identification of the target horizons of these both sites is based on correlation between each site of Leg 208 by tracing the target horizons along the seismic profiles. Table 2.1 summarizes the depths of the target horizons for each site of Leg 208.

	1262	1263	1264	1265	1266	1267
<b>Miocene Bolivina Acme</b>	53 mbsf	44 mbsf	159 mbsf	88 mbsf	115 mbsf	111 mbsf
<b>E/O boundary</b>	78 mbsf	100 mbsf	-	192 mbsf	207 mbsf	128 mbsf
<b>ELMO horizon</b>	115 mbsf	265 mbsf	-	241 mbsf	270 mbsf	179 mbsf
<b>PETM</b>	139 mbsf	335 mbsf	-	315 mbsf	306 mbsf	231 mbsf
<b>K/T boundary</b>	195 mbsf	-	-	-	-	298 mbsf

**Table 2.1:** Depth in mbsf of target horizons at each site of Leg 208 calculated using the velocity models of the synthetic seismograms and traveltime of the seismic data.

### Site 1262

Site 1262 (Fig. 2.4), at a water depth of ~4755 m and located on Profile GeoB01-035, is the deepest site of the drilling transect, situated at the edge of Angola Basin. The seismic profile is characterized by an undulating topography with a number of sedimentary ridges located on top of basement highs and small sedimentary basins in between. Several debris flows and/or slumps were imaged as transparent zones in the sedimentary basins. The total sediment thickness is between 150 and 220 m (Fig. 2.4). Site 1262 is located in one of the small sedimentary basins. The upper ~100 ms TWT is characterized by continuous reflectors with high amplitudes. A debris flow or slump is located in this depth interval directly west of the site. The upper ~100 ms TWT represents Neogene and Eocene sediments. The Miocene *Bolivina* Acme event is found in this interval at ~53 mbsf and can be characterized by a reflector with high amplitudes. At the depth of ~100 ms TWT, the seismic pattern changes with a clear decrease of amplitude at the E/O boundary at a depth of ~78 mbsf. Seismic data below ~100 ms TWT show interlayering of weak and strong reflector packages including the ELMO horizon and the PETM down to the basement at ~300 ms TWT. Both clay layers are



characterized by strong amplitudes. The ELMO horizon at ~115 mbsf appears as a single distinct continuous reflector, whereas the PETM at ~139 mbsf appears as the first reflector of a package of several reflectors with strong amplitudes. With the drilling depth of 209 mbsf it was possible to recover all critical transitions including the K/T boundary, which is characterized by a strong amplitude reflection close to the crystalline basement at a depth of ~195 mbsf.

### **Site 1267**

Site 1267, located on Profile GeoB01-030, is situated close to the edge of Angola Basin at a water depth of 4355 m (Fig. 2.5). The profile runs perpendicular to the ridge axis in a northwest-southeast direction. Sediment thickness in the northwest part of the profile is ~340 m. Site 1267 is located close to a basement high which results in mostly parallel and undisturbed but inclined reflectors. Upper Maastrichtian sediments, which were the oldest sediments drilled during Leg 208, were reached at a drilling depth of 329 mbsf. The interval 0-150 ms TWT consists of Quaternary and Neogene sediments and includes a package of disturbed reflectors embedded with parallel reflectors with strong amplitudes. The Miocene *Bolivina* Acme is the first reflector of a package of stronger reflectors at ~111 mbsf. The E/O boundary at ~128 mbsf is a strong continuous reflector. In contrast to Site 1262, underlying reflectors also show high amplitudes. The ELMO horizon at ~179 mbsf is characterized by a continuous distinct reflector with strong amplitudes surrounded by sediments with lower amplitudes. The PETM at ~231 mbsf is embedded within a package of parallel reflectors with average amplitudes. At Site 1267, the K/T boundary was reached at a drilling depth of ~298 mbsf. The reflector representing the K/T boundary is located only ~30 m above the crystalline basement and shows strong amplitudes. Because of the proximity of the K/T reflector to basement with its rough surface, the reflector is not continuous along the profile.

### **Site 1266**

Site 1266, in a water depth of 3798 m, is also situated on Profile GeoB01-30 at the flank of the ridge (Fig. 2.6). It reaches upper Paleocene sediments at a drill depth of 334 mbsf. Sediments of Profile GeoB01-030 in the vicinity of Site 1266 along the flank of the ridge have a thickness of ~370 m, which is only slightly more than those at Site 1267. The northwestern part of the profile is characterized by mostly undisturbed and parallel reflectors, but

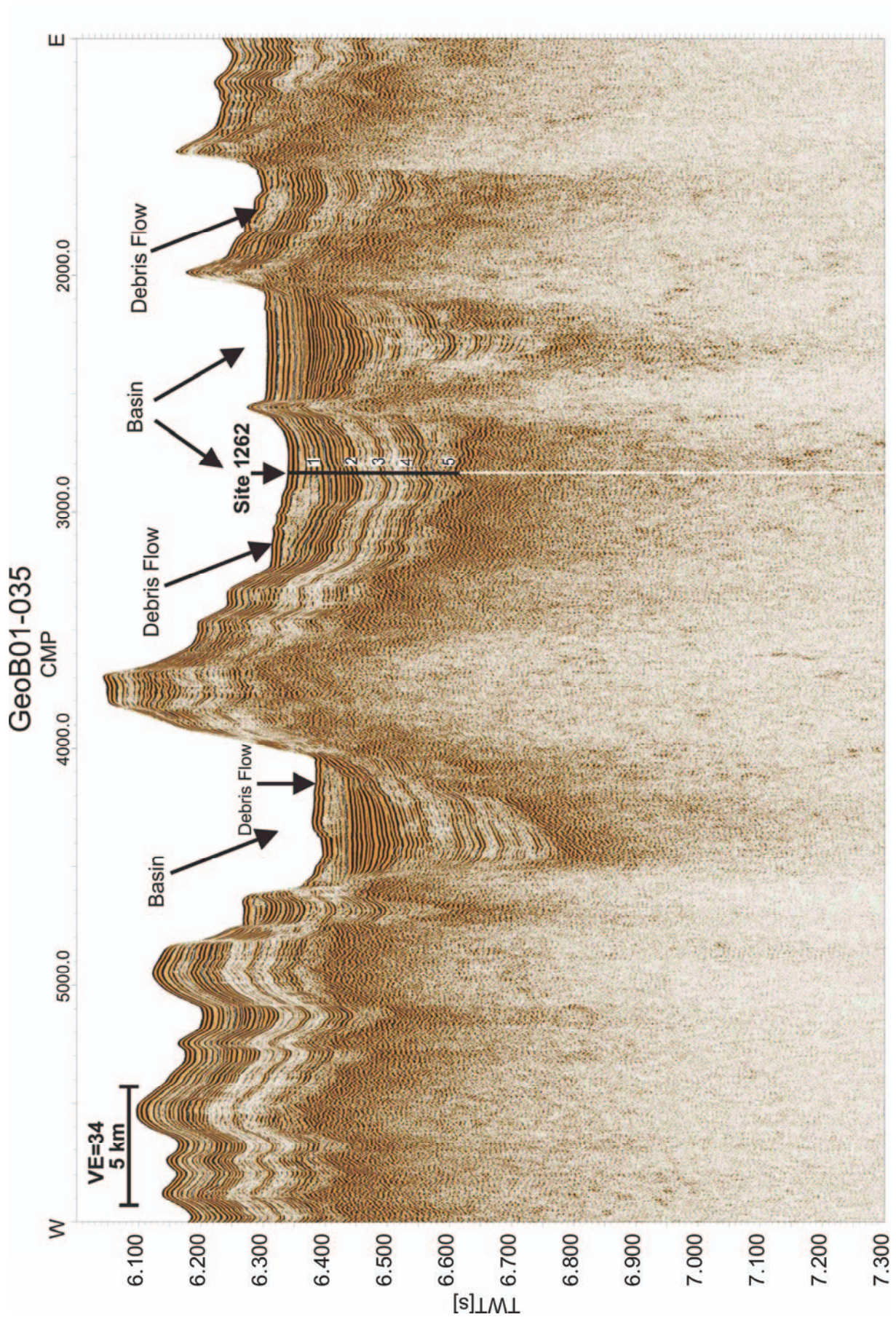


**Figure 2.4:** Seismic Line GeoB01-035 with Site 1262 (1) Miocene Bolivina Acme, (2) E/O boundary, (3) ELMO horizon, (4) PETM, (5) K/T boundary. VE = vertical exaggeration.



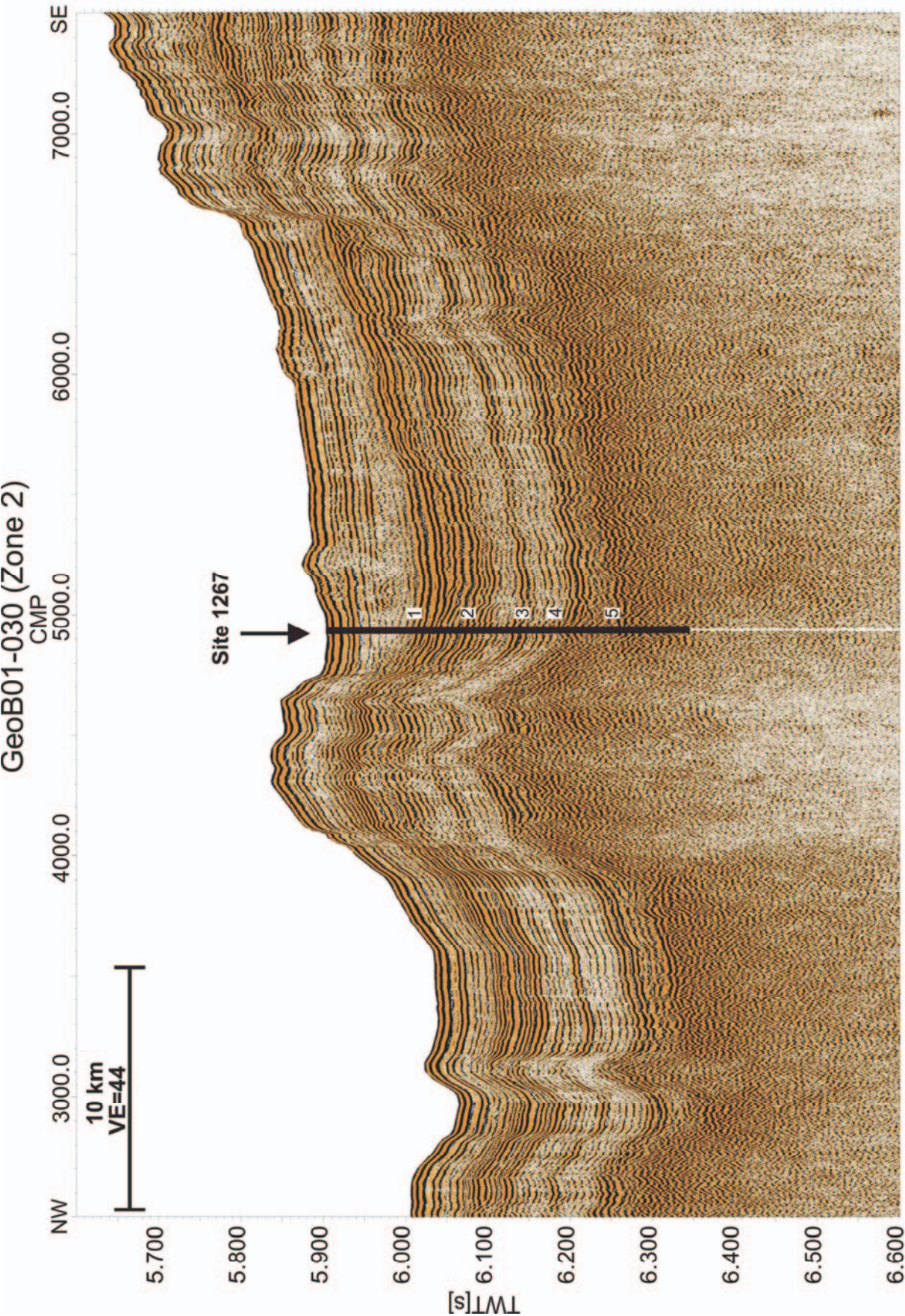


Figure 2.5: Part of the seismic line GeoB01-030 with Site 1267, (1) Miocene bolivina acme, (2) E/O Boundary, (3) ELMO horizon, (4) PETM, (5) K/T Boundary



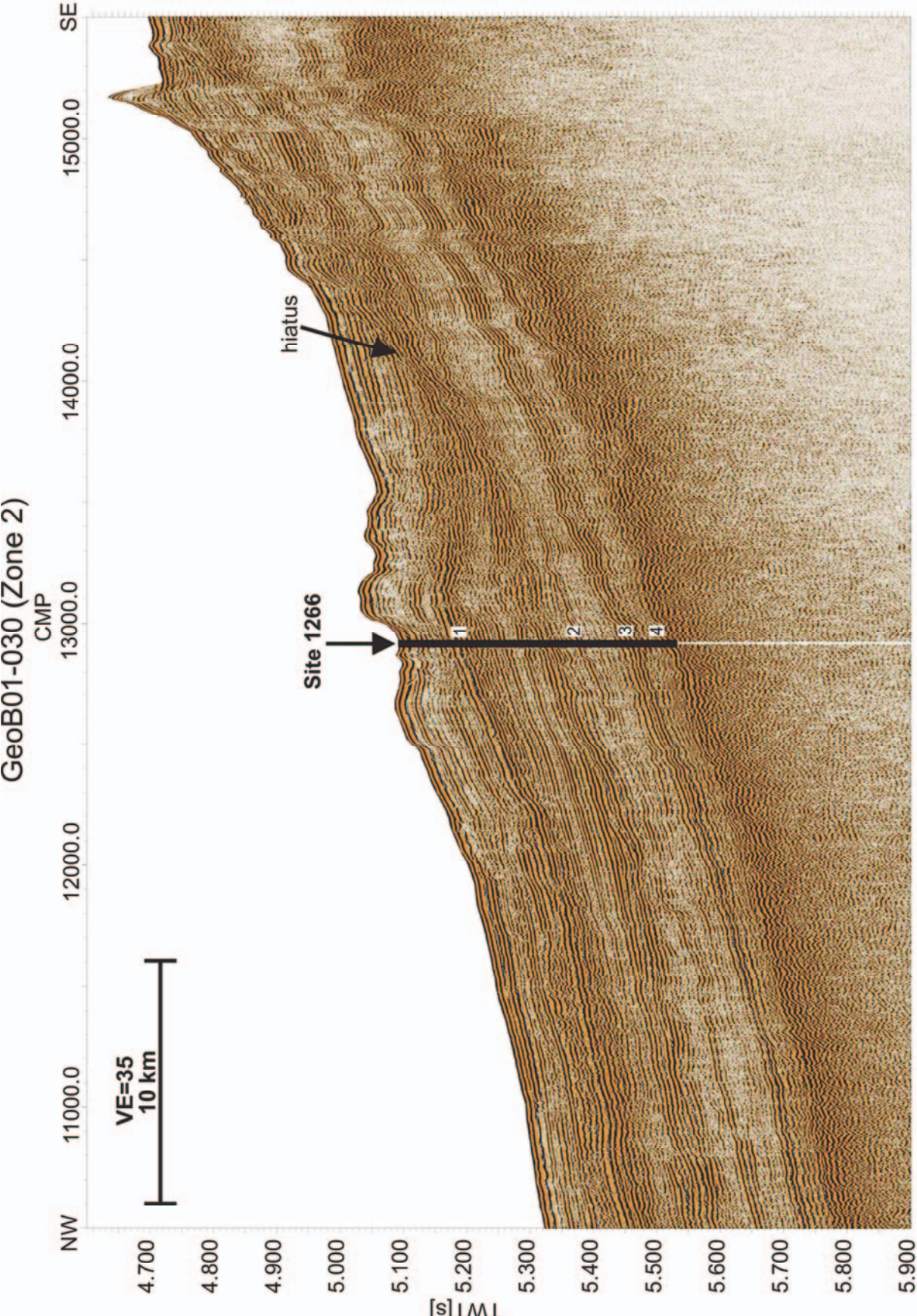


Figure 2.6: Part of the Seismic line GeoB01-030 with Site 1266, (1) Miocene bolivina acme, (2) E/O Boundary (3) ELMO horizon, (4) PETM, (5) K/T Boundary

in the direction of the ridge with decreasing water depth the pattern becomes more and more disturbed. Close to Site 1266 an unconformity occurs which results from a Neogene hiatus. Amplitudes of seismic reflectors at Site 1266 vary with depth, although only a few intervals with low amplitudes exist. The Miocene *Bolivina* Acme at ~115 mbsf is a continuous reflector with high amplitudes within a larger package of strong reflectors. The E/O boundary at ~207 mbsf is a transition from high amplitudes to a package of reflectors which are slightly disturbed and have lower amplitudes. The boundary is not as sharp as at Site 1262, for example (Fig. 2.4). The ELMO horizon at ~270 mbsf and the PETM at ~306 mbsf are part of packages with strong amplitudes. The package including the PETM is the lowermost sediment package which overlies the crystalline basement. The package consists of disturbed high amplitude reflectors.

### Site 1265

Site 1265 is located on Profile GeoB01-048, which is almost parallel to the axis of the ridge in a northeast-southwest direction (Fig. 2.7). The profile shows increasing sediment thickness up to ~450 m with decreasing water depth. Reflectors are mostly undisturbed and parallel except in a big channel structure in the center of the profile where Quaternary and Neogene sediments thin out. The reflectors of the flank of the channel are thinned out probably due to non-deposition. Additionally, the disturbed sedimentation pattern of the older sediments (e.g., Eocene) in the center of channel, likely indicates changing current activities. Expanded Neogene sediments shown in the northeast part of Profile GeoB01-048 are part of a morphologic high in which the shallowest Site 1264 (see below) was drilled. The morphologic high is characterized by the thickest sediments sequence at Walvis Ridge (up to 450 m). Site 1265 was drilled at the edge of the channel, where Quaternary and Neogene sediments are thin and older sediments are not disturbed by proximity to the channel. At a water depth of 3060 m and a drilling depth of 321 mbsf, Site 1265 reaches upper Paleocene sediments. The Miocene *Bolivina* Acme event within the uppermost 100 ms TWT at ~88 mbsf is characterized by a strong continuous reflector which is disturbed or absent in the center of the large channel. The E/O boundary at ~192 mbsf is situated in the interval between ~200 and 300 ms TWT. The boundary is not as sharp as at the other sites, but still a small change from higher to lower amplitudes beneath is notable. The boundary is not continuous, especially in northwest direction, where sedimentation was possibly disturbed variable current activities. The ELMO horizon at a depth of ~241 mbsf in the interval of ~300 to 400 ms TWT is not conspicuous because of only a small increase of the reflector amplitude. The PETM at



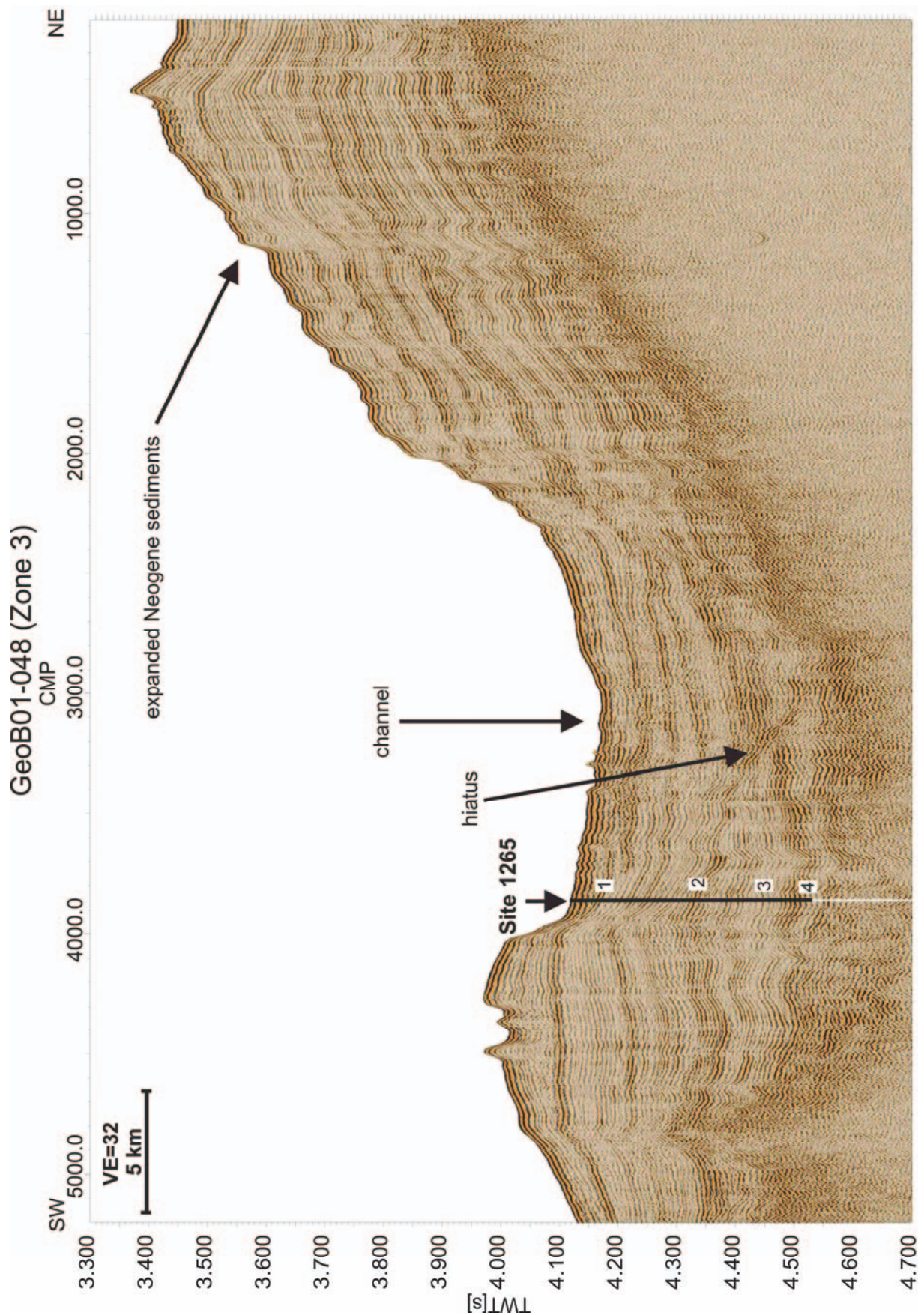


**Figure 2.7:** Seismic line GeoB01-048 with Site 1265, (1) Miocene bolivina acme, (2) E/O Boundary, (3) ELMO horizon, (4) PETM, (5) K/T Boundary

~315 mbsf is again part of the package with higher amplitudes but is not resolved as one continuous reflector.

### Sites 1263 and 1264

Sites 1263 and 1264, located on Profile GeoB01-046 (Fig. 2.8), were drilled close to the ridge flank where thickness of the sediment column varies from ~360 m at Site 1263 to ~450 m at Site 1264. Akin to Profile GeoB01-048 (Fig. 2.7), the profile shows a channel with thinned out reflectors at the flank and an expanded Quaternary and Neogene section. The western flank of the channel is not shown on the profile. The expanded section of Quaternary

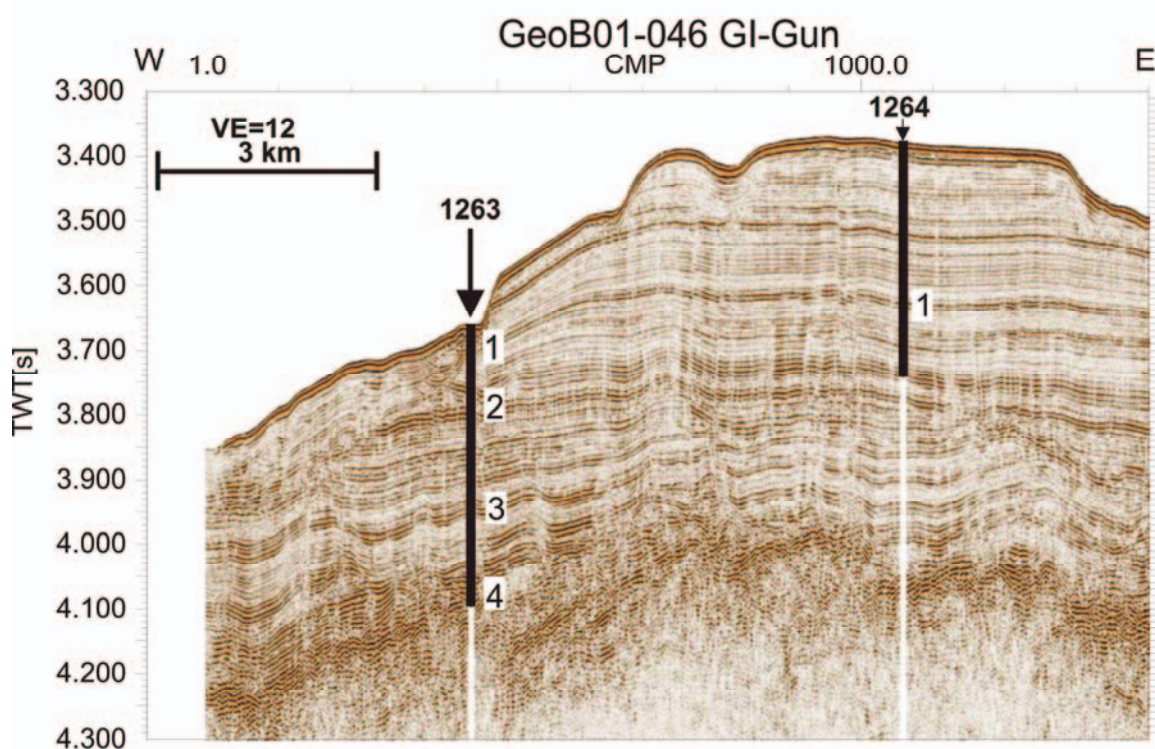


**Figure 2.8:** Seismic line GeoB01-046 with Sites 1263 and 1264, (1) Miocene bolivina acme (2) E/O Boundary, (3) ELMO horizon, (4) PETM, (5) K/T Boundary

and Neogene sediments shown in the eastern part of Profile GeoB01-046 are part of the morphologic high, which also appears on Profile GeoB01-048.

Site 1263, at a water depth of 2717 m, was drilled into an apparent bottom water channel where Quaternary and Neogene sediments are absent or thin and thus Paleogene sediments are shallow in depth. The upper ~100 ms TWT represents thinned out Quaternary and Neogene sediment sequences. It includes the Miocene *Bolivina* Acme at ~44 mbsf, which appears as a continuous reflector with high amplitudes. The parallel to sub parallel reflectors below ~100 to ~300 ms TWT show high amplitudes and good continuity. At ~100 mbsf the E/O boundary appears as a sequence of continuous reflectors with high amplitudes. Reflectors



below ~300 ms TWT start to undulate with depth. This unit shows varying amplitudes and includes the ELMO event as a strong reflector at ~265 mbsf. The site reaches Paleocene sediments including the PETM, which is surrounded by reflectors with high amplitudes at ~335 mbsf.

Site 1264 was drilled into an expanded section of Neogene sediments on the morphologic high close to the ridge flank. The location of the site is the crosspoint of Profiles GeoB01-046 (Fig. 2.8) and GeoB01-031 (Fig. 2.9). The morphologic high, illustrated on both profiles, is characterized by parallel layered sediment sequences. The sediments are disturbed by a slump or debris flow deposition shown in the south of Profile GeoB01-031 and smaller channels in the younger sediments in the north of the profile.

Site 1264, in a water depth of 2505 m, reaches Oligocene sediments at 282 mbsf. The parallel layered sediments represent a high-resolution data set of Quaternary and Neogene sediments with a pattern of varying strong and weak amplitudes in which the Miocene *Bolivina* Acme appears at ~159 mbsf as a continuous reflector with strong amplitudes.

## **2.5 Discussion**

### **2.5.1 Seismic characterization of target horizons**

The main objective of the project is stratigraphy and correlation between seismic and well data, which is based on pattern recognition of reflector sequences in the first place. Identification of the critical transition in the entire survey area is of great importance for this approach. As demonstrated above, we can identify the critical transitions in the seismic data at the locations of the Leg 208 drill sites; hence, demonstrating that our relatively simple event modeling is sufficient for this task. Seismic characteristics for each target horizons at Leg 208 drill sites were studied.

#### **Miocene *Bolivina* Acme event**

The Miocene *Bolivina* Acme event is a continuous reflector with strong amplitudes within the Neogene sediments. Depending on the thickness of the Neogene sequences, it is surrounded by sediments with lower amplitudes (Sites 1264 and 1265) or is part of a package with strong amplitudes (Sites 1262, 1266, and 1267).

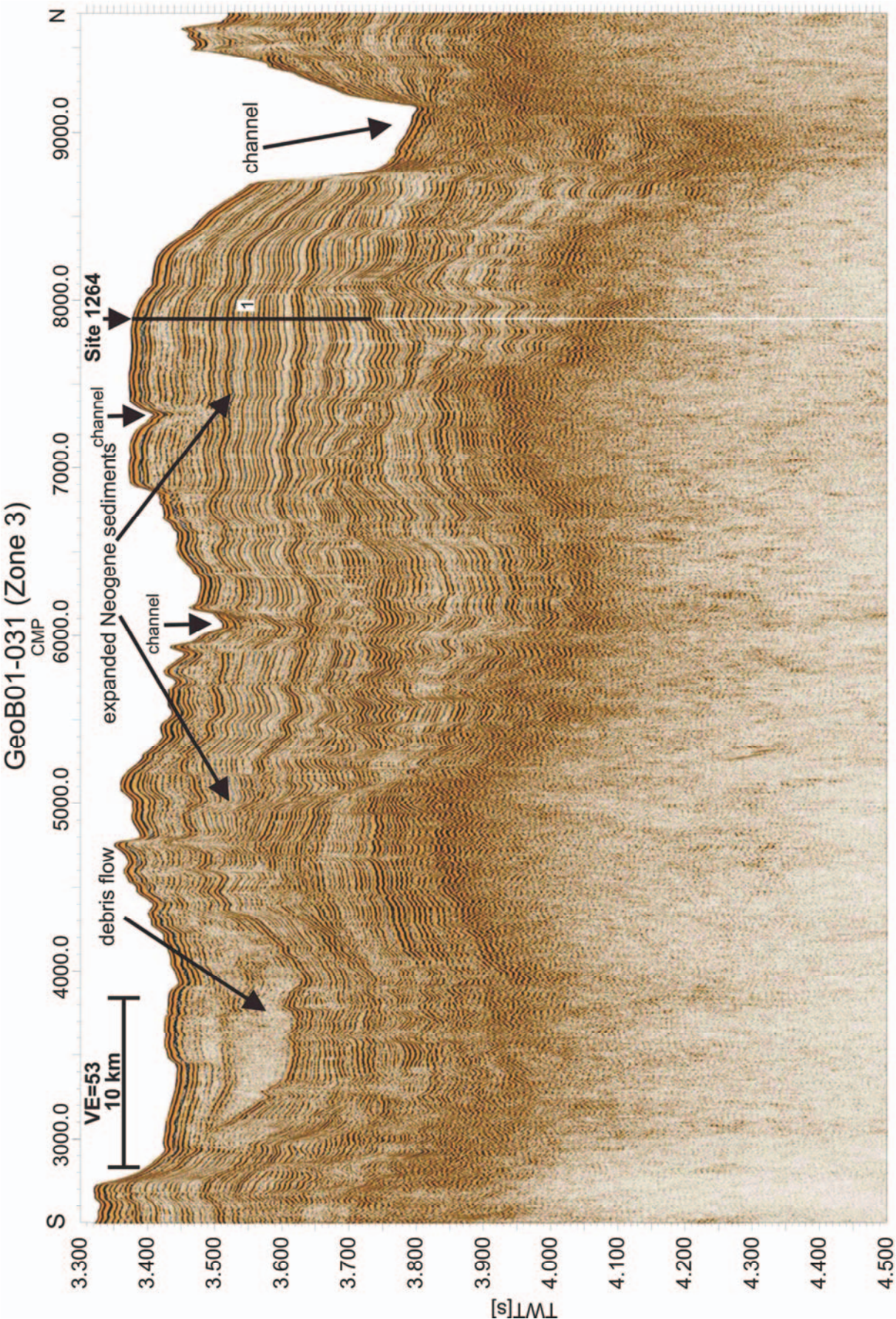


Figure 2.9: Seismic line Geob01-031 with Site 1264, (1) Miocene bolivina acme

**E/O boundary**

The E/O boundary in core samples is marked by a step increase in magnetic susceptibility (Zachos, Kroon, Blum, et al., 2004), which alludes to a change of the physical properties of the sediments. In seismic data the E/O boundary is represented by a sharp transition from a package of sediments imaged as reflectors with strong amplitudes to a package of sediments imaged with lower amplitudes at all sites except at Site 1266, where possibly synsedimentary slumping during the Oligocene disturbed the sedimentation pattern.

**ELMO horizon**

The ELMO horizon is represented as a strong continuous, mostly isolated reflector which is surrounded by sediments with lower amplitudes. The ELMO horizon, which is characterized by a 30- to 50-cm-thick layer with 10% higher density than the surrounding sediments, includes a drop in calcium carbonate content (Zachos, Kroon, Blum, et al., 2004). It has a strong impedance contrast resulting in a continuous reflector with high amplitudes.

**PETM**

The PETM is also characterized by low carbonate content and 10% higher density. Because of surrounding sediments with strong amplitudes, the 50- to 80-cm-thick clay layer (Zachos, Kroon, Blum, et al., 2004) cannot be resolved as an individual reflector with the GI gun data. Therefore, the PETM is not imaged as an individual reflector, but the sediments at the depth of the PETM are characterized by strong amplitudes at all sites except for Site 1264, which was not drilled to PETM depth.

**K/T Boundary**

The K/T boundary at Sites 1262 and 1267 occurs as the first reflector of a reflector package with strong amplitudes and a sharp transition immediately above basement. The basal contact of this clay layer is also sharply defined with an increase in magnetic susceptibility data.

**2.5.2 Sedimentary features on outer Walvis Ridge**

Most of the sediments at Walvis Ridge are characterized by undisturbed sediment sequences, but based on changing deposition conditions, varying basement structures, and/or influences of bottom water currents. Therefore it is possible to separate the study area into

three zones (Fig. 2.1). Zone 1 covers the north-western part of the study area, which is the beginning of Angola Basin. Basement is partly faulted as shown on profiles running parallel to the axis of the ridge which results in a rough basement topography (Fig. 2.4) with small basins filled with pelagic sediments. These sediments are generally undisturbed except some debris flow or slump structures in the younger sections. The shallow-dipping basement parallel to the flank of the ridge is mostly not faulted. Zone 1 is characterized by the smallest sediment thickness of ~150 to 200 m.

Zone 2 covers the flank of the ridge (Fig. 2.1). Sediment thickness increases toward the ridge axis. Basement is smoother compared to Zone 1, which probably indicates less tectonic activity. The sedimentation pattern is more disturbed than in the Zone 1, because of the flank's slope of  $0.7^\circ$  (Figs. 2.10, 2.11). A few channel structures at the flank of the ridge appear in a small part of Zone 2 (Figs. 2.1, 2.10, 2.11).

In Zone 3, sediment thickness reaches 450 m. Adjacent to some smaller channels with a width of 1–2 km (Fig. 2.9); there are larger channel structures with widths up to some tens of kilometers, indicating a large zone influenced by bottom water currents (Fig. 2.7). The thickness of Neogene sediments is significantly decreased in this area, while older sediment packages show a similar thickness as the surrounding areas. Hence, confined bottom currents occurred mainly in the Neogene. These changing deposition conditions offered the possibility to drill Sites 1263, 1264, and 1265 within a few kilometers with varying thickness of Neogene sediments (Figs. 2.7, 2.8, 2.9). No major faults were identified along the axis of the ridge, suggesting a mostly undisturbed sedimentary sequence.

## 2.6 Conclusions

The collected seismic data from Meteor expedition M49/1 are of high quality allowing excellent site selection for the drill-locations of Leg 208. Correlation of seismic data with borehole data was accomplished by calculating synthetic seismograms using GRA density measurements of the cores and an averaged velocity model. This method allowed “simple” event modeling to assign ages to the seismic reflectors and to identify key horizons/boundaries like the E/O and the K/T boundaries or the Miocene *Bolivina* Acme, ELMO, and PETM horizons. Characteristics of these target horizons show similar properties at the different sites, which is an indicating the regional distribution of each.



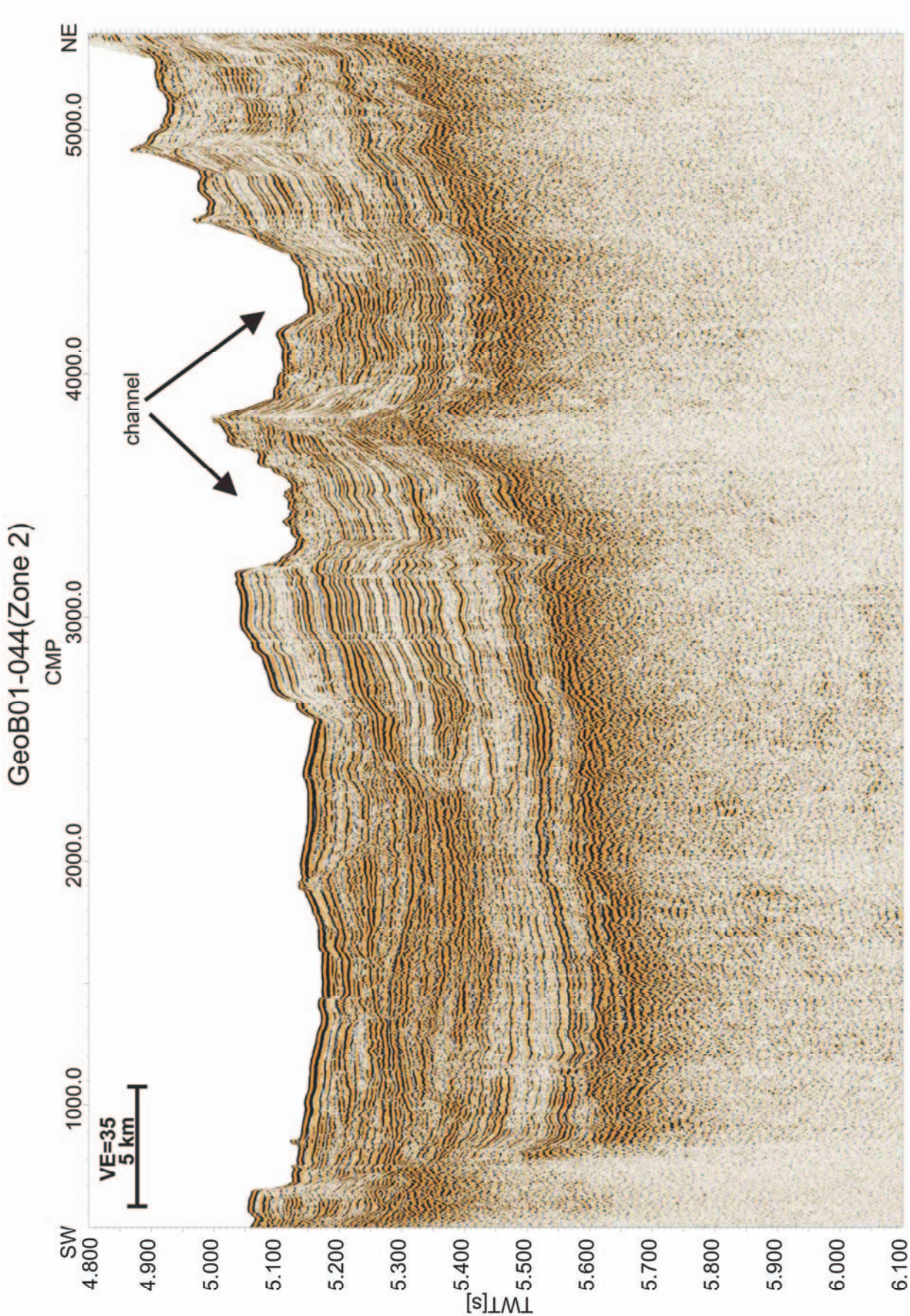
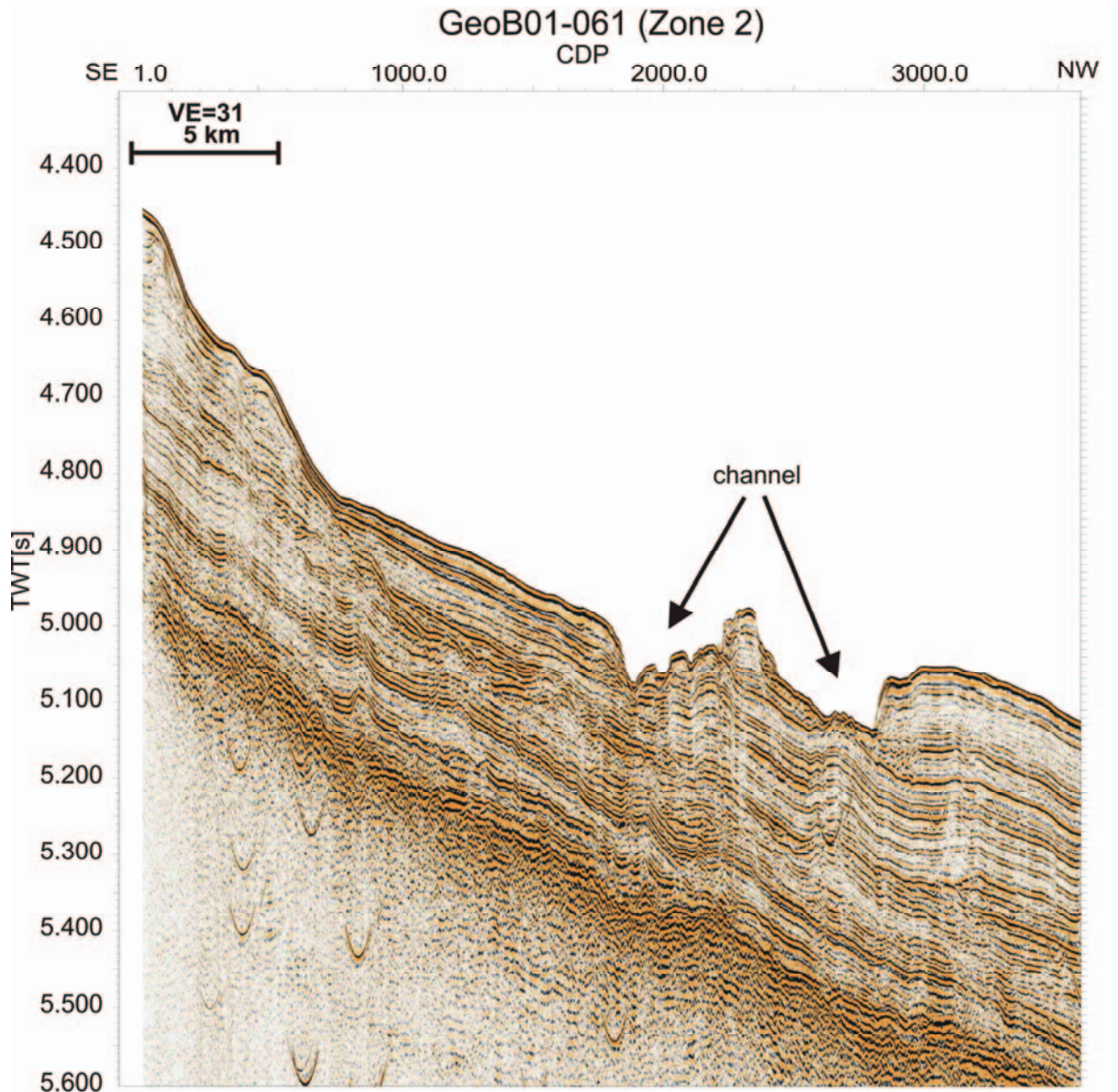


Figure 2.10: Seismic line GeoB01-044





**Figure 2.11:** Seismic line GeoB01-061

Sediment thickness of the study area increases from Angola Basin (~150 m) to the axis of Walvis Ridge (~450 m). Because of the changing deposition conditions the study area of Leg 208 is separated into three zones. Zone 1 is characterised by basement faulting which results in formation of a small basins at the beginning of Angola Basin. The basins are filled up with mostly undisturbed pelagic sediments, whereas the younger sediments in these basins partly constitute debris flow or slump deposits. Zone 2 on the flank of the ridge is characterized by an increasing sediment thickness and an area with several smaller channel structures indicating bottom water currents. Zone 3 at the axis of the ridge, shows the most varying sedimentation pattern. Among some expanded Neogene and Quaternary sections with the biggest sediment thickness of the study area, several erosive channels of variable width occur alluding to strong bottom current activities.

## 2.7 Acknowledgements

We are grateful for the support of the captain and the crew members as well as all cruise members of Meteor cruise M49/1 for their help during the expedition. We also want to thank the Scientific Shipboard Party of the ODP Leg 208, who did a great job, especially Jim Zachos for his comments and help during this study. This research used samples and/or data provided by the Ocean Drilling Program (ODP). ODP is funded by the U.S. National Science Foundation (NSF) and participating countries under management of Joint Oceanographic Institutions (JOI), Inc. This research was funded by Deutsche Forschungs Gemeinschaft, Grant Sp 296/24-1, "Sedimentation processes on Walvis Ridge - correlation of high resolution seismic records with ODP Leg 208 physical properties data".

## 2.8 References

- Adcock S., 1993, In search of a well tie: What if don't have a sonic log? *Leading edge*, 12: 1161-1164.
- Arhan M., Mercier H., Park Y.H., 2003. On the deep water circulation of the eastern South Atlantic Ocean, *Deep-Sea Research I* 50: 889-916.
- Badley M.E., 1985. *Practical seismic interpretation*. Ed. HDRC, Boston, 266 pp.
- Breitzke M., 1999. Physical properties of marine sediments. *Marine Geochemistry* edited by H.Schulz and M. Zabel, pp. 29-72, Springer-Verlag, New York.
- Hamilton E.L., 1976. Variations of density and porosity with depth in deep sea sediments. *Journal Sediment. Petrol.*, 46, 280-300.
- Kahio K., Arinobu T., Isishwatar R., Morgans H.E.G., Okada H., Takeda N., Tazaki K. Zhou G., Kajiwara Y., Matsumoto R., Hirai A., Niitsuma N., and Wada H., 1996. Latest Paleocene benthic foraminiferal extinction and environmental changes at Tawanui, New Zealand, *Paleoceanography*, 11:447-465.



Mendel J.M., Nahi N.E., Chan M., 1979. Synthetic seismograms using the state space approach, *Geophysics*, 44, 880-895.

Moore T.C. Jr., Rabinowitz P.D., Shipboard Scientific Party, 1984. Initial reports of the Deep Sea Drilling Project, Leg 74, U.S. Govt. Printing Office, 1-894.

Moscher D., Mayer L.A., Shipley T.H., Winterer E.L., Hagen R.A., Marsters J.C., Bassinot F., Wilkens R.H., Lyle M., 1993. Seismic stratigraphy of the Ontong Java Plateau. *Proc. Ocean Drill. Program Sci. Results*, 130, 33-49.

Rabinowitz P.D., Simpson E.S.W., 1984. Geophysical site survey results on the Walvis Ridge. In: Moore T.C. Jr., Rabinowitz P.D., et al., *Init. Repts. DSDP, 74*. Washington (U.S. Govt. Printing Office), 795-825.

Ricker N., 1953. The form and laws of propagation of seismic wavelets. *Geophysics*, 18, 10-40.

Rohr K.M.M., Gröschel-Becker H., 1994. Correlation of well logs, physical properties and surface seismic reflection data, Middle Valley, Juan de Fuca Ridge. *Proc. Ocean Drill. Program Initial Report*, 139, 585-596.

Smart C.W., Murray J.W., 1994. An early Miocene Atlantic-wide foraminiferal/ palaeoceanographic event, *Palaeogeography, Palaeoclimatology, Palaeoecology* 108: 139-148.

Weber M.E., Niessen F., Kuhn G., Wiedicke M., 1997. Calibration and application of marine sedimentary physical properties using a multi-sensor core logger. *Marine Geology*, 136, 151-172.

White R.E., Hu T., 1998. How accurate can a well tie be?, *Leading Edge*, 17, 1065-1071.

Zachos J.C., Kroon D. Blum P., et al., 2004. *Proceedings of the Ocean Drilling Program, Initial Reports Volume 208*, available on the web:

[http://www-odp.tamu.edu/publications/208\\_IR/VOLUME/CHAPTERS/IR208\\_01.PDF](http://www-odp.tamu.edu/publications/208_IR/VOLUME/CHAPTERS/IR208_01.PDF)

---

Zühlsdorff L., Spieß V., 2001. Modeling seismic reflection patterns from Ocean Drilling Program Leg 168 core density logs: Insight into lateral variations in physical properties and sediment input at the eastern flank of the Juan de Fuca Ridge. *J. Geophys. Res.* 106: 16119-16133.

### 3. Seismic imaging of thin clay layers deposited during extreme Cenozoic climatic events

Thomas Bartels\*, Sebastian Krastel, and Volkhard Spiess

#### 3.1 Abstract

Main objectives of Ocean Drilling Program (ODP) Leg 208 “the Walvis Transect” were to recover intact composite sequences of “critical” transitions like the Eocene/Oligocene (E/O) boundary, the Chron C24n ELMO event, or the Palaeocene/Eocene Thermal Maximum (PETM). The study area is located in the eastern South Atlantic at Walvis Ridge and characterized by complete undisturbed sediment sequences without terrigenous input, which are not affected by tectonics and local upwelling. R/V Meteor Cruise M49/1 in early 2001 was the main seismic pre-site survey for ODP Leg 208. A high-resolution multi-channel seismic system of the University of Bremen was used to select drill site positions that promise recovery of undisturbed, complete, and possibly expanded Cenozoic sequences. Then, a total of six sites were drilled at water depths between 2500 m and 4770 m on the northeastern flank of Walvis Ridge during Leg 208.

High resolution seismic data were recorded using a Generator Injector (GI) Gun and a Watergun in an alternating mode, covering a frequency spectrum of 200 Hz to 1600 Hz. The multi frequency approach was chosen to achieve best possible resolution at different depth levels of the sediment sections. The seismic response of the Watergun and the GI-Gun is dominated by changes of the acoustic impedance caused by density variations on different scales and thus emphasizes different sediment features. Whereas the resolution of GI-Gun data, with a wavelength of  $\sim 7.5$  m (200 Hz), is below the sub-meter scale of the “critical” climatic horizons layers (0.5-0.8 m), a Watergun with a shorter wavelength of  $\sim 3$  m ( $>400$  Hz) is required to resolve such thin layers in the seismic data.

A comparison of the seismic data with the magnetic properties of the borehole data of Leg 208 shows, that it is possible to image single horizons, representing “critical” climatic events as the PETM or the ELMO event. The thin clay layers at Walvis Ridge, with a thickness of 0.5 m to 0.8 m, are interbedded in homogenous sediments, which provide favourable conditions to image them in the seismic data. They occur as individual reflectors which do not suffer from signal interference of other closely spaced layers.

### 3.2 Introduction

The Paleogene represents a climatically dynamic period in Earth's history. Stable isotope and other temperature proxy records reveal a rather complex sequence of gradual and rapid warming and cooling, characterized by periods of both gradual and rapid change (Miller et al., 1987; Miller and Katz, 1987; Stott and Kenett, 1990; Zachos et al., 2001; Zachos et al., 1994). Extreme climatic events of the Paleogene include a) the PETM (Paleocene Eocene Thermal Maximum; 55 Ma), where isotope records suggest that at ~55 Ma the deep ocean and high-latitude surface waters warmed by 4°C and 8°C, respectively (e.g. Kaiho et al. 1996, Tripathi and Elderfield, 2005), b) the Chron C24n ELMO event (53.2 Ma), which has similar geochemical and biotic characteristics as the PETM but of smaller magnitude and represents a second global thermal maximum (Lourens et al., 2005), c) the Mid-Paleocene biotic event (~58.8 Ma) also called ELPE event (Ursula Röhl, University Bremen, pers. com.), which can be characterized by an increase in clay content and also represents a global climatic event (Zachos, Kroon, Blum et al., 2004), and d) the K/T boundary, where biostratigraphy reveals a well-established abrupt change in plankton assemblages (e.g. Luterbach and Premoli-Silvia, 1964; Thierstein, 1982; Monechi; 1985). Undisturbed sediment sequences of these periods were the primary stratigraphic targets of Leg 208, which was drilled in spring 2003 on the outer Walvis Ridge (Zachos, Kroon, Blum et al., 2004).

The northeast-southwest trending aseismic Walvis Ridge at 28°S effectively divides the eastern South Atlantic Ocean into two separate basins, the Angola Basin to the north and the Cape Basin to the south (Fig. 3.1). Here, paleoceanographic and paleoclimatic studies on longer time scales studies find favorable conditions due to the deposition of mostly undisturbed pelagic sediments of primarily carbonaceous origin and an absence of terrigenous input and local upwelling. This leads to low sedimentation rates of few cm per 1000 years, and Paleogene sediments are therefore found in relatively shallow depth below the sea floor of a few hundred meters (Zachos, Kroon, Blum et al., 2004), lacking an early diagenetic overprint and preserving high resolution paleoceanographic signals. The thickness of the full pelagic sediment cover down to basement varies from ~200 m on the deep (water depth >4.5 km) seafloor adjacent to the ridge to ~530 m near the summit (~2.5 km water depth).

R/V Meteor Cruise M 49/1 (Spiess et al., 2003) was the main pre-site survey cruise for Ocean Drilling Program (ODP) Leg 208. Generator Injector (GI) Gun (Sodera Inc.) data were acquired to search for appropriate drill sites to reach the main objectives of Leg 208, that are to recover complete and undisturbed sequences of these “critical” Cenozoic climatic events.

This turned out to be a successful enterprise (Zachos, Kroon, Blum et al., 2004). Most of these events are documented on Walvis Ridge as low-carbonate clay-rich layers with a thickness on a meter to sub-meter scale (0.5 m – 0.8 m) within carbonate-rich sequences (Zachos, Kroon, Blum et al., 2004).

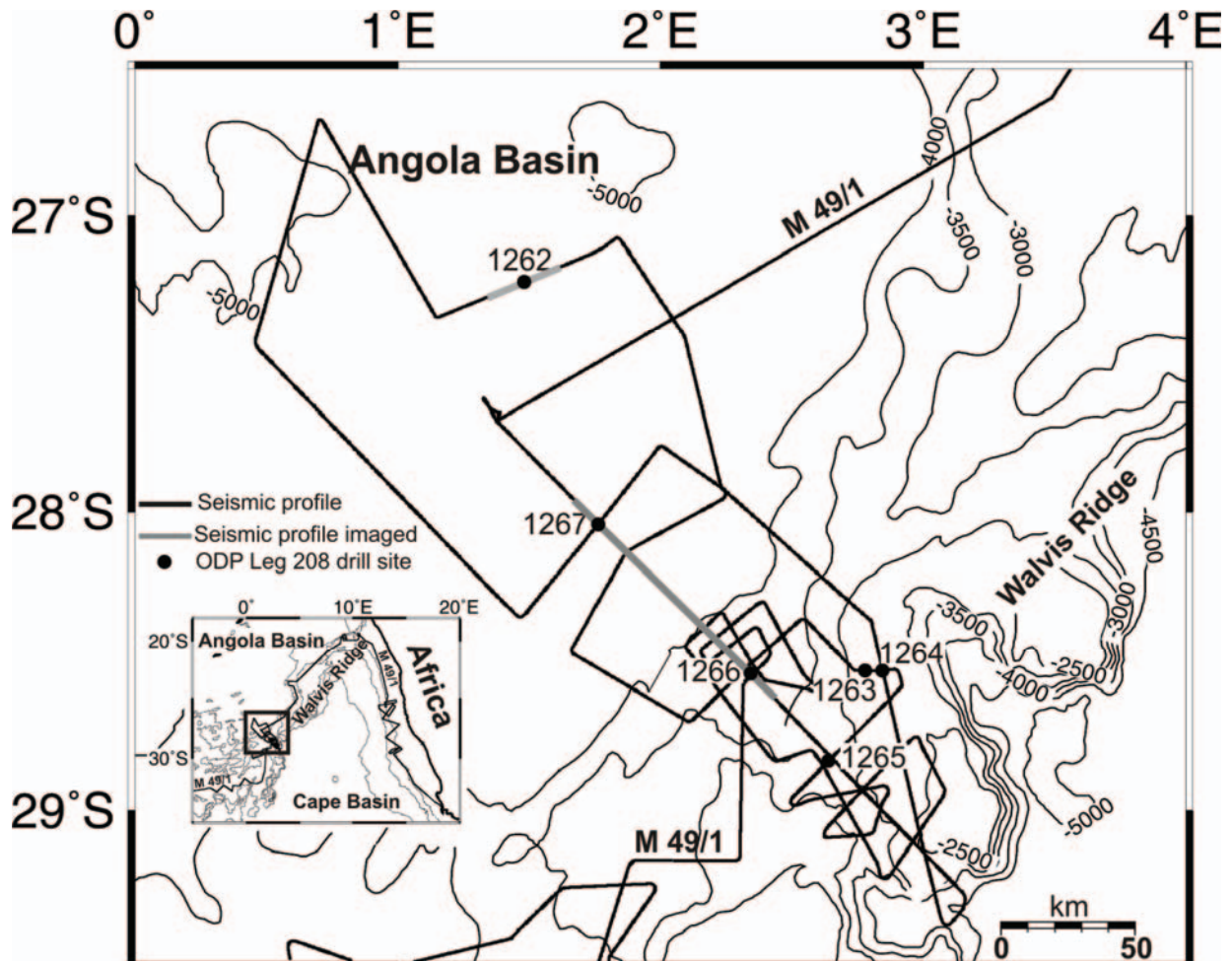


**Figure 3.1:** Overview study area ODP Leg 208 Walvis Ridge. Bathymetry is from GEBCO 2003 Digital Atlas, BODC, © National Environmental Research Council. Black lines: Seismic lines of R/V Meteor Cruise M49/1, gray lines: Seismic lines figured in this chapter, black dots: ODP Leg 208 Sites.

The seismic "measure" is a wavelength. In order for two nearby reflective interfaces to be distinguished well, they have to be about 1/4 wavelength in thickness. This is also the thickness where interpretation criteria change. For smaller thicknesses than 1/4 wavelength the amplitude is the only criteria to judge the layer thickness. For thicknesses larger than 1/4 wavelength the wave shape can be used to judge the bed thickness (Sheriff, 1991). Given a frequency spectrum of a GI-Gun between 100 Hz and 500 Hz with a main frequency of ~200 Hz and a wavelength of ~7.5 m, it is evident that sub-meter scale layers representing "critical" climatic events are difficult or not possible to identify in the seismic data.

Instead, according to a simple model using synthetic seismograms, frequencies around and above 400 Hz ( $\lambda = \sim 3$  m) will be required to unequivocally image these thin layers. Since an additional data set was recorded simultaneously with the GI-Gun, using a S-15 Watergun (Sodera Inc.) of 0.16 l with a frequency spectrum of 200 Hz to 1600 Hz, we analyzed this data set for the presence and seismic characteristics of the thin layers. The very high-frequency multichannel seismic reflection data generated by a Watergun allow detailed high-resolution studies of sedimentary structures of the order of one to few meters (Gutowski et al. 2002). However, a standard processing of such data will not be sufficient, since changes in the acquisition geometry due to wave action, which can be on the order of a wavelength, needed to be carefully corrected to reach a sufficient quality in stacking and in imaging of coherent reflectors (Gutowski et al. 2002). Otherwise, the consequence is a lack of coherency and a significant reduction in data quality.

To optimize the quality of the Watergun data, we developed a processing procedure to particularly improve static correction. A comparison of the GI-Gun data with the Watergun data illustrates clearly that the sedimentary structures appear different in the light of different frequencies which can be attributed to a general presence of signal interference from closely spaced layers. Processed Watergun data are less affected by interference and clearly reveal the presence and a spatial coherence of the relevant thin clay layers, which were then compared to the acquired borehole data of Leg 208.

### 3.3 Seismic Data

The multichannel seismic system of the University of Bremen is especially designed to collect seismic data with high lateral and vertical resolution. The alternating operation of a small chamber Watergun (0.16 l; 200 – 1600 Hz), a GI-Gun with reduced chamber volume (0.4 l; 100 – 500 Hz), and a GI-Gun with normal chamber volume (1.7 l; 100 Hz – 500 Hz) yields three seismic data sets, collected quasi-simultaneously. A 96-channel Syntron streamer of 600 m length, equipped with separately programmable hydrophone-groups, was used for recording. 48 channels, consisting of 13 hydrophones each, a group length of 6.25 m at a group distance of 12.5m, were used for recording the GI-Gun data, while 48 groups in between, consisting of 9 hydrophones and a group length of  $\sim 2$  m were used for the Watergun data. The shot interval was 9 sec, resulting in a shot distance of  $\sim 25$  m when sailing with an average speed of 6 knots. Ten cable levellers (birds) kept the streamer at a constant water depth of 3 m within a range of 1 m. A magnetic compass at each bird allowed determining the positions of the hydrophone groups relative to the ship's course. GI-Gun data were digitally

recorded at a sampling frequency of 4 kHz over a record length of 3000 ms. The sampling frequency of the Watergun was 8 kHz, record length was 1500 ms. Positioning was based on GPS (Global Positioning System). For processing of GI-Gun data, a combination of 'in house' and the commercial 'Vista' software (Seismic Image Software Ltd.) was used. Standard seismic processing procedures employed included trace editing, setting up geometry, static and delay corrections, velocity analysis, normal move-out (NMO) corrections, bandpass frequency filtering, stack and time-migration. A common midpoint (CMP) distance of 10 m was chosen for the processing.

The recorded Watergun data have to be specifically corrected for statics, because vertical variations of source and receiver depth during acquisition are of the order of the seismic wavelength. Standard static correction and stacking procedures, using the depth information from the birds, are not sufficient, since the residual unknown component of vertical streamer movement is of the same order as the dominating wavelength of the source signal. In order to improve the quality of the very high resolution seismic data, static correction has to be optimized. This procedure consists of two steps: (1) First arrivals of NMO-corrected Common Mid Point gather (CMP-gather) are automatically picked and leveled to the same arbitrary time level. Due to the short wavelength the automatic picker needs to be very accurate. To get optimum picking results, negative values of the traces are deleted and the resulting trace is squared. The modified traces are used as input for our custom-picking algorithm, which uses a moving window of a length of a few ms whose values are summed to identify the maximum peak of each trace. Finally, the NMO-corrected and leveled gathers are stacked. (2) To superimpose the morphology (which is lost during leveling), the first arrivals of the stacked GI-Gun profiles are picked manually or automatically and used as delay corrections. The GI-Gun wavelets are suitable for this task, because of their high quality, continuity and their low noise for picking the first arrivals. The disadvantage of this approach is that small scale bathymetric variations may be lost which could be resolved in Watergun data but not in GI-Gun data due to the smaller Fresnel zone. The quality of the stack on steep slopes may be limited, and the described process cannot be successfully applied at all if the first arrivals are dominated by diffraction hyperbolas. However, if water depth variations along the seismic line are sufficiently smooth, this procedure should lead to a significant increase in quality of Watergun CMP stacks.

To illustrate the different seismic reflection patterns observed in CMP stacked and time migrated GI-Gun and Watergun data, Figure 3.2 compares both data sets on the flank of Walvis Ridge. Watergun data resolve many more details of the sediment section than GI-Gun



data. Some higher amplitude horizons, which could be considered to be key horizons for interpretation in GI-Gun data, are also recognized in Watergun data, but Watergun data indicate some additional distinct horizons (e.g. at 3.59 s TWT (Two Way Traveltime)) which are not resolved in the GI-Gun data. Though depth penetration of Watergun data is limited compared to GI-Gun data, but it is still sufficient for the Paleogene objectives.

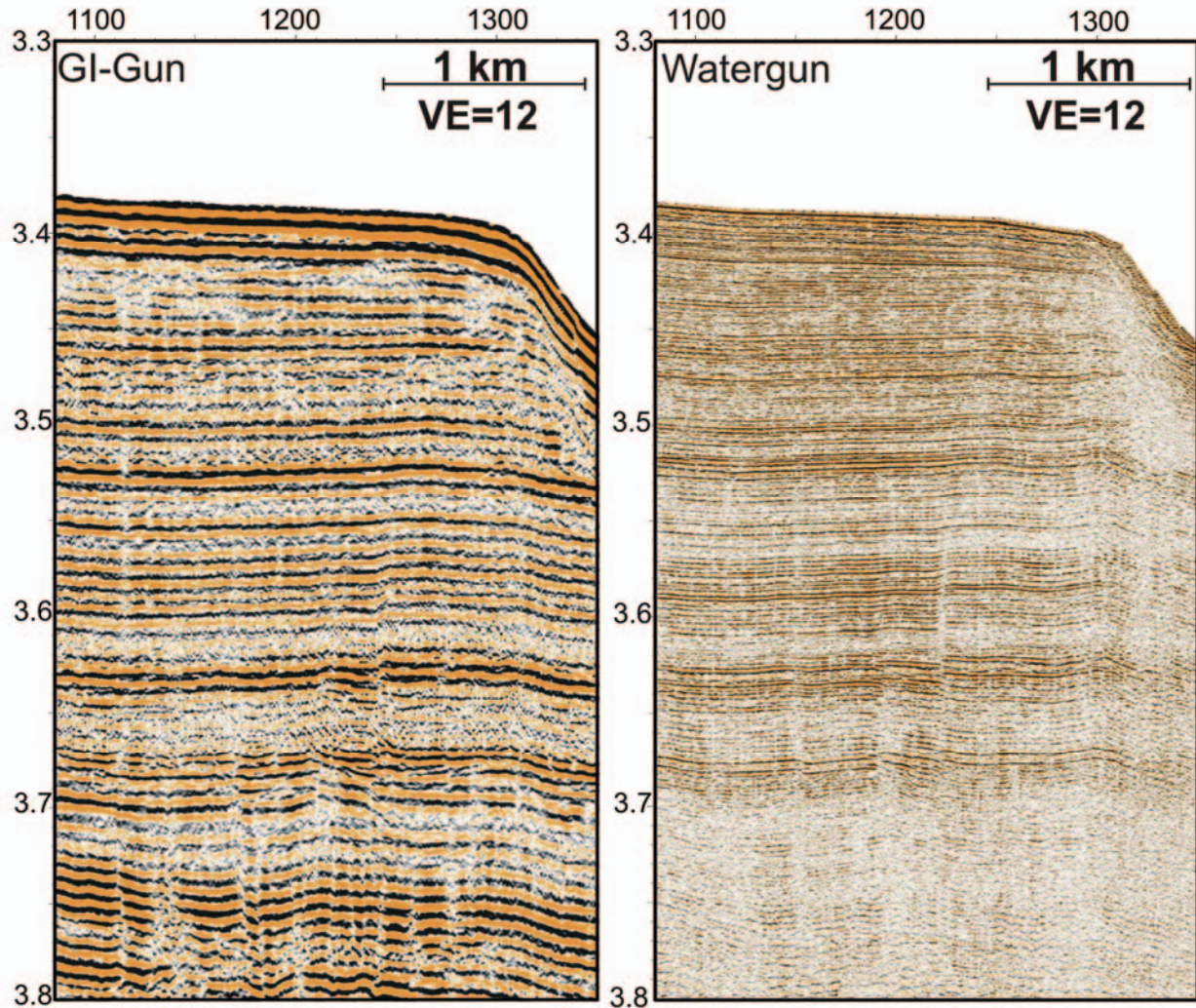


**Figure 3.2:** Comparison of GI-Gun (left, 1.7 l, 100 – 500 Hz) and Watergun (right, 0.16 l, 200 – 1600 Hz) data. The data show a profile from the flank of Walvis Ridge, both images are plotted at the same scale.

### 3.4 Borehole Data

Interpretation of seismic sections with respect to individual horizons, which are indicative for extreme climatic events, requires a comparison with borehole data. In this study, the magnetic susceptibility logs from ODP Sites 1262, 1266 and 1267 (Zachos, Kroon, Blum et al., 2004) were used instead of density and velocity measurements of the cores, which suffered too much by voids, cracks, or gas bubbles or which were not recorded at the same sample frequency along the whole core sections of the sites.

The three sites reached Paleogene sediments including “critical” transitions as the E/O boundary, the ELMO event, the PETM and the ELPE event. Sites 1262 and 1267, which were the deepest of the depth transect of Leg 208, even reached Maastrichtian sediments, hence both sites included the K/T boundary. The Lower Eocene and Upper Paleocene sediments at Walvis Ridge lie within the longest, most stratigraphically continuous and astronomically tuned sequence of marine sediments of the deep sea (Röhl et al., 2007). The three Sites 1262, 1266 and 1267 contain sharp transitions between carbonate-rich and clay-dominated facies, which are an expression of the deepening of the Carbonate Compensation Depth (CCD) and related changes in ocean carbon chemistry and/or circulation. The carbonate-rich facies includes the Pleistocene, Pliocene, Lower Oligocene, Paleocene and Lower-Middle Eocene intervals. The clay rich facies includes the Miocene and the Middle to Upper Eocene as well as separate layers as the ELMO event, the PETM, the ELPE event or the K/T boundary. The E/O boundary can be characterized by a transition from clay-rich (Eocene) to carbonate-rich (Oligocene).

The thickness of the individual clay layers, the ELMO event the PETM and the ELPE event, varies from 0.3 m to 0.8 m. Smaller variations of the thickness of each layer occur because of spatially varying sedimentation rates. The PETM and the ELMO event can be characterized by decreasing carbonate content ( $\text{CaCO}_3$ ) down to 0 wt%. Both clay layers are characterized by sharp basal color contact and an increase in the magnetic susceptibility because of a higher ferrous content in the sediment (Zachos, Kroon, Blum et al., 2004, Lourens et al., 2005). The ELPE event has a thickness of >0.8 m and can be characterized by decreasing clay content and an increasing magnetic susceptibility. It occurs as a prominent 0.3 m thick dark brown clay-rich layer which shows a pronounced peak in magnetic properties (Zachos, Kroon, Blum et al., 2004).

For a comparison of the magnetic susceptibility with the seismic data to identify lithological changes, depth values are transformed from a meter below seafloor (mbsf) scale to a TWT scale. For the transformation the velocity measurements of Leg 208 on sediment cores were used. Additionally, erroneous values or data gaps are automatically edited to generate continuous data sets for each site. Before comparison, the susceptibility measurements were normalized to the highest peak of each data set.

### **3.5 Modelling**

The use of high-frequency sources allows imaging of thin layers on different scales. The main frequency of the Watergun provides a wavelength of ~3 m, which is still large

compared to a layer thickness of 0.5 – 0.8 m. But a 0.5 m thick layer with a density difference in the range of 6-12 %, typical for the PETM (Zachos, Kroon, Blum et al., 2004), should definitely cause a distinct reflection from a 3 m long wavelet. Possibly with a resolution of  $\sim 1/4$  wavelength (Sheriff, 2001), it is should be suitable to resolve the upper and lower boundaries of the “critical” climatic events. To confirm this theoretical conclusion, we calculated simple synthetic seismograms.

The reflection coefficient between two media of densities  $\rho_1$  and  $\rho_2$  and velocities  $v_1$  and  $v_2$  is given for vertical incidence of plane waves by  $R = (\rho_1 v_1) - (\rho_2 v_2) / (\rho_1 v_1) + (\rho_2 v_2)$ . A careful analysis of the velocity and the GRA density measurements on sediment cores of Leg 208 at an interval of high quality of both data sets shows, that the density data are positively correlated with velocity data (Fig. 3.3 and Bartels et al., 2007). Since the two parameters are not independent we used a constant velocity model of 1500 m/s for the calculation, because the density values vary on a higher scale. A constant increase of the velocity with depth, which occurs in the sediments in situ, is neglectable because it does not influence on the amplitude of the reflection coefficients.

An analysis of the GRA density variations of core measurements of Leg 208 shows that the density variations vary strongly with depth. While the standard deviation of the density values of the Oligocene sediments (0-100 mbsf) of the deeper Sites of Leg 208 (1262, 1266 and 1267) average to  $\sim 100 \text{ kg/m}^3$ , the standard deviation of the Eocene and Paleocene sediments (200 – 300 mbsf) ranges between  $30 \text{ kg/m}^3$  and  $40 \text{ kg/m}^3$  (Fig.3.4). Therefore, we calculated two models with random distributions of density values for both types of sediments of Walvis Ridge. Upon this we added to both data sets a layer with a thickness of 0.8 m and 10% density to simulate a “critical” climatic event. The resulting series represents a synthetic impedance curve with a spike for the clay layer, which is then convolved with synthetic wavelets, varying in frequency from 200 Hz to 800 Hz to correspond to the main frequencies of GI-Gun and Watergun data.

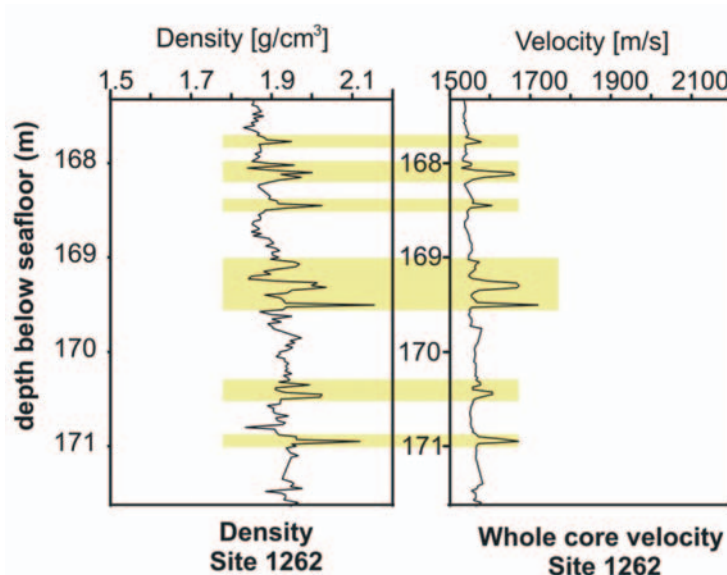


**Figure 3.3:** Correlation of GRA density measurements and velocity measurements of Site 1262 at a depth where both data are characterized by a high quality and a high resolution.

The results of the model (Fig 3.5) show that imaging and identifying of a “critical” horizon is much easier in sediments with a smaller standard deviation. Whereas the added horizon in the synthetic seismograms with a standard deviation of  $100 \text{ kg/m}^3$  is masked by surrounding reflections, the added horizon in the synthetic seismogram with a deviation of  $30 \text{ kg/m}^3$  is easily to identify. Hence, the Eocene/Paleocene sediments at Walvis Ridge, which are target of our observations, are suitable to image the “critical” climatic horizons.

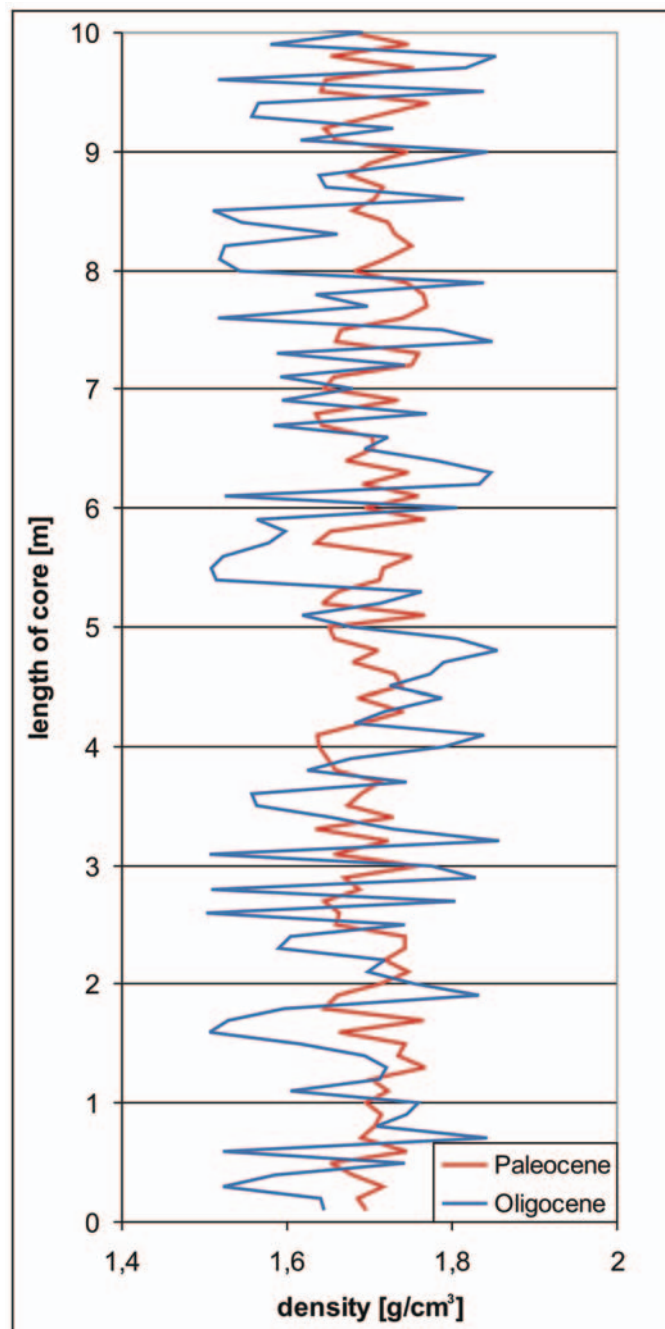


**Figure 3.4:** Correlation of GRA density measurements of Site 1262. Blue: Density values of Oligocene sediments with a standard deviation of  $100 \text{ kg/m}^3$ , Red: Density values of Paleocene sediments with a standard deviation of  $30 \text{ kg/m}^3$ .

The seismic response of a sedimentary sequence depends on the shape and the bandwidth of the source wavelet as well as on the nature and spacing of impedance contrasts. Thus, a comparison of seismic signatures for different source frequency ranges provides additional information about the nature of individual key reflectors and the way they are imaged by different types of seismic data. A comparison of the lower frequency traces (e.g. 200 Hz) in Figure 3.5 with the higher frequencies (400 – 800 Hz) traces illustrates clearly that the “sedimentary” structures of the random distribution appear in a different light, which can be attributed to signal interference from the closely spaced reflection coefficients. For higher frequencies layer imaging is less affected by interference, wherefore individual layers can be more likely identified.

This simple theoretical experiment illustrates that it should be possible to image a 0.5 m thick layer with a density contrast of about 10 % in the high resolution Watergun data which has a frequency spectrum between 200 – 1600 Hz. Also this model consideration is still a theoretical one without noise, the special setting of the Paleocene/Eocene sediments of Walvis Ridge with the availability of high quality core data including thin clay layers allows to prove this hypothesis.

### 3.6 Results

Figure 3.6 shows a comparison between GI-Gun data (1.7 l; spectrum 100 –500 Hz) and Watergun data (spectrum 200 - 1600 Hz) which are plotted at the same scale. In principal we observe the same features in the vicinity of Site 1262, e.g. the parallel to sub-parallel layering of undisturbed pelagic sediments, a transparent, irregularly shaped body representing a debris flow or slump deposit within the uppermost 100 ms and a sharp boundary which occurs at a depth of 6.45 s TWT at the location of the drill site. A closer view shows differences between these two data sets in terms of seismic facies. Especially for the sediment sequences beneath the boundary at 6.45 ms in the Watergun data four separated reflectors or reflector packages of sediments with higher amplitudes occur, which are not resolved as separated packages in the GI-Gun (compare arrows in Fig 3.6). In contrast, an interpretation of GI-Gun data would rather suggest gradual transitions of physical properties changes between the PETM and the ELPE event. The sharp interfaces possibly caused by thin layers like the PETM or the ELPE event, which have a density contrast of 10% are not resolved.



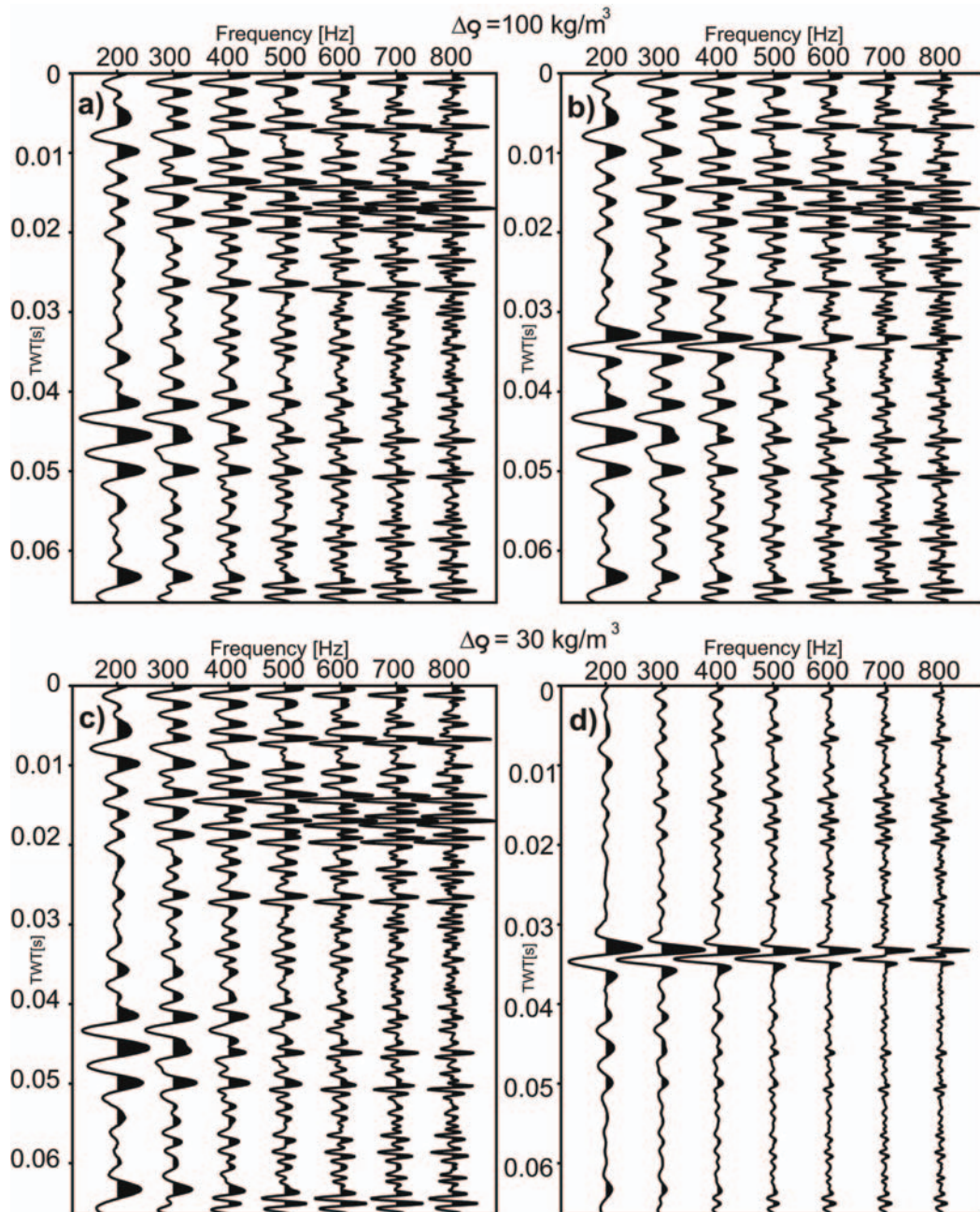


**Figure 3.5:** Synthetic seismograms with random distribution of density values and frequencies from 200 Hz - 800 Hz.

**3.5a)** Random distribution of density values with standard deviation of  $100 \text{ kg/m}^3$ , typical for Oligocene sediments at Walvis Ridge.

**3.5b)** Same density distribution as in a), but with synthetic clay layer with 10 % higher density and 0.8 m thickness between 0.03 s and 0.04 s.

**3.5c)** Random distribution of density values with standard deviation of  $30 \text{ kg/m}^3$ , typical for Eocene and Paleocene sediments at Walvis Ridge.

**3.5d)** Same density distribution as in c) but with synthetic clay layer with 10 % higher density and 0.8 m thickness between 0.03 s and 0.04 s.

An increase of the clay content of the sediment is reflected by a peak in the magnetic susceptibility data (e.g. Zachos, Kroon, Blum et al. 2004). Therefore the magnetic susceptibility data can be used to check whether the individual reflectors correspond to clay layers in the sediments. As an example, Figure 3.7 shows a part of the core measurements of the magnetic susceptibility measurements of Sites 1262 and 1267 vs. age with marked “critical” climatic events. The identification of the “critical” events in the sedimentary sequence is based on the preliminary results, developed during Leg 208 by the Shipboard Scientific Party (Zachos, Kroon, Blum et al., 2004). A comparison of this magnetic susceptibility data with the seismic data is used to identify seismic reflectors that are associated with key layers characterized by low or no carbonate content.

Figure 3.8 shows the comparison of magnetic susceptibility data with Watergun data for Sites 1262, 1266 and 1267. All data sets are plotted on a TWT scale. The fit of pronounced variations in the magnetic data with variations in the seismic reflection pattern is very good.

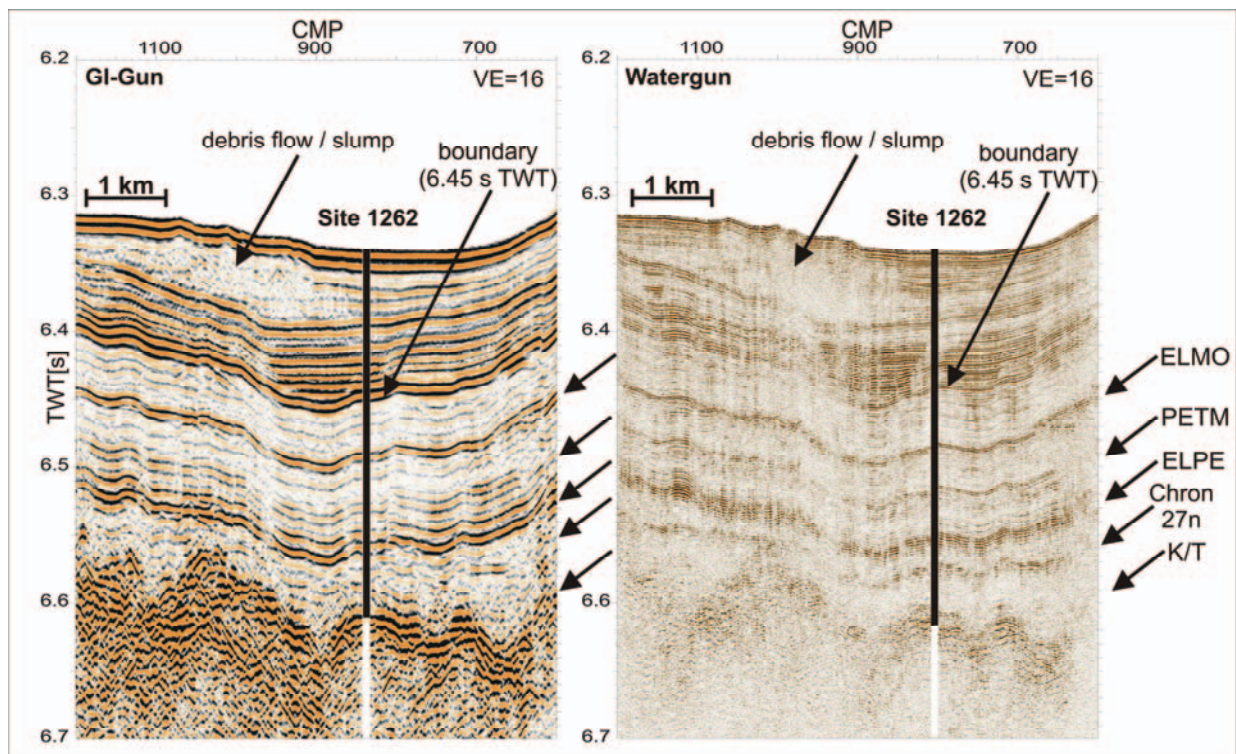


**Figure 3.6:** Seismic Data of the drill location of ODP Site 1262 Leg 208. Left: GI-Gun data, right: Watergun data. Both data sets are plotted at the same scale. Arrows indicate key layers: ELMO event, PETM, ELPE event, K/T boundary.



Site 1262 (Fig. 3.8a), situated at the edge of the Angola Basin, is the deepest site of Leg 208 with a water depth of 4755 m. It is characterized by the lowest sediment thickness of ~250 m, i.e. allowing drilling Paleogene sediments in shallow depths. As the first key layer the E/O boundary occurs as a sharp transition from carbonate rich Oligocene sediments to the clay rich Upper Eocene sediments at 6.45 s TWT. Whereas the Oligocene sediments with their larger density variations are characterized by high amplitudes, the Paleocene sediments occur as homogenous sections with few reflections. The beneath the E/O boundary following key layers are the ELMO event and the PETM. These clay layers occur as strong individual seismic reflectors in-between the homogenous carbonate-rich Paleogene sections. Both peaks of the magnetic data correlate well with seismic reflectors. As predicted using the model calculation, the Watergun with its wavelength of ~3 m is able to resolve the prominent clay layers ranging on a sub-meter scale as individual seismic reflectors. Beneath the PETM the ELPE event occurs as the first reflector of a package of three to four reflectors with higher amplitudes at a depth of ~6.55 s TWT. Different to the ELMO event and the PETM, it is not possible to resolve this event as an individual reflector in the Watergun data. Instead, the seismic response is more affected by interference effects from surrounding closely spaced layers, caused by more changing density and velocity values.

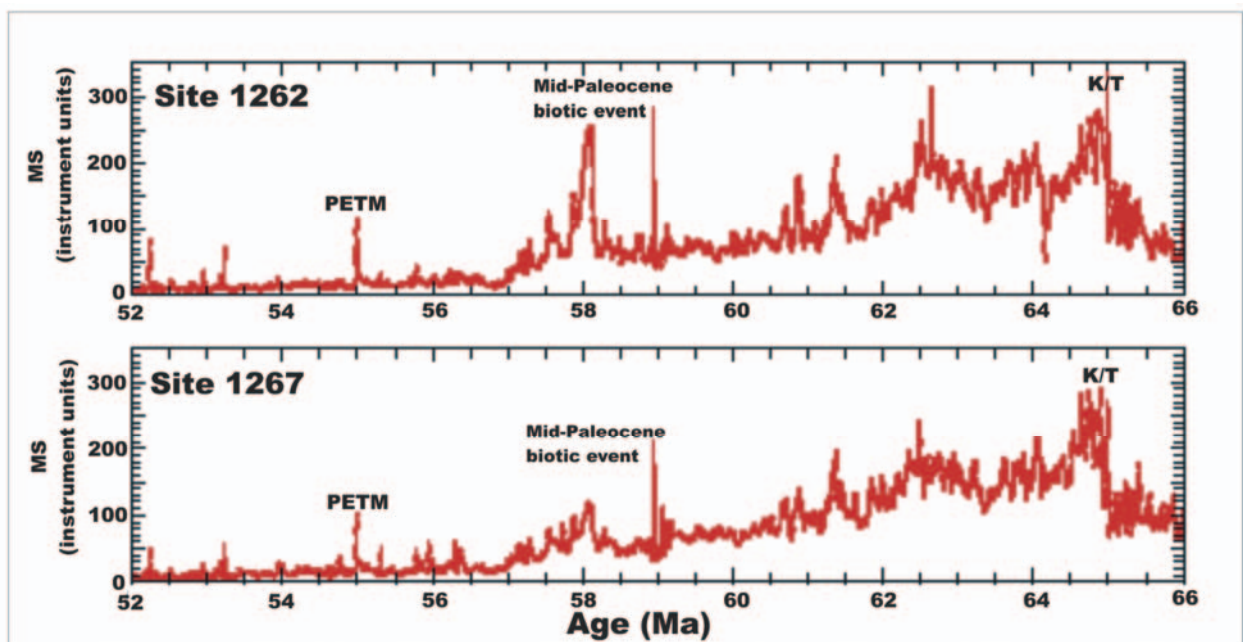


**Figure 3.7:** Magnetic susceptibility vs. age for 52 to 66 Ma time interval of Sites 1262 and 1267. Image and assignment of “critical” climatic events (PETM, Mid-Paleocene biotic event (ELPE event) and K/T boundary) after Zachos, Kroon, Blum et al. 2004.

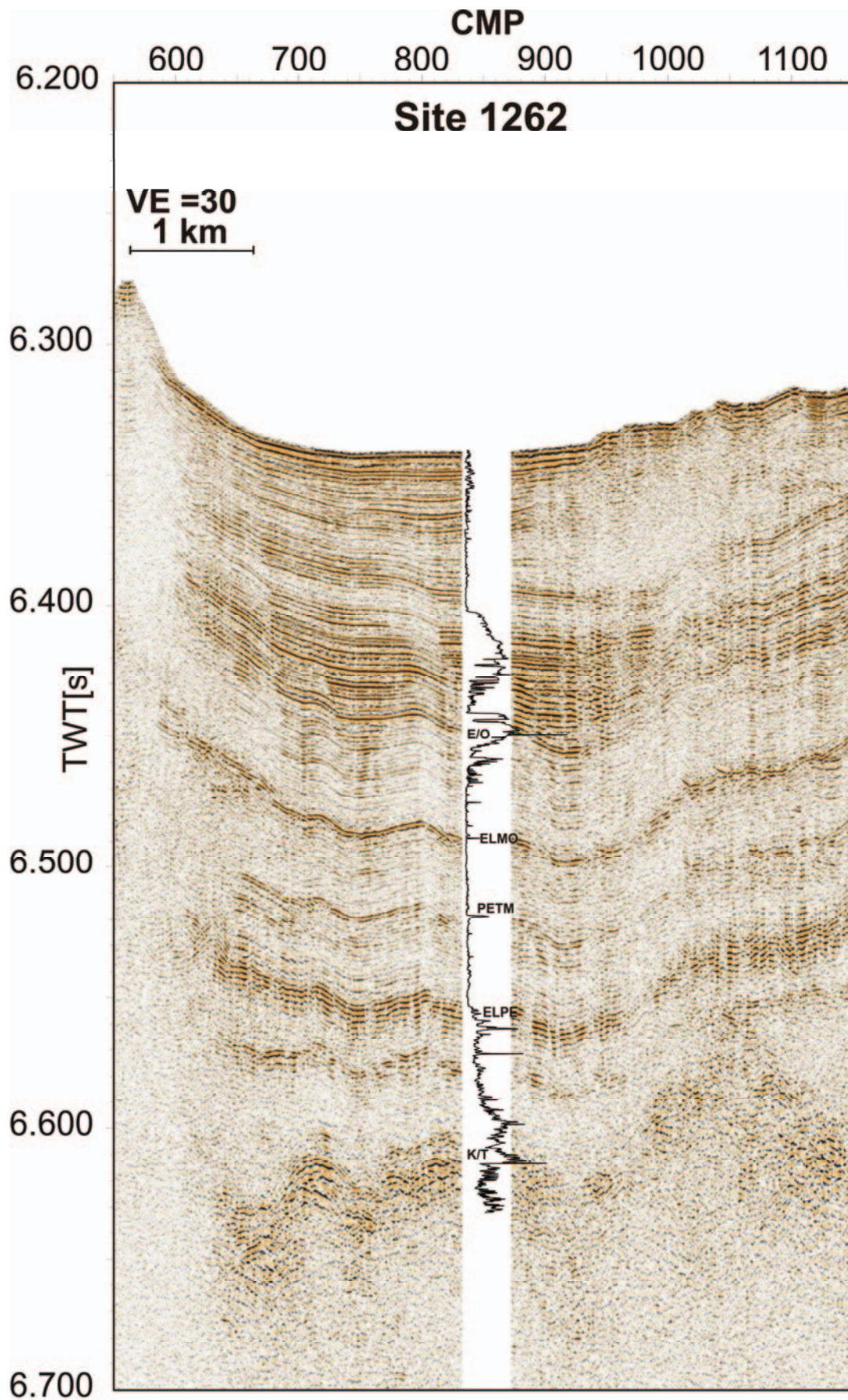


**Figure 3.8a:** Watergun data of ODP Sites 1262 compared with magnetic susceptibility measurements. Key layers: E/O Boundary, ELMO event, PETM, ELPE event and K/T boundary are marked in the data.



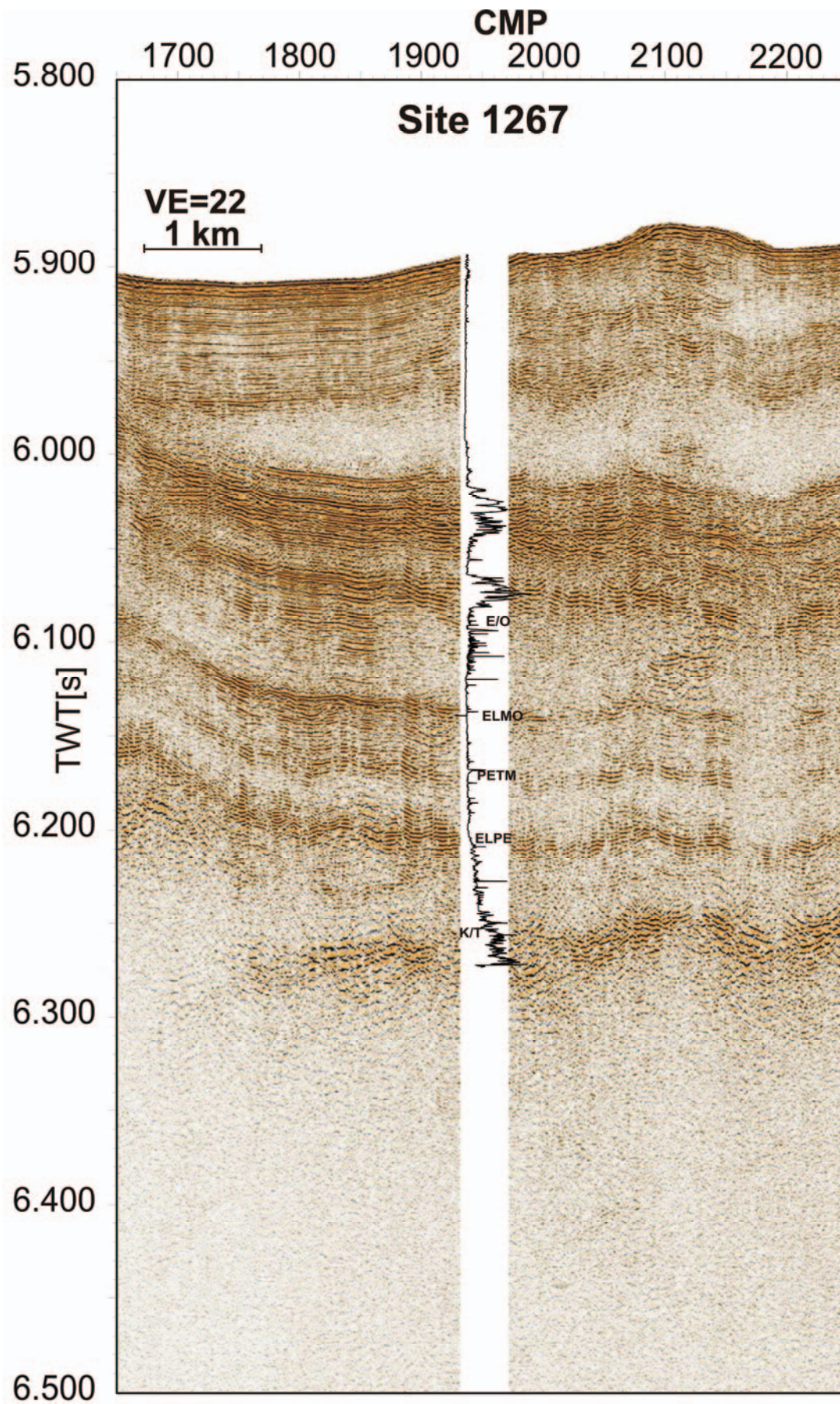


**Figure 3.8b:** Watergun data of ODP Sites 1267 compared with magnetic susceptibility measurements. Key layers: E/O Boundary, ELMO event, PETM, ELPE event and K/T boundary are marked in the data.



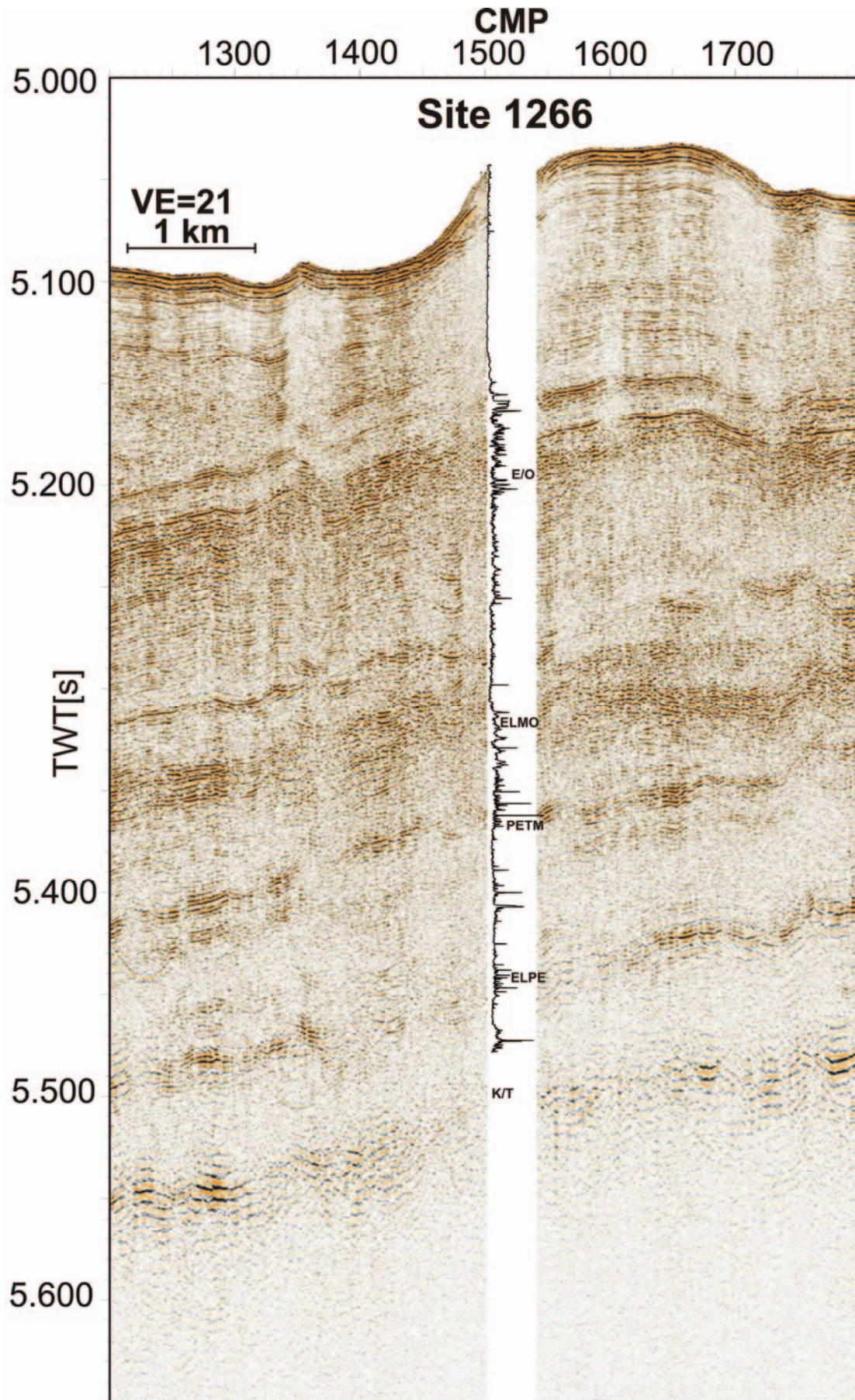


**Figure 3.8c:** Watergun data of ODP Sites 1266 compared with magnetic susceptibility measurements. Key layers: E/O Boundary, ELMO event, PETM, ELPE event and K/T boundary are marked in the data.

At ~6.58 s TWT at the location of the site another separated reflector package with higher amplitudes is resolved. At this depth the Scientific Shipboard Party of Leg 208 identified another clay horizon in the Chron 27n, which potentially represents a global climatic event with a smaller magnitude than the ELMO event or the PETM. Until now, the data are not evaluated, yet (Ursula Röhl, University Bremen, pers. com.). As the deepest key layer resolved in the seismic data, the K/T boundary occurs as a transition from lower to higher amplitudes at ~6.62 s TWT. Again the peak in the magnetic data correlates well with the seismic data. Because of its small distance to the rough crystalline basement and a decreasing penetration of the high frequency signal of the Watergun, the boundary is not resolved as a continuous reflector, although its spacial distribution can be obviously identified in the figure.

Site 1267 (Fig. 3.8b) at a water depth of 4355 m is situated at the flank of Walvis Ridge. It can be characterized by a sediment thickness up to ~350 m. Beyond the carbonate-rich Oligocene sediments at depth of 5.98 s to 6.00 s TWT, a disturbed package of low-amplitude reflections can be observed. Beneath this package, the data reveal almost parallel undisturbed sequences of the pelagic sediments typical for the study area, although the sedimentation pattern at the flank of the ridge is more disturbed than in the basin (Bartels et al., Chapter 2, 2007). The comparison of the magnetic data with the seismic data at Site 1267 fits sufficiently with the seismic reflections just as at Site 1262 and shows almost the same results: High amplitudes reflections in the Oligocene sediments and low amplitude reflection in the Paleocene sediments, although the E/O transition from clay rich to carbonate rich sediments is not as sharp pronounced as in the seismic data at Site 1262. The key layers (ELMO event, PETM, ELPE event) in-between the carbonate-rich homogenous Paleogene sediments occur as separated layers. Different to Site 1262 the ELMO event and the PETM occur, same as the ELPE event, as a part of a smaller reflector packages consisting of two to three reflectors. The occurrence of an additionally reflector between the ELPE event and the K/T boundary, as observed at Site 1262 is not evident here.

Site 1266 (Fig. 3.8c), in a water depth of 3798 m, is situated at the flank of the ridge close to the ridge axis. The sediments, which are mostly undisturbed, have a thickness of ~370 m, which is slightly more than at Site 1267. In the Neogene part of the sediments, the varying thickness causes an undulating topography of the seafloor. Same as at Sites 1262 and 1267 the E/O boundary occurs as a transition from high amplitudes (Oligocene) to low amplitudes (Eocene) at a depth of ~5.33 s. Similar to Site 1267 the transition is not as sharp pronounced in the seismic data as in the basin at Site 1262. Beneath the E/O boundary, the

ELMO event, the PETM and the ELPE event are imaged as a part of smaller reflector packages consisting of two to four reflectors. Same as at Sites 1262 and 1267, the in-between the key layers accumulated carbonate-rich Paleogene sediments occur as homogenous sections with low amplitudes. The K/T boundary was not drilled at this site but can be expected in the seismic data at a depth of  $\sim 5.51$  s as the deepest transition from lower amplitudes to higher amplitudes.

Figure 3.9 shows a part of Watergun Profile GeoB01-030 of Meteor Cruise M49/1. The profile, which runs in NW-SW direction, is situated at the flank of Walvis Ridge. The thickness of the surface sediments increases in southeastern direction, wherefore the total sediment thickness varies between  $\sim 340$  m in the NW to  $\sim 370$  m in the SE. As the first key layer, we correlated the E/O boundary between the two drill sites. The correlation shows, that the seismic attributes of the Oligocene sediments change along the profile. While in the northwestern part at Site 1267, the boundary occurs as a distinct transition from high amplitude Oligocene sediments to low amplitude Eocene sediments, which is typical for the sediments at the beginning of Angola Basin (compare Fig. 3.6 and 3.8), in southeastern part the characteristics of the Oligocene sediments change significantly. Instead of an undisturbed package of high amplitude reflectors, the Oligocene sediments are intermitted by a sediment section characterized by low amplitudes, although the E/O boundary as the last reflector of the package is characterized by strong amplitudes along the whole profile. The next resolved key layers are the ELMO event and the ELPE event, which occur as continuous reflector packages of two to three reflectors with high amplitudes interbedded in the homogenous Paleogene sections. Both events are imaged as distinct boundaries which can be easily correlated between the drill-sites. The responses of the PETM, which are expected to be resolved between the ELMO event and the ELPE event, are too weak for an explicit identification, although, especially in the vicinity of Site 1267, another continuous reflector between the ELMO event and the ELPE event can be suspected. As the last reflector, the K/T boundary occurs close to the crystalline basement. It is characterized by high amplitudes and can be easily correlated between the drill sites.



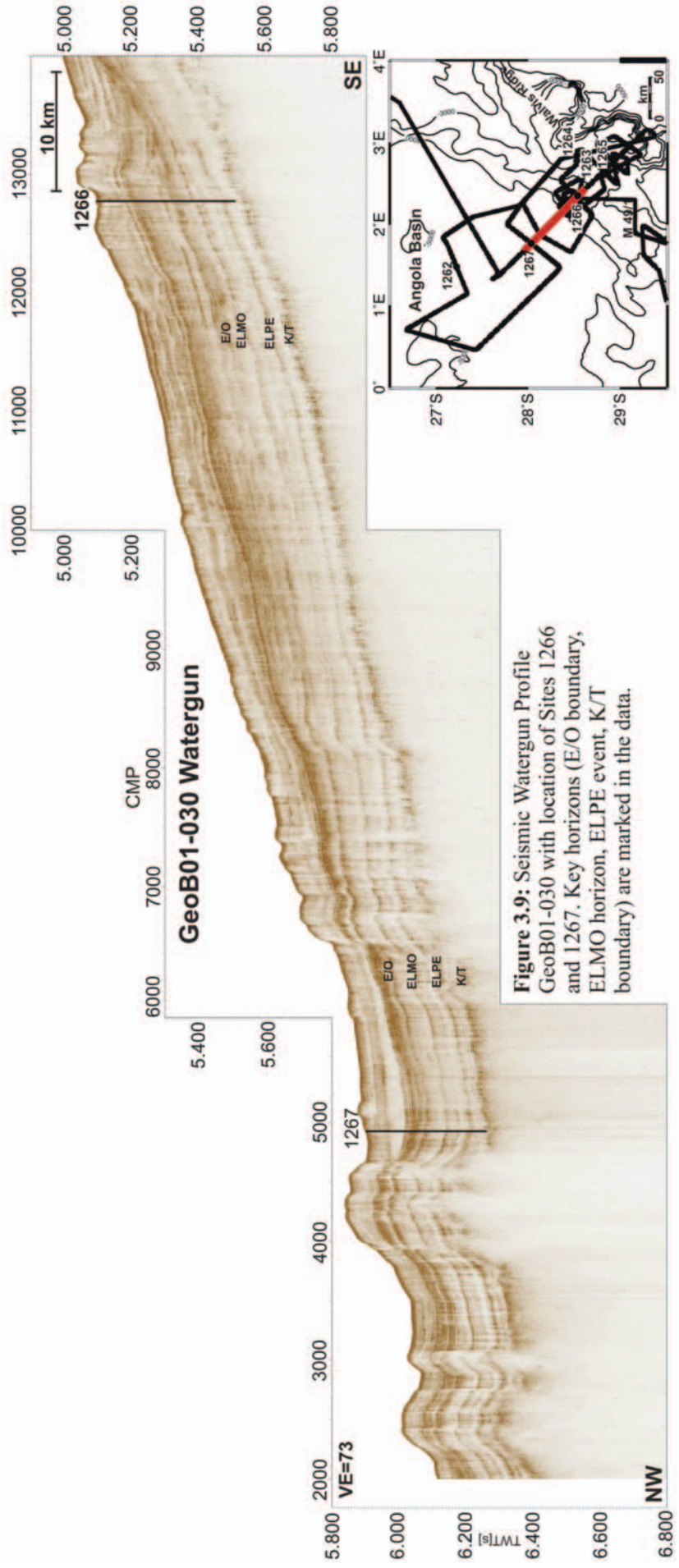


**Figure 3.9:** Seismic Watergun Profile GeoB01-030 with location of Sites 1266 and 1267. Key horizons (E/O boundary, ELMO horizon, ELPE event, K/T boundary) are marked in the data.

### 3.7 Discussion

To ground truth the seismic response, Figure 3.10 illustrates the three key layers (ELMO event, PETM and the ELPE event) in the vicinity of Site 1262, in a detailed view. To illustrate the continuity of the seismic reflectors all horizons are manually picked in the seismic data and flattened on the same time level. Figure 3.10 images the amplitude plots, the wiggle plot and the phase-spectra of the three flattened seismic reflectors, representing the key layers. The ELMO event and the PETM are imaged as singled continuous horizons with high amplitudes in between the homogenous Paleogene sections which are distinguished by low amplitudes and non continuous reflections. The positive density contrasts of the clay layers cause negative reflection coefficients, which are conspicuous to identify in the amplitude and in the wiggle plot. A good continuity of the phase of the recorded wavelets proofs, that the recorded wavelets are reflected from the same continuous horizon. In contrast, the surrounding Paleogene sediments are characterized by numerous changes of the phase, which is a result of the homogenous structure without significant parallel layered density contrasts. Different to the PETM and the ELPE event, the ELMO event occurs as the first reflector of a package of high amplitude reflectors with a constant phase of the wavelet, although the surrounding Middle Paleogene sediments have the same homogenous character. Probably, because of different depositional conditions in terms stronger variations of the density contrasts (compare Fig. 3.8) short above and beneath the ELPE event, the clay horizon is not resolved as an individual reflector, although a distinct transition between the reflector package and the surrounding Middle Paleogene sediments is conspicuous to identify.

As the discussed example of Site 1262 with its favourable conditions shows, the Watergun has the potential to resolve the 0.5 m to 0.8 m thick sediments layers which are characterized by a density contrast of ~10 %. But if the boundary conditions change in terms of increasing density and velocity variations of the surrounding sediment layers or a more disturbed sedimentation pattern, the seismic response is more affected by interference effects of the closely spaced layers and the resolution of the signal of the Watergun gets at its limit.

As this example of Profile GeoB01-030 shows (Fig. 3.9), the clay layers representing the key layers as the ELMO event or the ELPE event occur as separated individual reflectors distinctly separated from the homogenous Paleogene sediments. They are characterized by good continuity, wherefore it is possible to trace them over long distances of several kilometers and to correlate them between the drill sites.



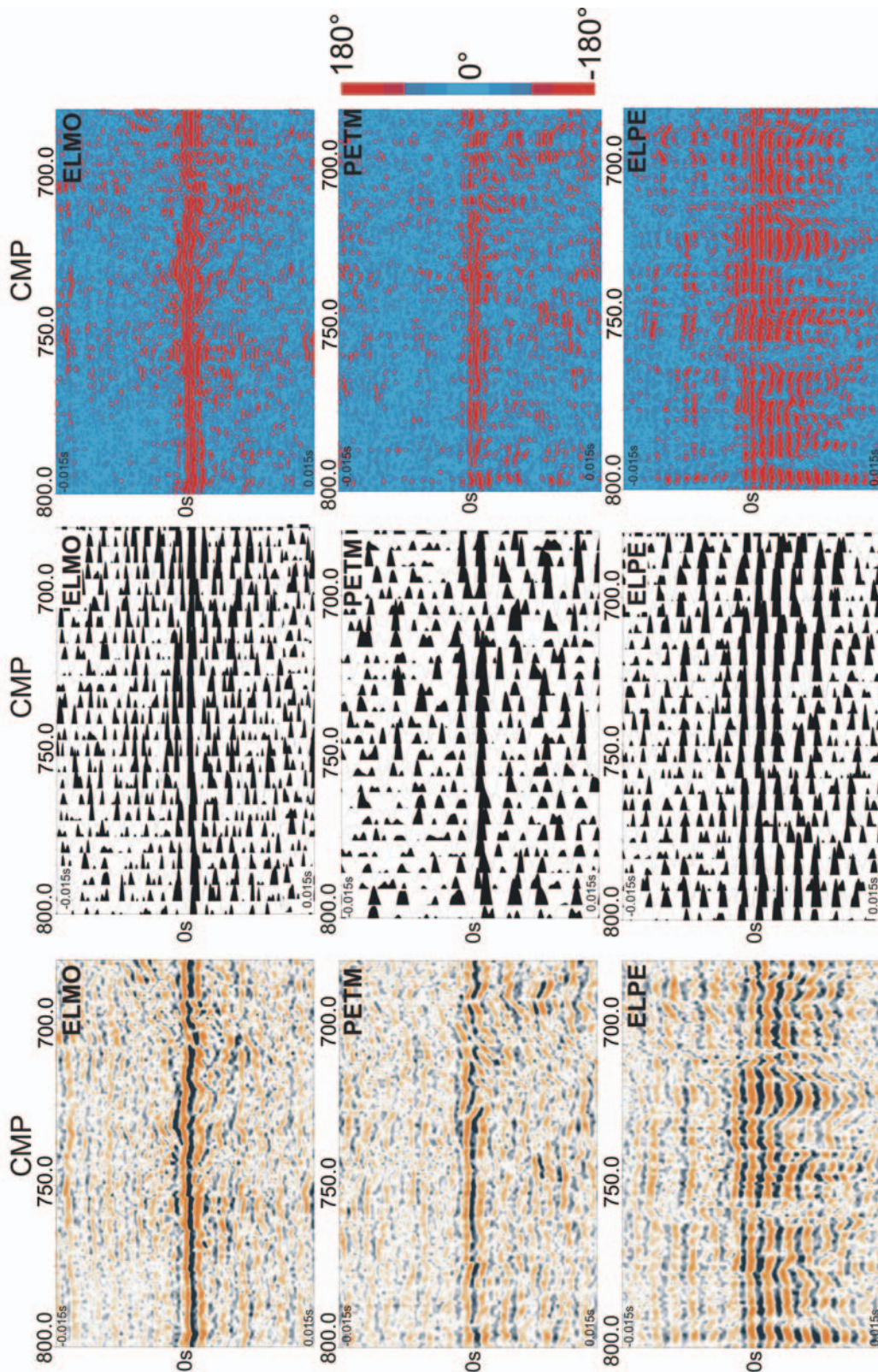


**Figure 3.10:** Detailed images of flattened manually traced horizons at Site 1262

Down: Amplitudes plots of ELMO event, PETM and ELPE event. Orange: negative amplitudes, black: positive amplitudes

Mid: Wiggle plots of ELMO event, PETM and ELPE event

Up: Phase plots of ELMO event, PETM and ELPE event

The weak appearance of the PETM, which is not imaged as a continuous reflector along the profile, illustrates that the changes of the impedance responds sensitive, hence, we are close to the limit of the resolution of the Watergun.

### **3.8 Conclusions**

As both, the model prediction and a comparison of Watergun data with magnetic susceptibility measurements, indicate, it is possible to image 0.5 m to 0.8 m thick sediments layers which are characterized by a density contrast of ~10 % in deep sea sediments using very high resolution Watergun data. The seismic response, which is limited by the wavelength of the source (Watergun ~3 m), is caused by the interference of the reflections of closely spaced layers and changes in sediment deposition and have different effects on images acquired with different frequencies. Whereas in GI-Gun data the clay horizons (ELMO event, PETM, ELPE event) occur as parts of sediment packages with high amplitudes, the Watergun is able to resolve them as individual reflectors or reflector packages with high amplitudes separated by homogenous low amplitude sediment sequences. The acoustic impedance at the key layers changes significantly because of the lower carbonate content. This change of the physical properties of the layers and is caused by a CCD shoaling during the climatic events. Because of different depositional conditions the impulse response of the clay horizons (ELMO event, PETM, ELPE event) changes from one separated layer at the beginning of Angola Basin at the location of Site1262 to small packages of two to four reflectors which include the clay rich horizons. But all events still occur as separated individual layers which can be clearly identified in the seismic data.

As the example of the Profile GeoB01-030 (Meteor Cruise M49/1) shows, it is possible to trace the thin clay layers like the ELPE event and the ELMO event over long distances and tie them in between the different drill locations. The weak appearance of the PETM, which does not occur as a continuous reflector along the Profile GeoB01-030, illustrates that the impedance responds sensitive; hence, we are close to the limit of the resolution of the Watergun.

### **3.9 Acknowledgements**

We are grateful for the support of the captain and the crew members as well as all cruise participants of Meteor cruise M49/1 for their help during the expedition. We also want to thank the Scientific Shipboard Party of the ODP Leg 208, who did a great job. This

research used samples and/or data provided by the Ocean Drilling Program (ODP). ODP is funded by the U.S. National Science Foundation (NSF) and participating countries under management of Joint Oceanographic Institutions (JOI), Inc. This research was funded by Deutsche Forschungs Gemeinschaft, Grant Sp 296/24-1, "Sedimentation processes on Walvis Ridge - correlation of high resolution seismic records with ODP Leg 208 physical properties data".

### 3.10 References

Bartels T., Krastel S., Spiess V., 2007. A correlation of high resolution seismic data with ODP Leg 208 borehole measurements. ODP Leg 208 Scientific Results, [http://www-odp.tamu.edu/publications/208\\_SR/204/204.htm](http://www-odp.tamu.edu/publications/208_SR/204/204.htm), Chapter 2).

Gutowski M., Breitzke M., Spiess V., 2002. Fast static corrections methods for high-frequency multichannel seismic reflection data: A high-resolution seismic study of channel-levée systems on the Bengal Fan. *Marine Geophysical Researches*, 23: 55-75.

Kaiho K., Arinobu T., Isishwatar R., Morgans H.E.G., Okada H., Takeda N., Tazaki K., Zhou G., Kajiwaru, Matsumoto, R., Hirai A., Niitsuma N., Wada, H., 1996. Latest Paleocene benthic foraminiferal extinction and environmental changes at Tawanui, New Zealand, *Paleoceanography*, 11: 447-465.

Luterbach, H.P., Premoli Silva, I., 1964. Biostratigrafia del limite Cretaceo-terziario nell'Appennino centrale. *Riv. Ital. Paleontol.* 70, 67-117.

Miller K.G., Janecek T.R., Katz M.E., Keil D.J., 1987. Abyssal circulation and benthic foraminiferal changes near the Paleocene/Eocene boundary. *Paleoceanography* 2: 741-761.

Miller K.G., Katz M.E., 1987. Oligocene to Miocene benthic foraminiferal and abyssal circulation changes in the North Atlantic. *Micropaleontology* 33: 97-149.

Monechi, S., 1985. Campanian to Pleistocene calcareous nannofossil stratigraphy from the northwest Pacific Ocean, Deep Sea Drilling Project Leg 86. In Heath, G.R., Burckle, L.H., et al., *Init. Reports DSDP 86*, Washington (U.S. Govt. Print. Office).

Lourens J., Sluijs A., Kroon D., Zachos J.C., Thomas E., Röhl U., Bowles J., Raffi I., 2005. Astronomical pacing of late Paleocene to early Eocene global warming. *Nature*, 435, 1083-1087.

Röhl U., Westerhold T., Bralower T.J., Zachos J.C., 2007. On the duration of the Paleocene-Eocene thermal maximum (PETM). *Geochemistry, Geophysics, Geosystem* Volume 8, 12: 1-13 p.

Sheriff, R.E., 1991, *Encyclopedic Dictionary of Exploration Geophysics*, Third Edition: Society of Exploration Geophysicists, 384 p.

Spieß V., Cruise Participants, 2003. Report and preliminary results of Meteor Cruise M49/1, Capetown (South Africa) - Montevideo (Uruguay), 04.01.2000 - 10.02.2000. *Berichte Fachbereich Geowissenschaften, Universität Bremen*, No. 205: 1- 57.

Stott L.D., Kenett J.P., 1990. Antarctic Paleogene planktonic foraminifer biostratigraphy: ODP Leg 113, Sites 689 and 690. In: Barker PF, Kenett J.P., et al. (eds) *Proc. ODP, Sci. Results*, 113. College Station, TX (Ocean Drilling Program): 549-569.

Thierstein H.R., 1982. Terminal Cretaceous plankton extinctions: a critical assessment. In Silver, L.T., and Schultz, P.H. (Eds.), *Geological Implications of Impacts of Large Asteroids and Comets on the Earth*. *Spec. Pap.-Geol. Soc. Am.*, 190:385-399.

Tripathi A., Elderfield H., 2005. Deep-Sea Temperature and Circulation Changes at the Paleocene-Eocene Thermal Maximum. *Science*, 308: 1894-1898.

Zachos J.C., Stott, L.D., Lohmann, K.C., 1994. Evolution of early Cenozoic marine temperatures. *Paleoceanography* 9: 353-387.

Zachos J.C., Pagani, M., Sloan, L., Thomas, E., Billups, K., 2001. Trends, rhythms and aberrations in global climate 65 Ma to present. *Science* 292: 686-693.

Zachos, J.C., Kroon, D. Blum, P., Scientific Shipboard Party 2004. *Proceedings of the Ocean Drilling Program, Initial Reports Volume 208*, available on the web:

[http://www-odp.tamu.edu/publications/208\\_IR/VOLUME/CHAPTERS/IR208\\_01.PDF](http://www-odp.tamu.edu/publications/208_IR/VOLUME/CHAPTERS/IR208_01.PDF)



## **4. Cenozoic evolution of central Walvis Ridge paleotopography**

Thomas Bartels\*, Sebastian Krastel, and Volkhard Spiess

### **4.1 Abstract**

During R/V Meteor Cruise M49/1 more than 1800 km of high resolution seismic profiles were collected at the northeastern flank of Walvis Ridge between 28°- 29.5°S and 2°- 4°E. The data were used as the pre-site survey for Ocean Drilling Program (ODP) Leg 208, where six sites were drilled at different water depths between 2500 m and 4770 m to recover intact composite sequences of Lower Cenozoic sediments from a wide range of depth. The correlation between seismic and borehole data allowed to assign ages to prominent reflectors. These seismic reflectors, which were mapped for the entire study area, represent the paleotopography of the seafloor at selected time intervals after being corrected for subsidence. The resulting model of the paleotopography illustrates that bottom water activities had a significant influence on sedimentation processes at Walvis Ridge. No major bottom water currents were identified for Pre-Miocene times, but since the Middle Miocene bottom water activities increased and cut through the central Walvis Ridge sediment cover, forming a deep water passage from the Cape Basin to the Angola Basin. This newly established pathway might have influenced the development of modern ocean thermohaline circulation.

### **4.2 Introduction**

Walvis Ridge is a northeast-southwest trending aseismic ridge that effectively divides the eastern South Atlantic Ocean into two basins, the Angola Basin to the north and the Cape Basin to the south (Fig. 4.1). It forms a well known, nearly impassable, barrier for bottom waters, which avoids an exchange of bottom water masses between the two basins (Arhan et al., 2003). Only two passages in excess of 4000 m are known in the southern part of Walvis Ridge, one near 37°S called the Walvis Passage (Connary and Ewing, 1974) and another at 32°S called the Walvis Kom (Shannon and Chapman, 1991), that possibly allow some exchange of NADW and AABW between the Cape Basin and the Angola Basin (Fig. 4.1). The Namib Col located at the northeastern part of Walvis Ridge (~22°S) close to the continental margin represents an another possible pathway for deep water masses due to the lower elevation of Walvis Ridge at this location (Fig. 4.1) (Arhan et al., 2003).

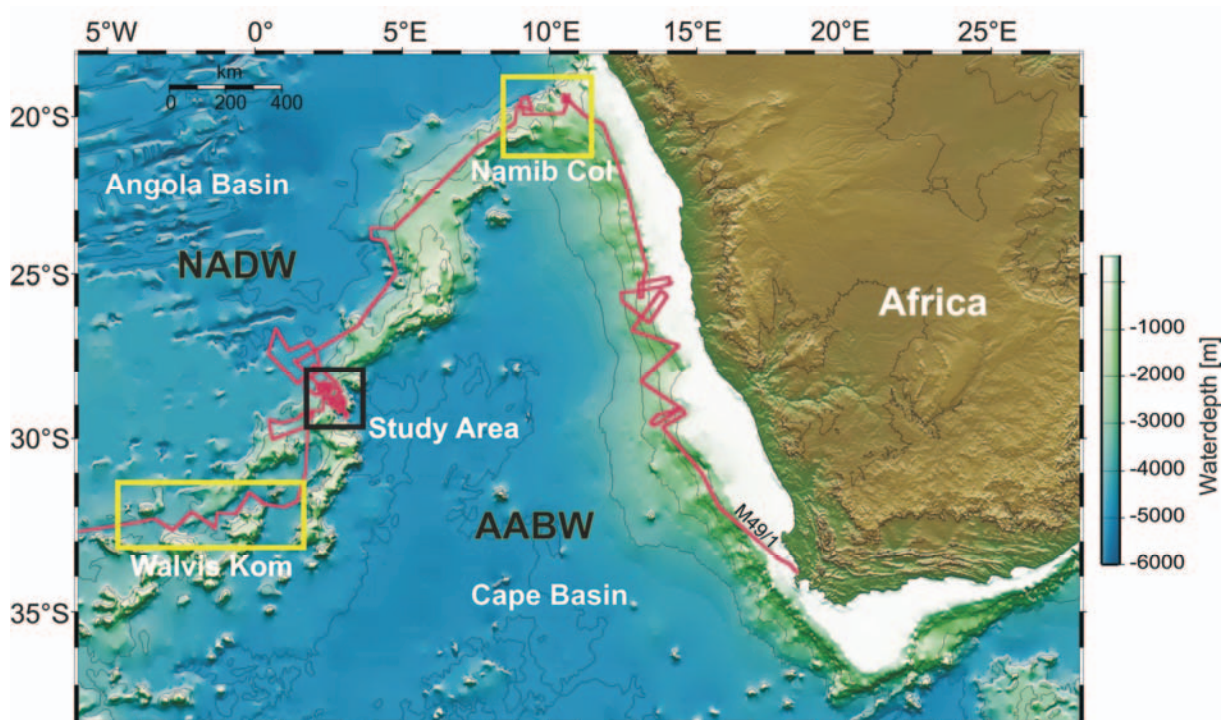


**Figure 4.1:** Cruise track of R/V Meteor Cruise M49/1 Cape Town -Montevideo 2001. Yellow boxes: Gateways of AABW across Walvis Ridge. Black box: Study area. Bathymetry is from GEBCO 2003 Digital Atlas, BODC, © National Environmental Research Council.

In 2001 R/V Meteor Cruise M 49/1 acted as main seismic pre-site survey for Ocean Drilling Program (ODP) Leg 208 (Spiess et al. 2003), which was realized in spring 2003 (Zachos, Kroon, Blum et al., 2004). Main aim of ODP Leg 208 was to recover complete and undisturbed sequences of “extreme” Cenozoic climatic events. More than 1800 km of Generator Injector (GI) Gun (Sodera Inc.) data were acquired during R/V Meteor Cruise M49/1 to search for appropriate drill sites in an area between 28°S and 30°S. In this area, Arhan et al. (2003) suggest another potential flow path for bottom water exchange across the ridge. A detailed stratigraphic analysis of this area was done by Bartels et al. (2007) based on a correlation of the borehole data of Leg 208 with the seismic data of R/V Meteor Cruise M 49/1. The combination of the subsidence history of Walvis Ridge and the stratigraphic analysis allows to reconstruct the evolution of the paleotopography of the study area.

Main objectives are to search for indications of bottom water currents across the ridge in order to emphasize the idea of a bottom water exchange, and possibly answer the question, during which time periods significant changes of the current activities at 28 °S at Walvis Ridge occurred.

### 4.2.1 Geologic Setting

Walvis Ridge is an aseismic topographic high formed by a series of offset north-northwest trending crustal blocks. This set of blocks form a roughly linear NE-SW oriented ridge that separates the eastern South Atlantic into two basins (Fig. 4.1), i.e. the Angola Basin to the north and the Cape Basin to the south (Borella, 1984). In the study area of Leg 208 the ridge slopes gradually into the Angola Basin to the northwest and steeply into the Cape Basin in the southeast. Magnetic and gravity anomalies indicate that the ridge was formed by hotspot volcanism near the mid-ocean ridge as the basin gradually widened (Rabinowitz and Simpson, 1984). Walvis Ridge nowadays acts as barrier for deep water currents and isolates the Angola Basin from Antarctic Bottom Waters (AABW), which dominates the deep waters of the Cape Basin below 4000 m (Fig. 4.1) (Arhan et al. 2003).

No major tectonic events are known for the ridge during the last 60 Ma. Hence, Moore et al. (1984) assume that the ridge has followed a simple thermal subsidence of ~1.1 km since the Maastrichtian. Pelagic sediments drape most of the ridge and generally increase in thickness toward the continental margin (Zachos, Kroon, Blum et al., 2004). The thickness of the pelagic sediments of the study area varies from ~200 m on the deep (>4.5 km) seafloor adjacent to the ridge to ~530 m near the summit (~2.5 km). The sediments are primarily calcareous oozes and chinks that range in age from Campanian to Holocene. Nannofossil and foraminiferal nannofossil oozes with relatively high carbonate contents up to 90 wt% dominate in the Neogene. Some intercalated slumps and turbidites were identified in the Neogene deposits. The Lower to Middle Miocene sections are characterized by lower carbonate content with values from 0 wt% to 20 wt%. The Paleogene sediments are dominated by nannofossil and foraminifer bearing nannofossil oozes to chalk. The sediments have high contents of carbonate up to 80 wt% through out most of the Paleocene, Eocene and Oligocene. Some smaller carbonate-poor intervals indicate episodes of CCD shoaling (Zachos, Kroon, Blum et al. 2004).

### 4.2.2 Oceanographic setting

The study area of ODP Leg 208 (Fig. 4.1) lies beneath the generally northward-flowing surface currents in the eastern parts of the central subtropical gyre. It is approximately 800 km off the coast of Africa, well outside of the eastern boundary current (Beguella Current) and the associated regions of high productivity. With the possible exception of storm induced

currents, the near surface conditions in the study area are rather uniform in recent times and most likely also in the past (Moore et al., 1984). The sediments of the area probably received a nearly uniform supply of biogenic and detrital material since the Maastrichtian. The calcium carbonate lysocline at the northeastern flank of Walvis Ridge is at a depth of ~5 km, therefore all sites of Leg 208 which were drilled at depths ranging from 2500 m and 4770 m lie above this boundary. Today all sites are covered by North Atlantic Deep Waters (NADW) (Zachos, Kroon, Blum et al., 2004), which dominate the deep and bottom waters of the Angola Basin (Moore, et al. 1984).

AABW is widely distributed throughout Cape Basin, which is dominated by few exchanges of the depth waters with the surrounding ocean basins (e.g. Tucholke and Embley, 1976; Faugères et al., 1992). It occurs at water depths greater than 3800 m (e.g. Wüst, 1936, Fuglister, 1960, Arhan et al., 2003) and is pushed by Coriolis force to the western margin of the basin against Walvis Ridge, which leads the water flowing to the north where it reaches the continental margin (Dingle et al., 1987).

## **4.3 Methods**

### **4.3.1 Seismic data**

R/V Meteor Cruise M 49/1 in early 2000 from Cape Town (South Africa) to Montevideo (Uruguay) was the main seismic pre-site survey for Leg 208 (Spiess et al., 2003). Main objectives of ODP Leg 208 were to collect high resolution seismic reflection profiles to identify drill sites that promise recovery of undisturbed, complete and possibly expanded Palaeogene sequences in different water depths. The multichannel seismic system of the Geoscience Department, University of Bremen, is designed to optimize lateral and vertical resolution. It is possible to work with high shot and sampling rates for the collection of very high resolution data sets. A GI-Gun (1.7 L) was used as seismic source providing a frequency range of 100 Hz -500 Hz. The gun was attached to floats to keep it at a constant depth under the water line. For recording a 96-channel Syntron streamer of 600 m length equipped with separately programmable hydrophones was used. 48 channels consisting of 13 hydrophones with a group length of 6.25 m were used for recording the GI-Gun data. The shot interval was 9 seconds resulting in shot point distance of ~12m when sailing with an average speed of 5 knots. For remote control 10 birds kept the streamer at a constant water depth within a range of 1 m. A magnetic compass at every bird allowed to determine the positions of the hydrophone groups relative to the ship's course. The seismic data were digitally recorded at a



sampling frequency of 4 kHz over a time of 3 s. Positioning was based on GPS (Global Positioning System). For processing of the seismic data a combination of ‘in house’ and the commercial ‘Vista’ software (Seismic Image Software LTD.) was used. Standard seismic processing procedures employed included trace editing, setting up geometry, static and delay corrections, velocity analysis, normal move-out (NMO) corrections, bandpass frequency filtering, stack and time migration. The selected spacing of the common midpoints (CMP) was 10 m throughout the survey.

### 4.3.2 Model of the paleotopography and age determination

A correlation of the seismic data with the borehole data was done by using synthetic seismograms calculated out of the density and velocity measurements of Leg 208 (Bartels et al., 2007). This procedure allowed to assign ages to the seismic reflectors. The reflectors, which can be traced almost over the entire study area, represent the paleotopography considering vertical tectonic movements. No major tectonic events are known for Walvis Ridge since the Maastrichtian (Moore et al., 1984). Hence we assume that Walvis Ridge follows a simple thermal subsidence model based on the  $t^{1/2}$  subsidence law for an aseismic ridge (Detrick et al., 1977). Total subsidence sums up to ~1.1 km since the Maastrichtian (Moore et al., 1984).

We selected eight prominent seismic reflectors including the seafloor, which could be traced almost over the entire study area. The depths and the age information of the mapped reflectors are used for the calculation of the paleotopography of the seafloor. Four of the selected reflectors are prominent seismic reflectors which are characterized by strong amplitudes and good continuity along all profiles. Their ages were determined using the correlation of the seismic data with the borehole data based on the biostratigraphy of Leg 208 (Zachos, Kroon, Blum et al., 2004). The remaining three reflectors represent ‘critical’ transitions like the Miocene Bolivina Acme Event (18 Ma), which represents a foraminiferal assemblage dominated by small, smooth, thin-walled bolivinids (Smart and Murray, 1994), the Eocene/Oligocene (E/O) boundary (35.7 Ma), as well as the ‘Eocene layer of mysterious origin’ (ELMO horizon, 53.2 Ma) which is characterized by a drop of calcium carbonate content in the sediments (Zachos, Kroon, Blum et al., 2004) and represents a global thermal maximum (Lourens et al. 2005).

Figure 4.2 shows the study area which is used for the calculation of the paleotopography model. As we want to grid the depth of the paleoseafloor we need to convert

travel times to depth. This is done by using the velocity models based on the velocity measurements of the cores of Leg 208 (Zachos Kroon, Blum et al., 2004), which were also used for the correlation of the seismic data with the borehole data (Bartels et al., Chapter 2). The correction for the subsidence of each time step results in the paleotopography.

Assuming non-deposition conditions in the channel structures, because very slow current velocities, age determinations of the channel structures were done by tracing the base reflector of the channel to one of the Leg 208 boreholes. Using the same correlation of the borehole data with the seismic data, which was used for the calculation of the model, it is possible to estimate the age of the channel structures.

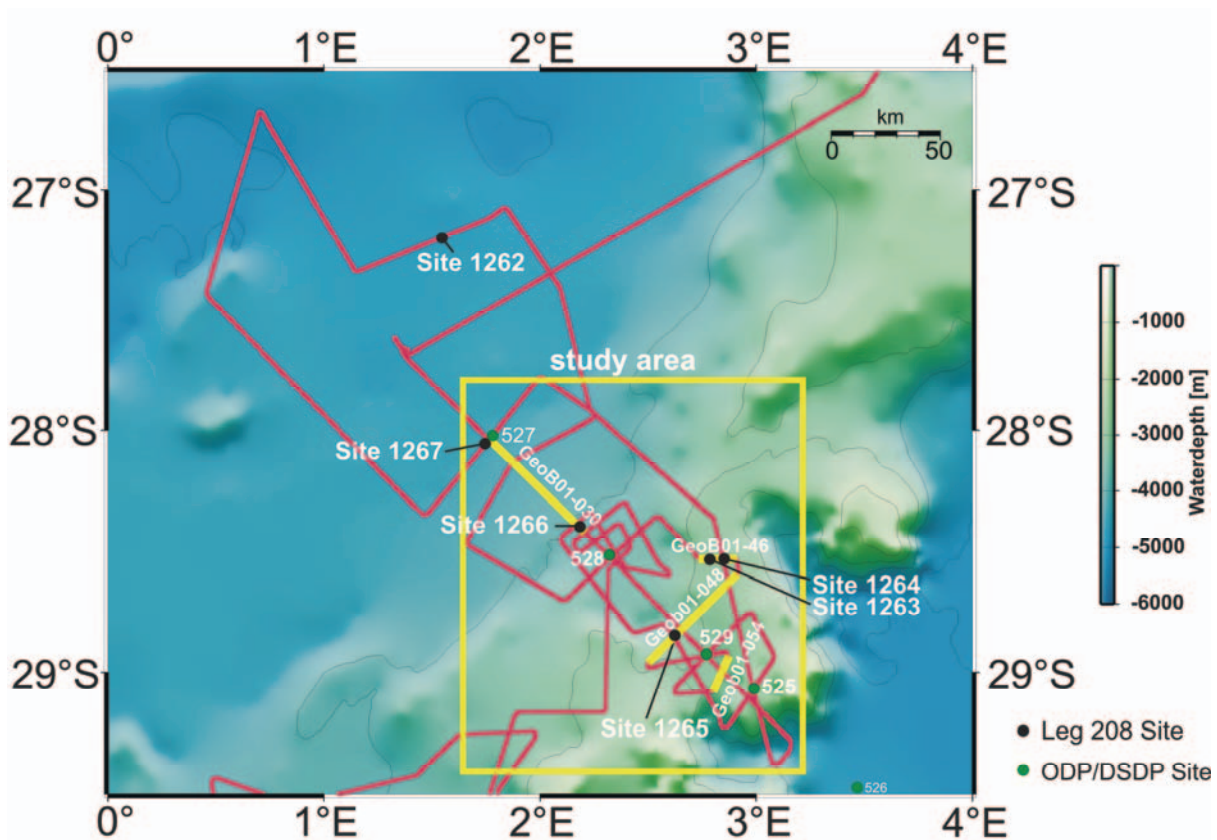


**Figure 4.2:** Study area of ODP Leg 208 with drill sites. Yellow box: Study area used to model the paleotopography. Yellow lines: Seismic profiles imaged in this chapter) Bathymetry is from GEBCO 2003 Digital Atlas, BODC, © National Environmental Research Council.

## 4.4 Results

### 4.4.1 Model of the paleotopography

Figure 4.3 shows a part of the GI-Gun Profile GeoB01-030 at the flank of Walvis Ridge. Two ODP Sites of Leg 208, 1267 in the northwest and 1266 in the southeast, are

located in different water depth on the profile. The pelagic sediments are mostly undisturbed and follow the structures of the top of the basement, supporting the interpretation of Moore et al. (1984) that no major tectonic events occurred in the last 60 Ma. Reflectors can be traced with great confidence between drill sites (Fig. 4.3). The selected reflectors shown in Fig. 4.3 represent ‘critical’ climatic events, like the Miocene Bolivina Acme (18 Ma), the E/O boundary (35.7 Ma), the ELMO horizon (53.2 Ma), and the PETM (Paleocene Eocene Thermal Maximum, 55 Ma). In contrast to the other events, the PETM cannot be correlated between the drill Sites 1266 and 1267, because it directly overlies the rough topography of the basement. The discontinuous reflector cannot be traced manually along the seismic profiles of the study area. Hence, the model of the paleotopography starts at 53.2 Ma during the ELMO event, which is the first traceable reflector for the entire survey area. The seismic lines are dense enough to calculate depth grids for the selected horizons, which in turn represent the paleotopography after being corrected for subsidence

Figure 4.4 shows the results of the model of the Cenozoic evolution of central Walvis Ridge paleotopography. The model starts at 53.2 Ma, during the ELMO event. The time steps of the model depend on the ages of selected prominent horizons; hence the time intervals between the steps of the model vary. For imaging, a not continuous depth scale with a sharp step in colour at ~2600 m water depth is used to visualize the elevation of the seafloor and its alteration in the southeast of the study area. Additionally, the applied subsidence model is shown in Figure 4.4.

The results of model show that the depths of the in the northwest adjoining Angola Basin does not change significantly from one step of the model to the next. Accumulation rate on the one hand and subsidence on the other hand are in the same range. The water depth in the basin increases for about ~250 m since the ELMO event (53.2 Ma).

Only minor morphological variations occur in the first four steps of the model (53.2 Ma – 25 Ma). The time interval from the Paleocene to the Middle Miocene is characterized by a mostly uniform undisturbed sedimentation supply all over the study area which is compensated by the subsidence of the plate. The deposition conditions all over the four time steps seem to be nearly constant. In contrast, major changes are found for the last three time steps (18 Ma – today). The area characterized by water depths shallower than 2600 decreases significantly. Additionally, the isobath pattern changes and a major incision becomes visible in the southeastern survey area.

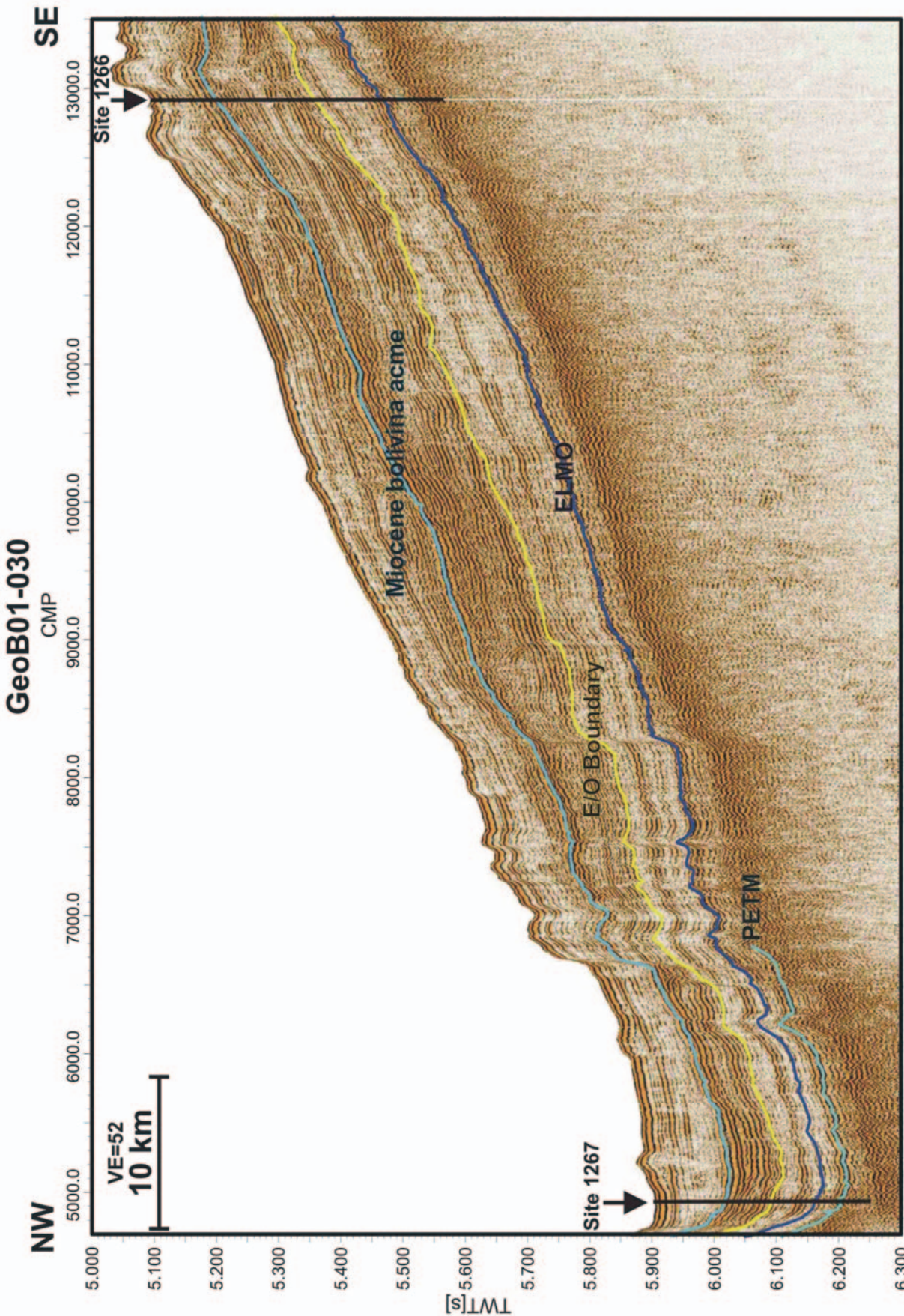
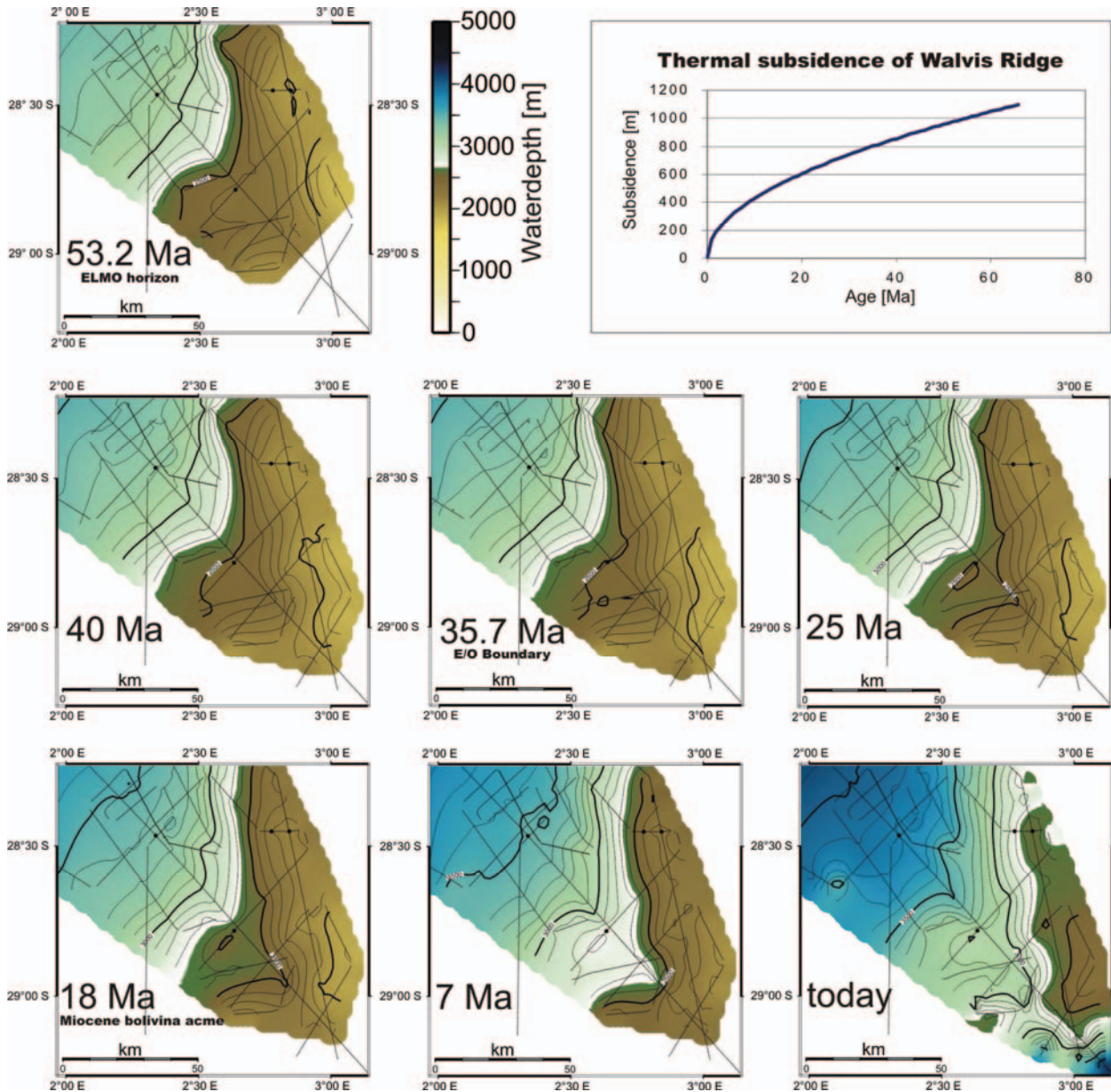


Figure 4.3: Seismic Profile GeoB01-030 with traced reflectors correlated between Sites 1267 and 1266. Location of profile is shown in Fig. 4.2.





**Figure 4.4:** Model of the paleotopography at Walvis Ridge. Subsidence model used for calculation implies the simple model that an aseismic ridge follows the  $t^{1/2}$  subsidence law after Detrick et al. (1977). Initial value for the calculation is a subsidence rate of 1.1 km since the Maastrichtian (Moore et al., 1984).

#### 4.4.2 Seismic data

Figure 4.5 shows a detailed view of the study area where channel structures which can be identified in the seismic sections, are mapped. These structures (red lines in Fig.4.5) which occur side by side at the axis of the ridge cut through the deposited surface sediments. As an example, Figure 4.6 illustrates such a channel structure on Profile GeoB01-048. The profile is almost parallel to the axis of the ridge in a NE-SW direction. The sediments of the profile can be characterized by an increasing thickness with decreasing water depth. They are mostly

undisturbed and parallel layered except in the channel which cuts through the sediments almost in the center of the profile. Site 1265 was drilled at the edge of this channel showing that that Upper Miocene to Quaternary sediments were not deposited (Zachos, Kroon, Blum et al., 2004). The northeastern part of the profile shows expanded Neogene sediments which are part of the morphologic high at the axis of Walvis Ridge, also visible in the eastern part of the paleotopography. This high is characterized by the greatest sediment thickness in the study area (Bartels et al., 2007).

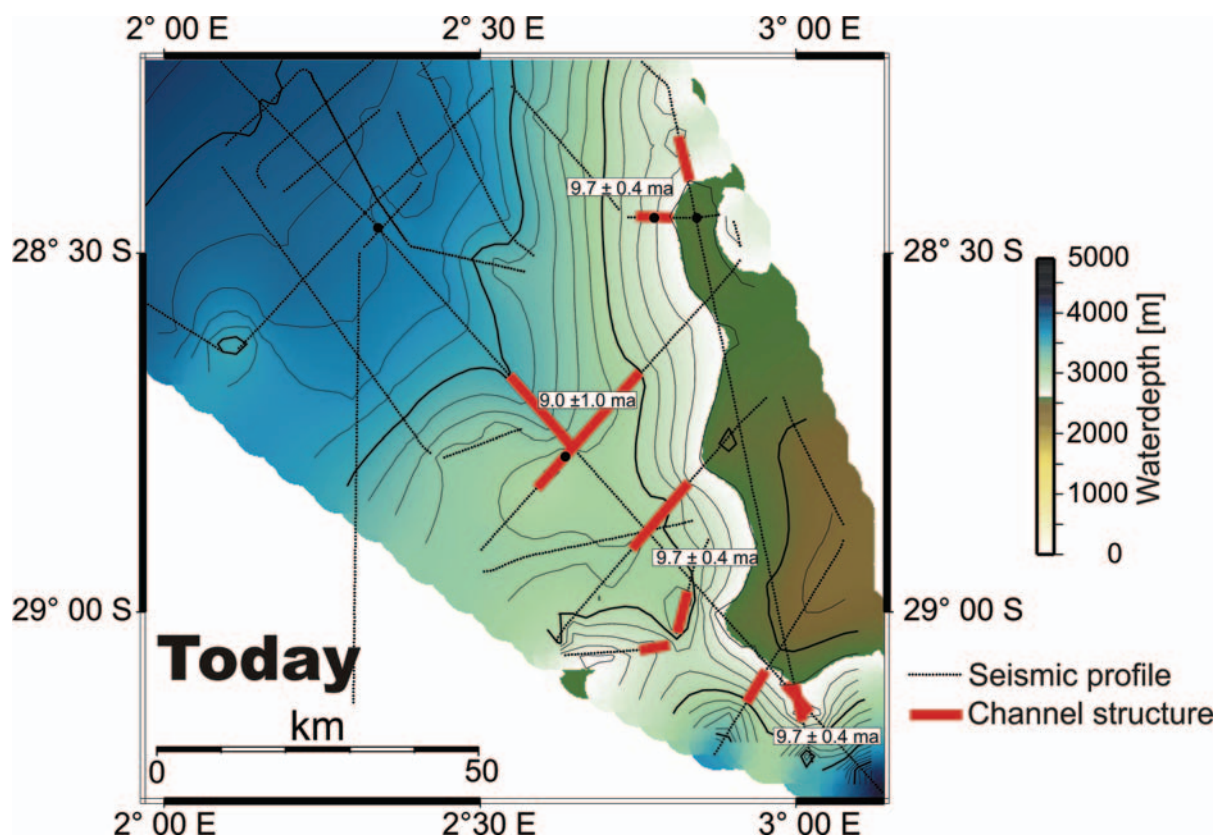


**Figure 4.5:** Topography of the seafloor today with dated channel structures identified in the seismic data.

#### 4.4.3 Ages of the channel structures

To evaluate the ages of the channels, which are cutting through the sediments of Walvis Ridge (red lines in Fig. 4.5), the base of the channels has been identified and correlated with borehole data of Leg 208 (Fig.4.7, 4.8). If we assume that the channels were mainly formed by non-deposition, the base reflector represents the initial age of the channel. Erosive channels might cut older sediments and the base reflector is older than the initial age of the channel. In this case the age of the base reflector represents the maximal for channel initiation. For correlation, Sites 1264 and 1265 are used which are both directly situated in the



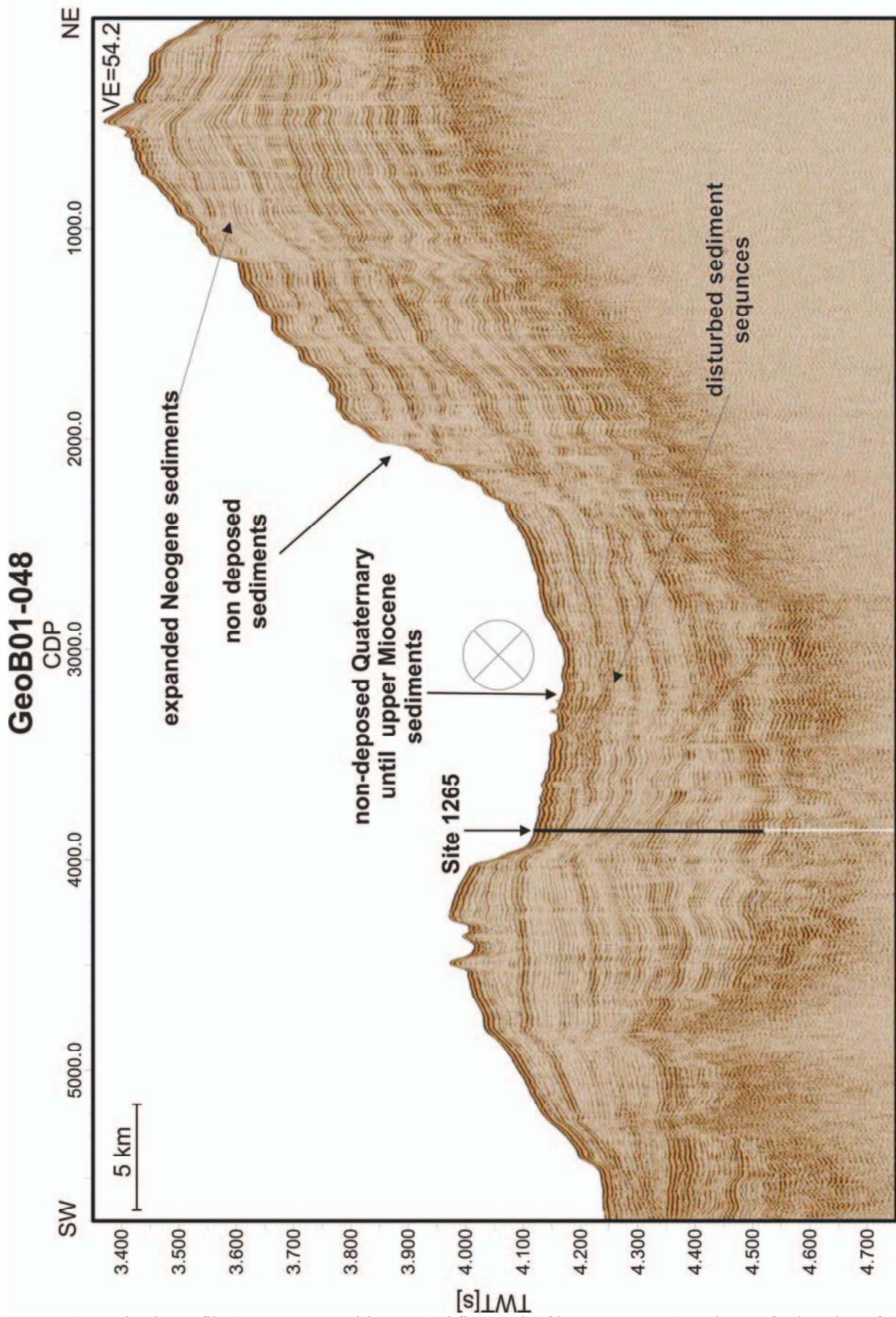
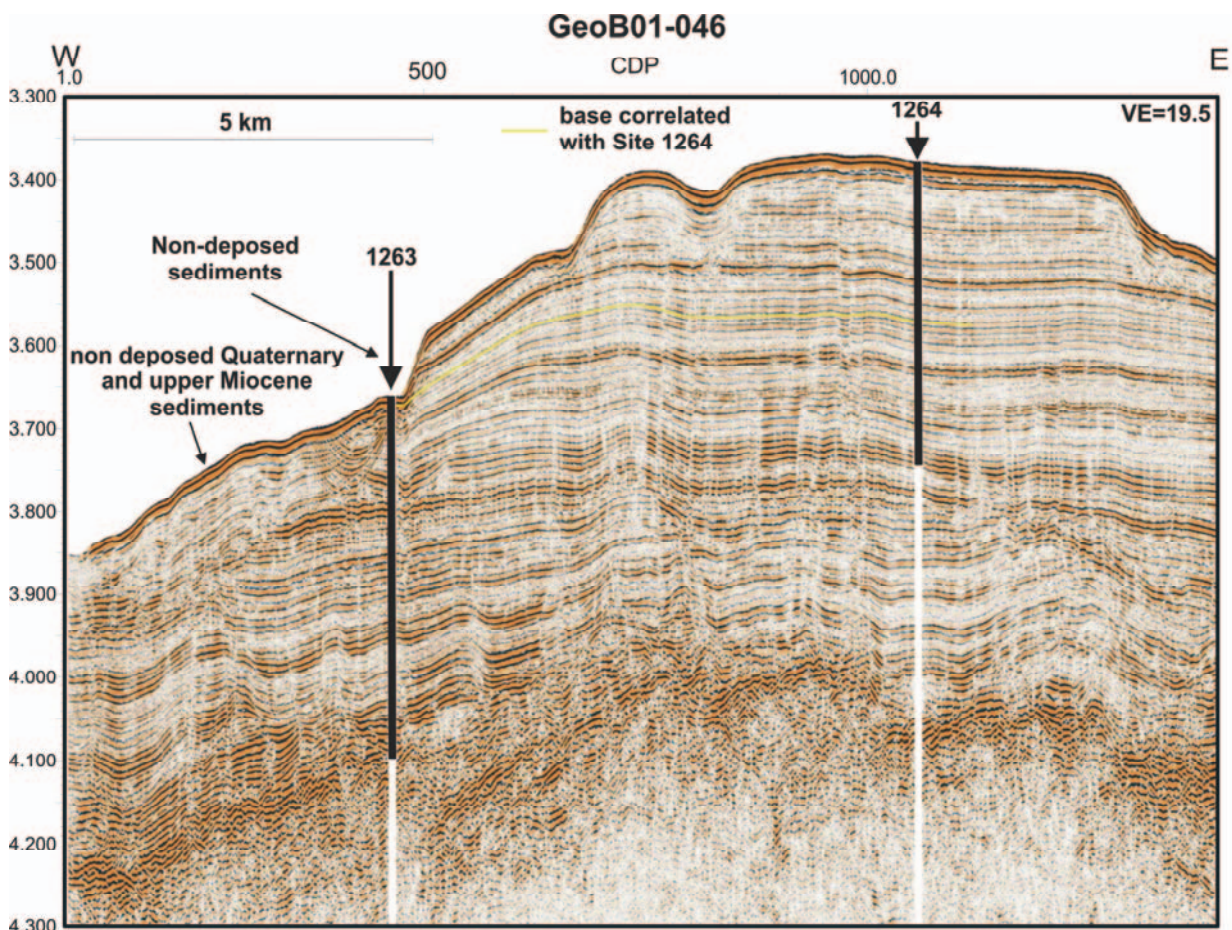


Figure 4.6: Seismic Profile GeoB01-048, with expected flow path of bottom water. See Fig. 4.2 for location of profile.



study area of the model of the paleotopography (compare Fig. 4.2). Site 1264 located on the profile GeoB01-046 (Fig. 4.7) was drilled into expanded Neogene sediments at the axis of the ridge. With a drilling depth of 282 mbsf it reaches upper Oligocene sediments, and therefore it represents a high resolution data set for Neogene times, which is suitable for the determination of the ages of the channels. Site 1265 was drilled at the edge of a channel on Profile GeoB01-048 (Fig. 4.6, Fig. 4.8). Although the resolution of this drill site is much lower because of thinned out or non-deposited Neogene sediments, this site reaches early Oligocene sediments at a depth of  $\sim 146$  mbsf.

The results show that most channel structures show a similar age of  $\sim 9.7 \pm 0.4$  Ma (Fig. 4.5), only one structure at the northwestern part of Profile GeoB01-048 (Fig. 4.9) seems to be slightly younger with an age of  $\sim 9.0 \pm 1.0$  Ma (Fig. 4.5).



**Figure 4.7:** Seismic line GeoB01-046 with Sites 1263 and 1264, yellow line: base of the channel. See Fig. 4.2 for location of profile.



## 4.5 Discussion

For the calculation of the model of paleotopography the picked horizons of the seismic data must be gridded and interpolated between the seismic profiles. The quality of the map depends on the density of the seismic lines. In this study, we think, that the horizontal resolution of the grid is sufficient enough to model the paleotopography, also the resolution is not sufficient to map boundaries of topographic features in detail. We are convinced, however, that the model is good enough to investigate large scale current activities at Walvis Ridge.

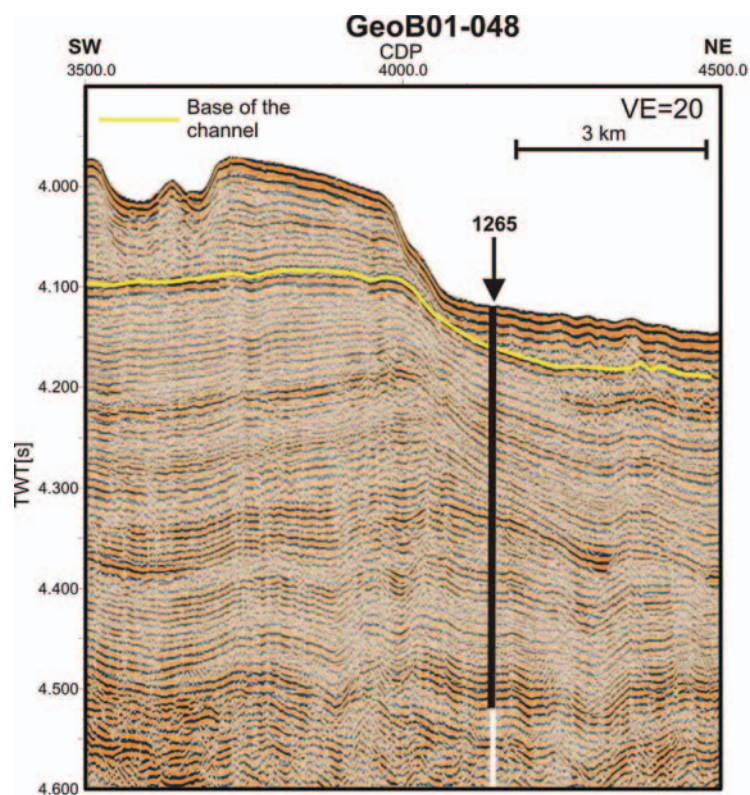


**Figure 4.8:** Part of the Seismic Profile GeoB01-048 with Site 1265, yellow line: base of the channel

As visible in the model of the paleotopography (Fig. 4.4) the isobath pattern of the last three steps of the model changes and a major incision becomes visible in the southeastern survey area. Such an increase of the water depth can be only effected by less deposition or erosion of sediments and is probably connected to increasing bottom water activities across the ridge, since the Miocene (Miocene Bolivina acme, 18 Ma).

A good age estimate for increasing bottom water currents can be done based on a detailed analysis of the channel structures. As described above, we made age estimates for the bases of the channels, which are the last continuous reflectors following the basement

topography below and beside the channel structures. These reflectors give a maximum ages for the channels or even the real age, if the channels were formed by non deposition and not erosion. The quality of the ages estimates are very much depending on seismic resolution. A GI-Gun with a main frequency of about 200 Hz generates a signal with a wavelength of about ~8 m. Additional smaller errors are caused by the velocity model which is used to transform the seismic time scale on a meter scale. Hence, we estimate the inaccuracy to be roughly 10 m. 10 m correspond to ~400 k.y. years in the biostratigraphy of Site 1264 and to ~1 Ma in the biostratigraphy of Site 1265 at the depth of the picked horizons. It is not possible to determine the ages of the channel structures more precisely using GI-Gun data in combination with the borehole data.

The results of the model of the paleotopography emphasize the idea of Arhan et al. (2003), that the general shallowing of Walvis Ridge at 28°S gives possible ways to flows deeper than 3000 m. Potentially, AABW, which is pushed by Coriolis force against the southern flank of Walvis Ridge (Dingle et al., 1977), crosses the ridge and enters the Angola Basin. The mapped and identified channel structures in the seismic profiles of Meteor Cruise M 49/1 indicate these bottom water activities between 28°S and 30°S. Further indicators for current activities are two hiatuses: one on Profile GeoB01-046 at Site 1263 (Fig.4.8) from the Upper Oligocene to the Pleistocene, the second on Profile GeoB01-048 at Site 1265 (Fig. 4.7, 4.9) between the Upper Miocene and the Quaternary (Zachos, Kroon, Blum et al., 2004). Using the biostratigraphy of Leg 208 allows the determination of the age of the bases of the channels which all show similar around 9.5 Ma. The model of the paleotopography indicate increasing current activities in the time step between 18 Ma and 7 Ma. The ages of the channels suggest that major changes occurred relatively close to the end of this time period.

Some of the most important changes to past ocean circulation and climate have been connected with tectonic events involving the closure or opening of oceanic gateways. One of the most recent events was the closure of the Central American Seaway between North and South America (Nisancioglu et al., 2003). The shoaling of the seaway is thought to have been gradual, beginning at 16 Ma at the Early to Middle Miocene boundary (Keller and Barron, 1983; Duque-Caro, 1990; Droxler et al., 1998) with final closure at about 3 Ma in the Middle Miocene (Keigwin, 1982; Marshall et al, 1982; Coates et al, 1992). The closure caused changes in the ocean circulation especially for the NADW, which production increased in the early Pliocene as the Central American Seaway closed (Nisancioglu et al., 2003). The increased bottom water currents crossing Walvis Ridge might be a result of the changing oceanographic conditions. This statement is supported by other examples in the Atlantic

Ocean. The Vema Channel is such an example for a channel structure, which developed in the Miocene and crosses an aseismic ridge (e.g. Faugères et al. 2002). The Vema channel represents a pathway across the Rio Grande Rise for bottom waters with potential temperatures below 2°C (Pätzold et al., 1996, Tarwell et al, 1994).

To sum up, ocean circulation in the South Atlantic changed significantly during the Miocene. Hence, the results of the model of the paleotopography and its temporal evolution are suitable, also the consequence, that the exchange at Walvis Ridge might have influenced the development of modern ocean thermohaline circulation, is a matter of speculation.

#### **4.6 Conclusions**

The detailed analysis of seismic data of the northeastern flank of Walvis Ridge allows to trace prominent dated seismic reflectors over long distances. These reflectors represent the paleotopography of the seafloor under consideration of the subsidence, but neglecting tectonic events which are unknown for this region during the last 60 Ma. Gridding these horizons lead to a model of the paleotopography since 53 Ma. The subsidence of Angola Basin was almost compensated by the increasing thickness of the sediment column. The model illustrates the importance of bottom water activities crossing the ridge between 28°S and 30°S. Increased bottom water activities started most likely around 9 Ma and resulted in an exchange of AABW and NADW between the Cape Basin and the Angola Basin. The exchange of bottom waters was initiated by a shallowing of the ridge between 28°S and 30°S. AABW, which is pushed by Coriolis force against Walvis Ridge, possibly crosses the ridge and enters Angola Basin. Increased bottom water activities at Walvis Ridge are most likely another piece of a dynamic period in the Middle Miocene where significant changes in the ocean circulation of the South Atlantic occurred.

#### **4.7 Acknowledgements**

We are grateful for the support of the captain and the crew members as well as all cruise members of Meteor cruise M49/1 for their help during the expedition. We also want to thank the Scientific Shipboard Party of the ODP Leg 208, who did a great job. This research used samples and/or data provided by the Ocean Drilling Program (ODP). ODP is funded by the U.S. National Science Foundation (NSF) and participating countries under management of

Joint Oceanographic Institutions (JOI), Inc. This research was funded by Deutsche Forschungs Gemeinschaft, Grant Sp 296/24-1, "Sedimentation processes on Walvis Ridge - correlation of high resolution seismic records with ODP Leg 208 physical properties data".

#### 4.8 References

Arhan M., Mercier H., Park Y.H., 2003. On the deep water circulation of the eastern South Atlantic Ocean, *Deep-Sea Research I* 50, 889-916.

Bartels T., Krastel S., Spiess V., 2007. A correlation of high resolution seismic data with ODP Leg 208 borehole measurements. ODP Leg 208 Scientific Results, Manuscript Number SR208-204, [http://www-odp.tamu.edu/publications/208\\_SR/204/204.htm](http://www-odp.tamu.edu/publications/208_SR/204/204.htm), Chapter 2).

Borella P.E., 1984, Sedimentology, Petrology and cyclic sedimentation patterns, Walvis Ridge transect, LEG 74, Deep Sea Drilling Project, Initial reports of the Deep Sea Drilling Project, Leg 74, U.S. Govt. Printing Office, 645-666.

Coates A.G., Jackson J.B.C., Collins J.S., Cronin T.M., Dowsett H.J., Bybell L.M., Jung P., Obando J.A., 1992. Closure of the Isthmus of Panama: The near-shore marine record of Costa Rica and western Panama. *Geol. Soc. Am. Bull.*, 104, 814-828.

Connary S.D., Ewing M., 1974. Penetration of Antarctic Bottom Water from the Cape Basin into the Angola Basin. *Journal of Geophysical Research* 79, 463-469.

Detrick R.S.; Sclater J.G.; Thiede J., 1977. The subsidence of aseismic ridges. *Earth and Planetary Science Letters*, 34, 185-196.

Dingle R.V., 1977. The anatomy of large submarine slump on a sheared continental margin (SE Africa). *J. Geol. Soc. London*, 134, 293-310.

Droxler A. W., Burke K.C., Cunningham A. D., Hine A. C., Rosencrantz E., Duncan D.S., Hallock P., Robinson E., 1998. Caribbean constraints on circulation between Atlantic and Pacific oceans over the past 40 million years, in *Tectonic Boundary Conditions for Climate Reconstructions*, edited by Crowley T.J. and Burke, K.C., 169-191, Oxford Univ. Press, New York, 1998.



Duque-Caro H., 1990. Neogene stratigraphy, paleoceanography and paleobiogeography in northwest South America and the evolution of the Panama Seaway. *Palaeogeogr., Palaeoclimatol. Palaeoecol.*, 77, 203-234.

Faugères J.C., Mézerais M.L., Stow D.A.V., 1992. Contourite drift types and their distribution in the North and South Atlantic Ocean basins. *Sedimentary Geology*, 82, 189-203.

Faugères J.C., Zaragosi S., Mézerais M.L., Massé L., 2002. The Vema contourite fan in the South Brazilian Basin. From: Pudsey, D.A.V., Howe, C.J., Faugères, J.C, Viana, A.R., 2002. *Deep-Water Contourite Systems: Modern Drifts and Ancient Series, Seismic and Sedimentary Characteristics*. Geological Society, London, *Memoirs*, 22, pp 209-222.

Fuglister F.C., 1960. *Atlantic Ocean Atlas of temperature and salinity profiles and data from the International Geophysical Year of 1957-1958*. Woods Hole Oceanographic Institution Atlas Series, 1, 209pp.

Keigwin L., 1982. Isotopic paleoceanography of the Caribbean and East Pacific: Role of Panama uplift in the Late Neogene time. *Science*, 217, 350-352.

Keller G., Barron J.A., 1983. Paleoceanographic implications of the Miocene deep sea hiatuses. *Geol. Soc. Am. Bull.*, 94, 590-613.

Lourens J., Sluijs A., Kroon D., Zachos J.C., Thomas E., Röhl U., Bowles J., Raffi I., 2005. Astronomical pacing of late Paleocene to early Eocene global warming. *Nature*, 435, 1083-1087.

Marshall J., Shott F., 1982. Open-ocean convection: Observations, theory, and models. *Rev. Geophys.*, 37(1), 1-64, J.

Moore T.C., Rabinowitz P.D., Shipboard Scientific Party, 1984. *History of Walvis Ridge. Initial reports of the Deep Sea Drilling Project, Leg 74*, U.S. Govt. Printing Office, 31, pp 873-894.

Nisancioglu K.H., Raymo M.E., Stone H.P., 2003. Reorganization of Miocene deep water circulation in response to the shoaling of the Central American Seaway. *Paleoceanography*, Vol.18, No.1 1006-1018.

Pätzhold J., Heidland K., Zenk W., Siedler G., 1996. On the Bathymetry of the Hunter Channel. From Wefer G., Berger W.H., Siedler G., Webb D.J., (eds) 1996, *The South Atlantic: Present and Past Circulation*. Springer-Verlag Berlin Heidelberg, pp 355-361.

Rabinowitz P.D., Simpson E.S.W., 1984. Geophysical site survey results on the Walvis Ridge. In: Moore TC, Rabinowitz PD, Shipboard Scientific Party (eds) *Init. Repts. DSDP*, 74. U.S. Govt. Printing Office, pp 795-825.

Shannon L.V., Chapmann, P., 1991. Evidence of Antarctic Bottom Water in the Angola Basin at 32°S. *Deep Sea Research*, Vol. 38, No. 10, pp. 1299-1304.

Smart C.W., Murray J.W., 1994. An early Miocene Atlantic-wide foraminiferal/ palaeoceanographic event, *Palaeogeography, Palaeoclimatology, Palaeoecology*, Volume 108, Issues 1-2, Pages 139-148.

Spiess V., Cruise Participants, 2003. Report and preliminary results of Meteor Cruise M49/1, Capetown (South Africa) - Montevideo (Uruguay), 04.01.2000 - 10.02.2000. *Berichte Fachbereich Geowissenschaften, Universität Bremen*, No. 205: 1- 57.

Tucholke B.E., Embley R.W., 1976. A continuous erosional zone in the Cape, Agulhas, and Mocambique Basins. *Geological Society of American Bulletin*, 88, 1337-1346.

Wüst G., 1936. Das Bodenwasser und die Gliederung der Atlantischen Tiefsee. *Wiss. Ergebnisse Deut. Atlantik Expeditionen Meteor*, 6(1), 3-107.

Zachos J.C., Kroon D., Blum P., et al., 2004. *Proceedings of the Ocean Drilling Program, Initial Reports Volume 208*, available on the web:

[http://www-odp.tamu.edu/publications/208\\_IR/VOLUME/CHAPTERS/IR208\\_01.PDF](http://www-odp.tamu.edu/publications/208_IR/VOLUME/CHAPTERS/IR208_01.PDF)

## **5. The Walvis Kom: A pathway for AABW from the Cape Basin to the Angola Basin?**

**Thomas Bartels\*, Sebastian, Krastel, Volkhard Spiess**

### **5.1 Abstract**

Several seismic, echosounder, and swathsonder profiles were shot at Walvis Ridge along a region east of the Walvis Passage which is called the Walvis Kom at 32°S in early 2001 during R/V Meteor Cruise M49/1. Walvis Ridge, which is known as a nearly impassable barrier for bottom waters, divides the south-eastern Atlantic into two basins, the Angola Basin to the north and the Cape Basin to the south. AABW is widely distributed in the Cape Basin at water depth >3800m, but Walvis Ridge avoids an exchange of AABW between the Cape Basin and the Angola Basin.

The acoustic data of this study are located between 2°E and 4°W at the Walvis Kom, which is a postulated leakage for AABW from Cape Basin to Angola Basin. Walvis Kom is surrounded by tectonic blocks of Walvis Ridge and represents a continuous flow path connecting the Cape Basin with the Angola Basin at water depth >3800 m. AABW is pushed by the Coriolis force into the flow path. Sedimentary waves, contourite-sheeted drifts and toplap structures identified in acoustic data supports the idea of past and recent continuous bottom current activities through Walvis Kom. An unconformity in the upper sediments along the flow path dates the initiation of current activities during the Lower Miocene. Recently the current induced structures at the seafloor indicate a still active exchange with slow current velocities which are too weak for erosion. Accumulation rates decrease from the Cape Basin to the Angola Basin since the initiation of the current, which is mainly caused by higher current velocities caused by a narrowing flow path.

### **5.2 Introduction**

Supan (1899) was the first to advocate that a temperature contrast of 1.5 °C between the bottom waters of the Angola Basin and the Cape Basin can be explained by a ridge that divides the basins and stretches from the Mid-Atlantic ridge to the African continent. Supan (1899) proposed the name Walvis Ridge. This aseismic feature consists of a series of interconnected crustal blocks that slope gradually toward the northwest and more steeply

toward the southeast (Rabinowitz and Simpson, 1984). The blocks form a roughly linear ridge that effectively divides the eastern South Atlantic into two basins, the Angola Basin in the north and the Cape Basin in the south (Borella et al., 1984).

Antarctic Bottom Water (AABW), which has a potential temperature  $<1.4^{\circ}\text{C}$ , salinity  $<34.82$  PSU and silicate concentration  $>80$   $\text{mmol m}^{-3}$ , is widely distributed throughout the Cape Basin at water depths  $>3800$  m (Wüst, 1936, Fuglister, 1960). Above 3800 m water depth, the AABW is overlain by North Atlantic Deep Waters (NADW), which is found in all basins of the South Atlantic (e.g. Siedler et al., 1996). The exchange of deep water between the Cape Basin and adjacent basins is limited to few pathways (e.g. Tucholke and Embley, 1976; Faugères et al., 1992). Measurements and models of thermohaline circulation show, that AABW enters and exits the Cape Basin through the Cape Passage (Tucholke and Embley, 1976) in the south, connecting to the Agulhas Basin (Fig. 5.1). The passage has a width of  $\sim 250$  km and a maximum water depth  $>4500$  m (Rogers 1987). After Dingle et al. (1987), AABW is pushed by the Coriolis force towards the western margin of the basin, where Walvis Ridge as a nearly impassable barrier guides the deep water currents to the north and northeast. From the northeastern corner, AABW is forced southward by the continental margin and out of the basin. This circular flow is associated with massive erosion in particular in water depths between 4000 m and 4500 m (Dingle et al., 1987). However, the today measured current velocities of the AABW are too slow for the transport of deep sea sediments. Therefore erosive zones in the surface sediments must be interpreted as relict structures from periods of more intensive bottom currents possibly in the Eocene (Tucholke and Embley, 1976).

The classical view of Wüst (1936), that the northward passage of AABW into the Angola Basin is completely blocked by Walvis Ridge, was first challenged by Shannon and van Rijswijk (1969). Connary and Ewing (1972, 1974), who published temperature and light scattering measurements, that confirm some leakage of AABW to Angola Basin through a channel near  $37^{\circ}\text{S}$  and  $7^{\circ}\text{W}$ , the so called Walvis Passage (see Fig. 5.1). Further northeast, the crest of Walvis Ridge is even shallower, and only two regions, the Namib Col near  $22^{\circ}\text{S}$  (Arhan et al., 2003) and one between  $28^{\circ}\text{S}$  and  $30^{\circ}\text{S}$  (Arhan et al., 2003, Bartels et al., Chapter 4) (Fig. 5.1), possibly allow deep-water exchange at water depth deeper than 3000 m.

Shannon and Chapman (1991) published temperature and salinity measurements which suggested another leakage of AABW across Walvis Ridge at the Walvis Kom at  $32^{\circ}\text{S}$ . However, because of no existing current or seismic measurements, the question of whether



the flow of AABW through the gap in the ridge is continuous or pulsed remained still open (Shannon and Chapman, 1991).

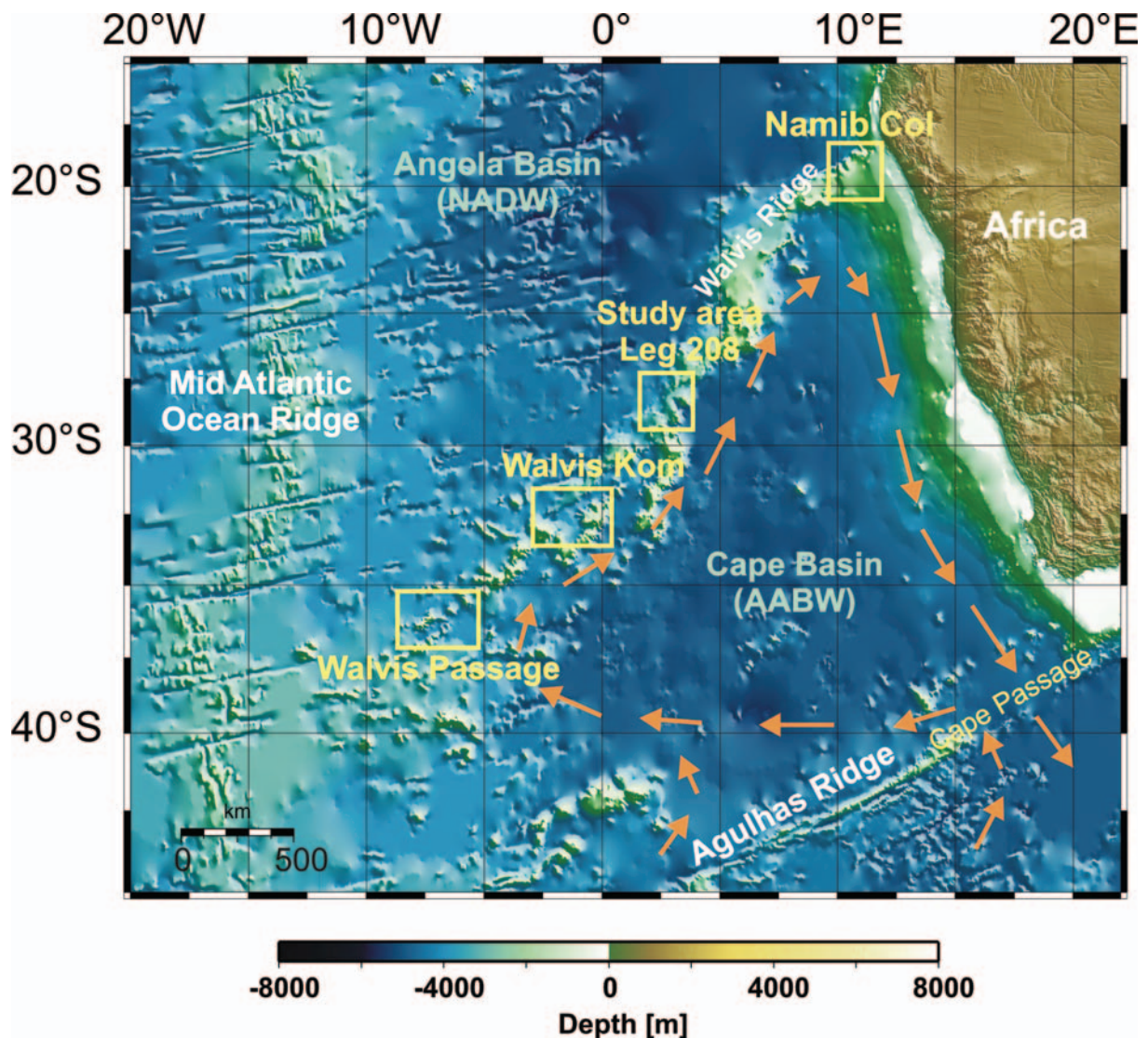


**Figure 5.1:** General oceanographic setting of Walvis Ridge. Arrows: Flow path of AABW through the Cape Basin after (Tucholke and Embley, 1984). Boxes: Bottom waters flow paths for exchanging NADW and AABW between the Angola Basin and the Cape Basin. Bathymetry is from GEBCO 2003 Digital Atlas, BODC, ©National Environmental Research Council.

In this study, we employ a combined analysis of seismic, echo-sounder, and swath-sounder profiles along the Walvis Kom at 32°S in order to describe and analyze the morphologic and sedimentological setting of this postulated flow path. We search for indications of bottom water currents in the younger sediment sequences of the pathway to emphasize the idea of a bottom water exchange between the two basins and possibly answer the question, whether the recent current activities, proofed by the evidence of AABW along the path way, are continuous or not. Furthermore the study intends to evaluate the temporal

evolution of the current activities due to the intensification of the thermohaline circulation in the South Atlantic during the Oligocene and Neogene.

### **5.3 Methods**

High resolution multi-channel seismic data, narrow beam sediment echo-sounder (Parasound) data and multibeam swath-sounder (Hydrosweep) data are presented in this study. All data were all collected during R/V Meteor Cruise M49/1 in early 2001 (Spiess et al. 2003). Eleven profiles with a total length of about 580 km were recorded using all acoustic systems at 32°S (Walvis Kom), where Shannon and Chapman (1991) provided evidence of AABW in the Angola Basin.

#### **5.3.1 Seismic data**

The multi-channel seismic system of the University of Bremen is designed to optimize lateral and vertical resolution. A Generator Injector (GI) Gun (Sodera Inc.) with chamber of 1.7 l was used as energy source. It provided a source frequency range of 100 Hz - 500 Hz. The gun was attached to floats which kept it at a constant water depth of ~1 m beneath the water line. For recording, a Syntron streamer with a length of 600 m and 96 hydrophone groups was used, half of which were used for GI Gun recording. The 48 hydrophone group are spread over a length of 6.25 m with a maximum of 13 hydrophones. The shot interval was at 9 seconds on average while surveying with a speed of ~5 knots. For remote control of the streamers depth, 10 cable levellers were used, which kept the streamer at a constant water depth of 3 m and within a range of +/-0.5 m. Magnetic compasses at every cable leveller (bird) measured the streamer orientation. These data are used to determine the position of each hydrophone group relative to the course of the ship. The positioning of the ship and the seismic equipment was based on GPS (Global Positioning System). For the digital recording of the data, a 4 kHz sampling frequency was chosen and a recording length of 3 s. For processing we used standard processing procedures, including trace editing, setting up the geometry, CMP binning at 10 m spacing, static and delay corrections, velocity analysis, NMO corrections, bandpass frequency filtering, stacking, and migration. The depths presented in this study were converted from two-way traveltime to depth using constant velocity models derived from seismic velocity analysis.

For Profile GeoB01-077 (Figure 5.3) only a brutestack data set over the first three channels of each shot exists, with a shot distance of ~5 m. The brutestacked profile is filtered and migrated using a constant velocity model of 1500m/s.

### **5.3.2 Sediment echo-sounder profiling**

The hull-mounted echosounder system (Parasound) generates a narrow beam, low frequency signal of 4 kHz by using the parametric effect. The much smaller footprint (~7% of the water depth) compared to conventional 3.5 kHz echosounders increases lateral resolution significantly and allows the imaging of small scale features as sediment waves on the sea floor. The system has also an enhanced vertical resolution of a few decimetres, signal penetration varies between 0 m and 200 m, depending on the type of sediment and attenuation (Grant and Schreiber, 1990). The collected data were digitized with a sampling rate of 40 kHz and stored using the ParaDigMA Software (Volkhard Spiess, Universität Bremen). For further processing and imaging of the profiles the 'in house' software package SENT (Hanno Keil, University Bremen) was used. The depths presented in the echo sounder profiles were converted from two-way travel time to depth using a constant velocity model of 1500 m/s.

### **5.3.3 Swath mapping data**

The Hydrosweep swathsonder system is hull-mounted, generating 59 pre-formed beams over an angle of 90° with an aperture of 2.3° for each beam. The system provides depth information for a swath with a width of twice the water depth (Grant and Schreiber, 1990). The system operates at a frequency of 15.5 kHz.

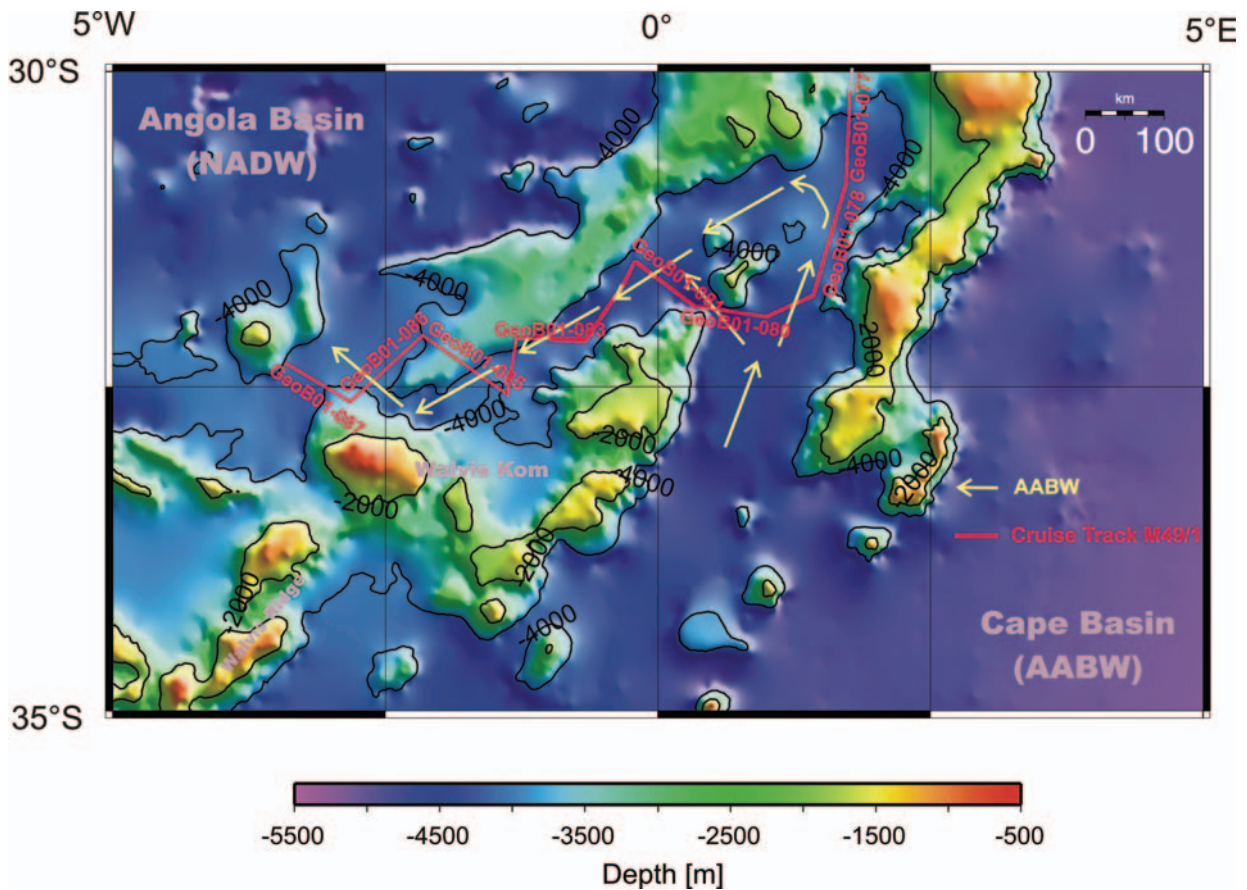
The processing and presentation of the bathymetric data were carried out with the public domain software package MultiBeam (Caress and Chayes, 1996) and the General Mapping Tools (Wessel and Smith, 1998). The processing includes correction of the navigation data and both an automatic and a manual editing of the bathymetric data as well as final gridding for display.

## **5.4 Results**

### **5.4.1 Bathymetry**

Walvis Ridge, which forms a more than 2000 m high barrier between the Angola Basin and the Cape Basin, is an impassable barrier for depth waters in depth greater than 3100

m (Arhan et al., 2003). At Walvis Kom, blocks of the ridge built a possibly flow path, which crosses the ridge and connects the two basins at water depth  $>3800$  m (Fig. 5.2). The water depth of the thalweg of this flow path decreases from  $\sim 4500$  m in the Cape Basin to  $\sim 4150$  m in the Angola Basin (Fig. 5.3, 5.4).



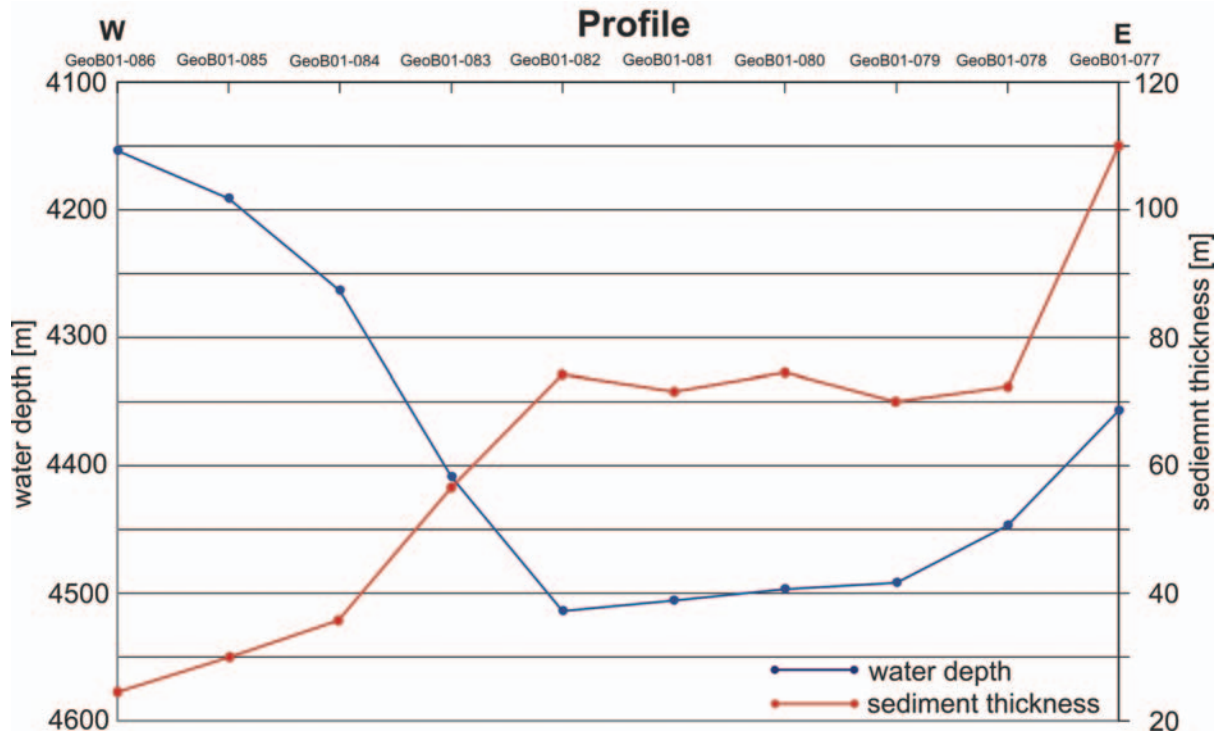
**Figure 5.2:** Bathymetric map of the western Walvis Ridge. Red straight lines: Seismic profiles of the Cruise M49/1. Yellow arrows: Assumed flow path of AABW after Shannon and Chapman, 1991. Bathymetry is from GEBCO 2003 Digital Atlas, BODC, ©National Environmental Research Council.

Figure 5.4 illustrates the bathymetry data of the Profiles GeoB01-083 - GeoB01-86. The quality of the bathymetry data of Profiles GeoB01-077 - GeoB01-082 unfortunately suffered from weather conditions, hence they are not shown. Additionally to the recorded data, the bathymetry data from GEBCO database (GEBCO, 2003) are implemented as contour lines into the plot as well. Black arrows indicate the suggested flow path of AABW through the Walvis Kom (Shannon and Chapman, 1991), which is surrounded by tectonic blocks of Walvis Ridge.

The results of the Figures 5.3 and 5.4 illustrate the trend of the decreasing water depth along the flow path in direction of the Angola Basin, which corresponds to the western spill of Walvis Ridge. Whereas the blocks of the ridge are characterized by steep flanks, the



bathymetry of the thalweg is characterized by only few variations in the range of some ten meters. In the south-eastern part of the flow path, a gap in the blocks the ridge builds a direct connection to an adjoining smaller basin in the south, which is, similar as the flow path, surrounded by the steep blocks of Walvis Ridge. The water depth of this basin amounts  $\sim 4180$  m.



**Figure 5.3:** Average water depths and average thickness of the current influenced sediments of the the thalweg at each seismic profile along the Walvis Kom.

#### 5.4.2 Seismic and echo-sounder profiles

Figure 5.5 shows the brutestack of Profile GeoB01-077 located at the northern edge of the suggested pathway (compare Fig. 5.2). It runs from the blocks of Walvis Ridge into the suggested pathway of the AABW. Here, the maximum thickness of the sediments amounts  $\sim 620$  m. The sediment column represents two depositional units: A lower unit with a thickness up to  $\sim 510$  m, which is represents the old undisturbed pelagic sediments which cover the rough topography of Walvis Ridge and an upper unit with a maximal thickness of  $\sim 110$  m, which shows undulating internal structures. The amplitude of the undulating surface structures vary between 20 m and 30 m. The small inset of the bathymetry data shows that the seafloor is characterized by a linear elongated pattern with a strike direction of  $11^\circ$ .

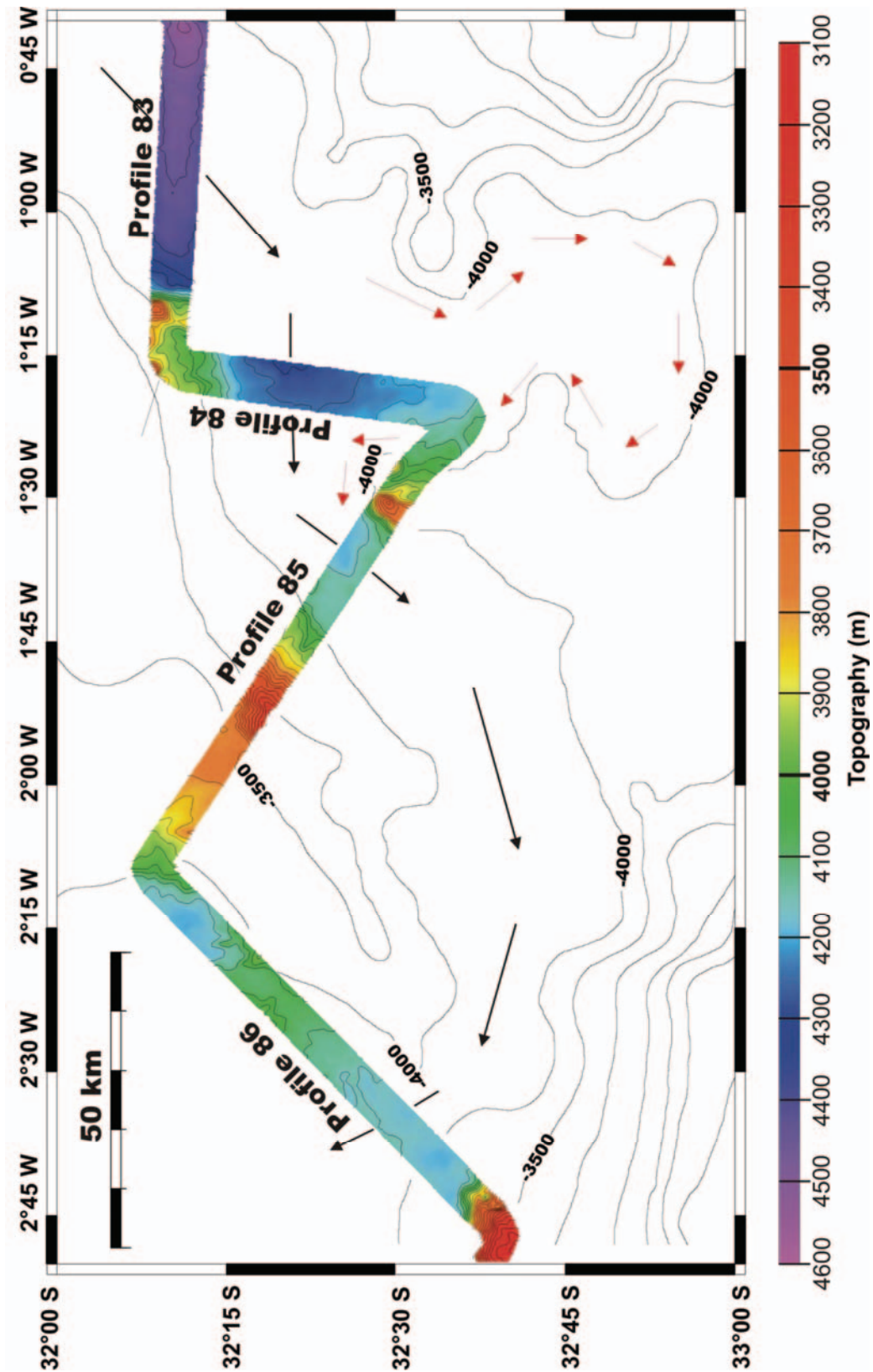


**Figure 5.4:** Swath bathymetric data of the Profiles GeoB01-083 to GeoB01-086. Black arrows show the suggested flow path of AABW after Shannon and Chapman, 1991. Red arrows: Possible flow path of AABW through an adjoining basin south of the main flow path. Bathymetry is from GEBCO 2003 Digital Atlas, BODC, © National Environmental Research Council.

The average thickness of the sediment column decreases in southern direction on Profiles GeoB01-078 (~470 m), GeoB01-079 (~370 m), and GeoB01-080 (~350 m) (not shown). The three profiles are characterized by mostly undisturbed pelagic sediment patterns covering the rough topography of the blocks of Walvis Ridge. In contrast to Profile GeoB01-077 (Fig. 5.5), the upper unit of the sediments, with a thickness of ~70 m, have no undulating structures.

Figure 5.6 images the seismic data of Profile GeoB01-081. The profile is directly located at the beginning of the suggested flow path, where AABW possibly enters the Walvis Kom. The water depth is ~4500 m, except at the eastern end, where parts of the blocks of Walvis Ridge are imaged. The profile has a length of ~62 km and crosses the pathway almost in perpendicular direction. Hence, the south-eastern part of the pathway amounts to more than 60 km. The sediment thickness varies between ~410 m in the south-eastern part and ~550 m in the north-western part. The deeper sections of the sediment column are characterized by mostly undisturbed pelagic sediments, which drape most of the profile and are only disturbed by topographic highs of the ridge. Several toplap structures, identified in the seismic data, separate the younger sediment cover from the older undisturbed pelagic sedimentation. In the south-eastern part of the profile the thickness of this cover amounts ~70 m, in the north-western part it increases up to ~130 m. At the surface of the seafloor four sediment bodies occur, of which the thicker ones in the north-western part are characterized by an internal undulating structure and continuous reflectors. The inset of the bathymetry shows that the elongated bodies are almost parallel arranged with a strike direction of ~5° (Fig.5.6).

Figure 5.7 shows the adjoining seismic Profile GeoB01-82. Similar to Profile GeoB01-081 undisturbed pelagic sediments drape the rough topography of Walvis Ridge. The total sediment thickness amounts ~465 m in the south-west and ~540 m in the north-east. The thickness of the sediment cover separated from the lower unit varies between ~70 m in the middle of the flow path and ~130 m in the north-eastern part of the profile. The boundary between the two sedimentation units is characterized by toplap structures. Just as on Profile GeoB01-081 four sediment drifts occur in the surface sequences. The thicker bodies have an internal structure of continuous reflectors, but of different characteristics. Whereas the eastern one is characterized by an undulating structure, the western one consists out of smooth parallel reflector packages.



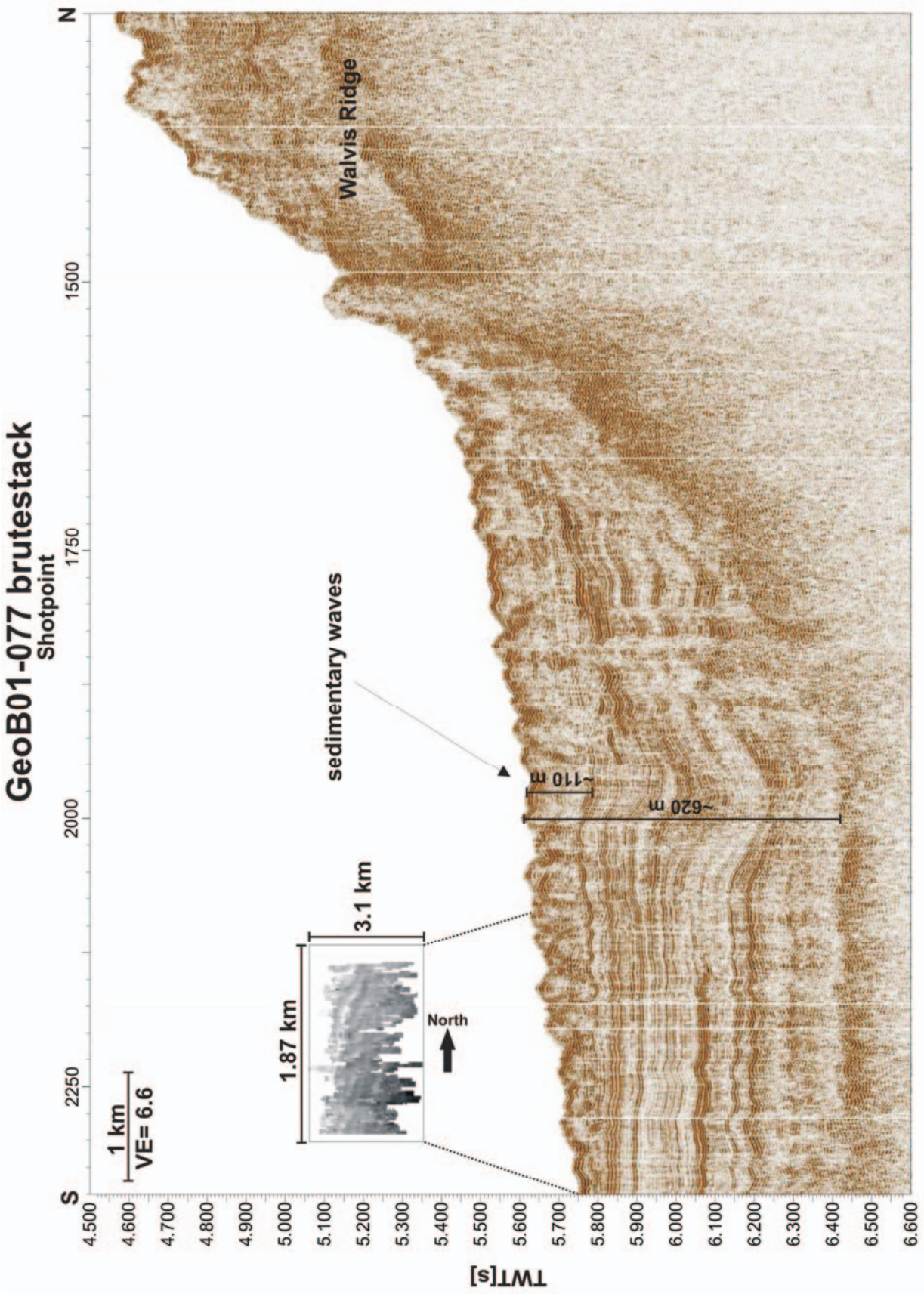
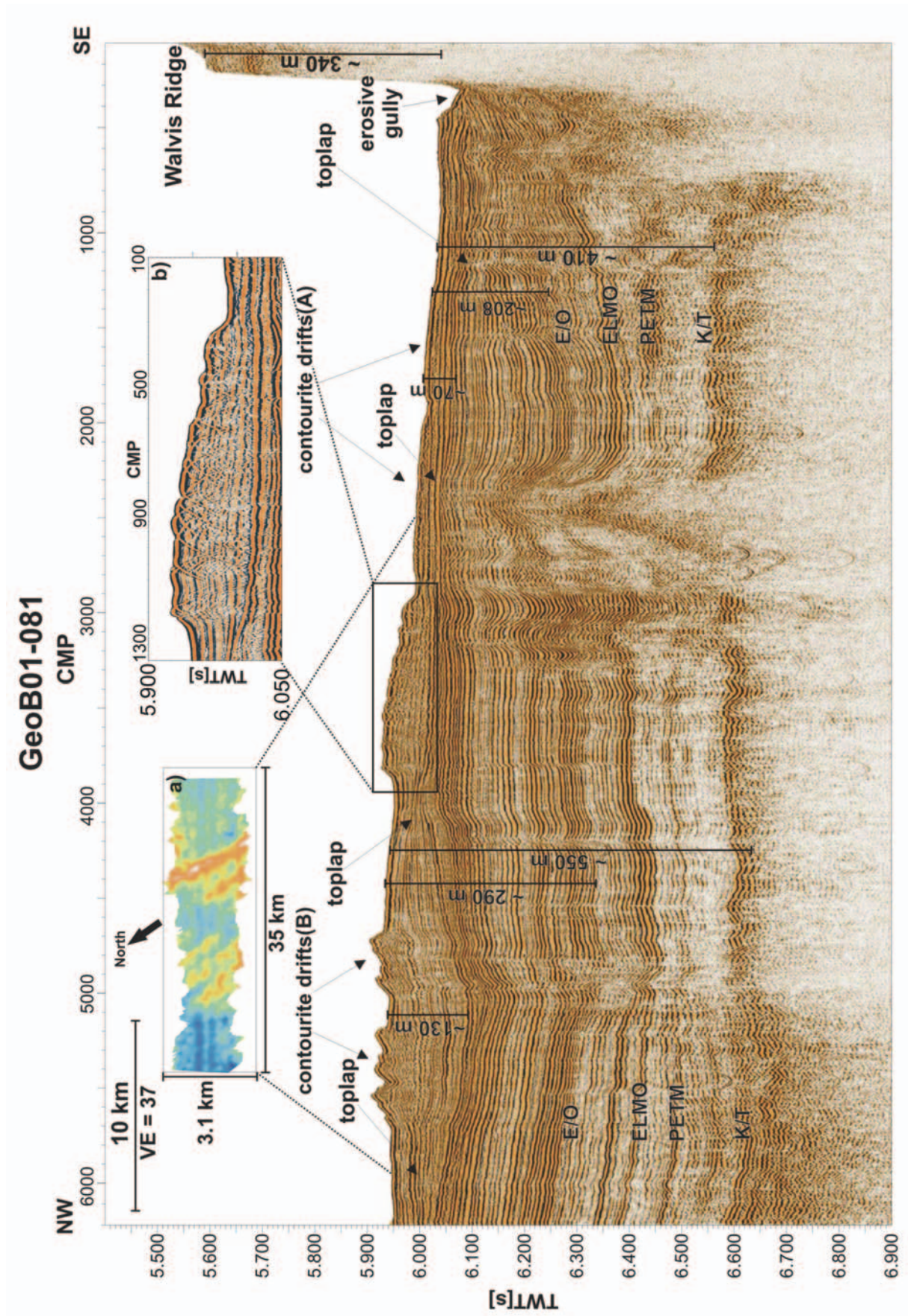


Figure 5.5: Brutestack of Profile GeoB01-077. Inset: Swathsonder data of the southern part of the profile.





**Figure 5.6:** Seismic Profile GeoB01-081. Inset a): Swathsounder data of sediment bodies in the north-western part of the profile. Inset b): Zoomed image of contourite-sheeted drift.



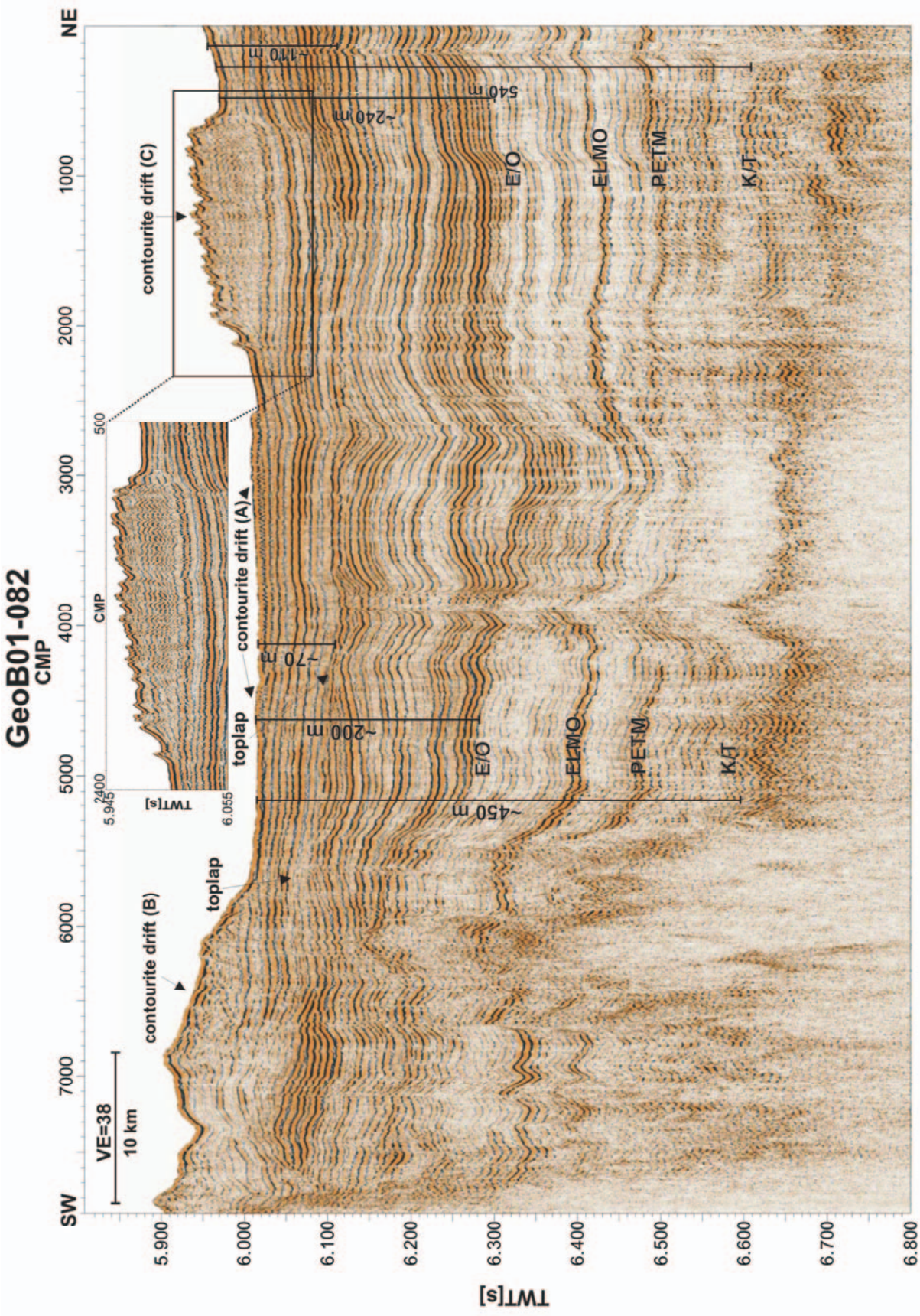


Figure 5.7: Seismic Profile GeoB01-082. Inset: Zoomed image of contourite-sheeted drift.

Figure 5.8 shows the echosounder data of Profiles GeoB01-081 and GeoB01-082, where the first 20 m to 30 m of the surface sediments are imaged with higher resolution. Both profiles show that the surface sediments are dominated by the sediment bodies already described for the seismic data (Fig. 5.6, Fig 5.7). Based on different characteristics the bodies can be separated into three categories (Fig. 5.6, Fig 5.7, Fig.5.8):

- A) thickness < than 15 m, internal structures are not clearly to identify; in the seismic data the bodies occur as an additional seismic reflector at the seafloor; the surface especially in the echo-sounder data indicates undulating structures.
- B) thickness > than 25 m, internal structures of regularly spaced sinusoidal conformable reflectors are imaged in the seismic data as well as the in echo-sounder data, surface has sinusoidal structure.
- C) thickness > than 25 m, internal structure of smooth conformable reflector packages which are probably thinned out at the edges.

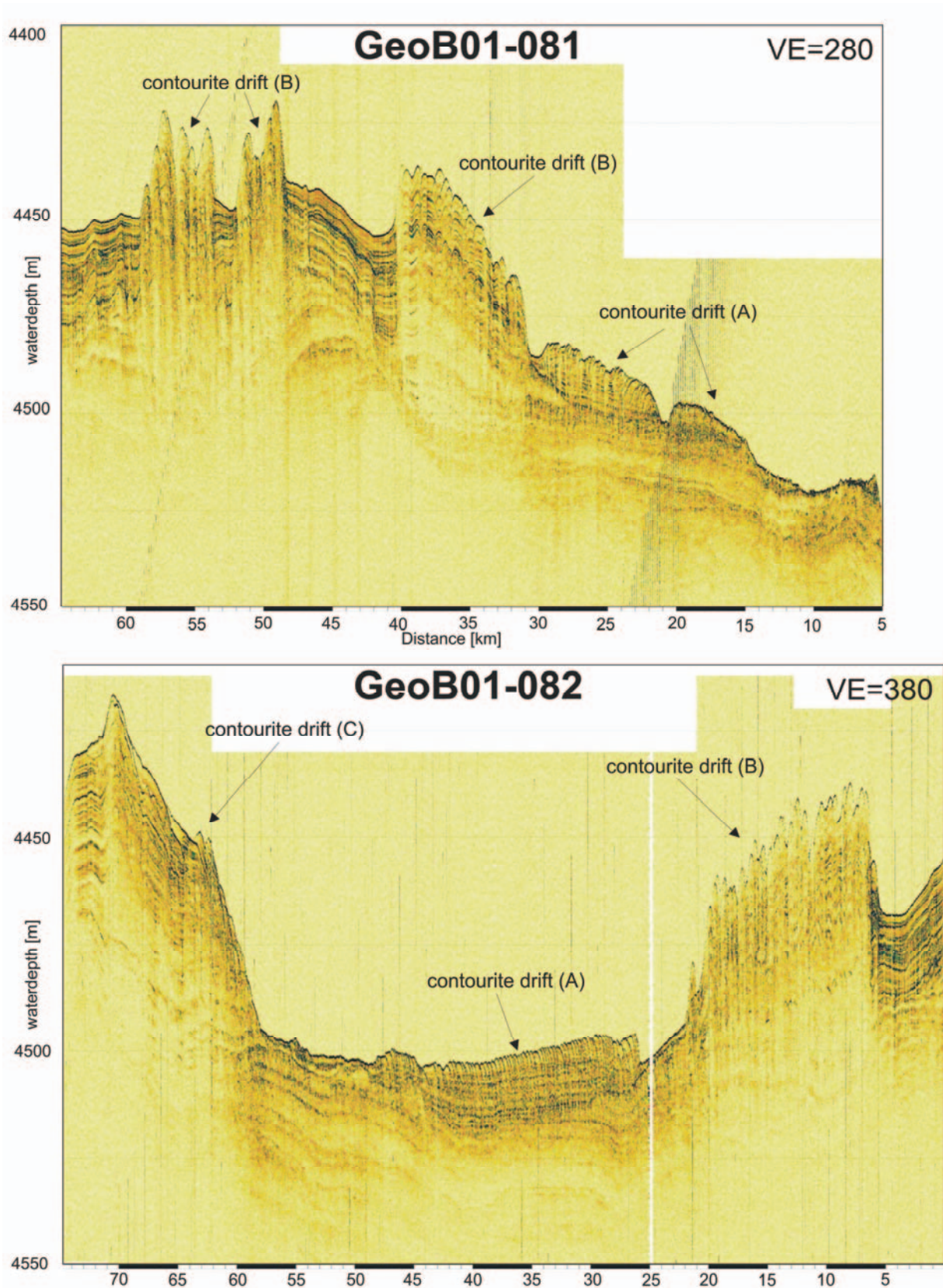
On the following Profiles GeoB01-083 and GeoB01-084 (not shown) the average sediment thickness decreases to ~450 m. Similar as on Profiles GeoB01-081 and GeoB01-082, the deep pelagic undisturbed sediments drape the rough basement of Walvis Ridge. The boundary characterized by toplap structures occurs at ~55 m below the seafloor on Profile GeoB01-083 and on ~45 m below the seafloor on Profile GeoB01-084.

Figure 5.9 shows the middle part of Profile GeoB01-085 which corresponds to the center of the suggested flow path, which is surrounded by the tectonic blocks of Walvis Ridge. With a width of ~30 km it narrows in comparison to Profiles GeoB01-081 and GeoB01-082 (Fig. 5.6 and Fig 5.7), where the width amounts to more than 60 km. The sediment thickness in the pathway is ~400 m (Fig. 5.9), while the top lap structures are found at a depth of ~40 m and shallower. In contrast to the former profiles the thin surface sediments are more disturbed without continuous reflectors. Besides contourite depositions directly at the surface, a depression structure filled with sediments is identified in the seismic data. At CMP number 4120 an almost vertical headwall is imaged, which is characterized by sharp truncated seismic reflectors.

Figure 5.10 shows the southern part of Profile GeoB01-085. The profile crosses an adjoining basin south of the main flow path. The basin is surrounded by tectonic blocks of Walvis Ridge. The sediments of this basin have a thickness of ~500 m. They are characterized by an undisturbed pelagic sedimentation pattern covered by contourite depositions at the surface. Different to the former profiles the boundary between the two sediment sections is



not marked by toplap structures. Because of an undulating surface the thickness of the upper unit varies along the profile with a maximum value of ~90m.



**Figure 5.8:** Parasound data of the Profiles GeoB01-081 and GeoB01-082. Categories A, B, and C of sediment bodies compare Chapter 5.4.2.



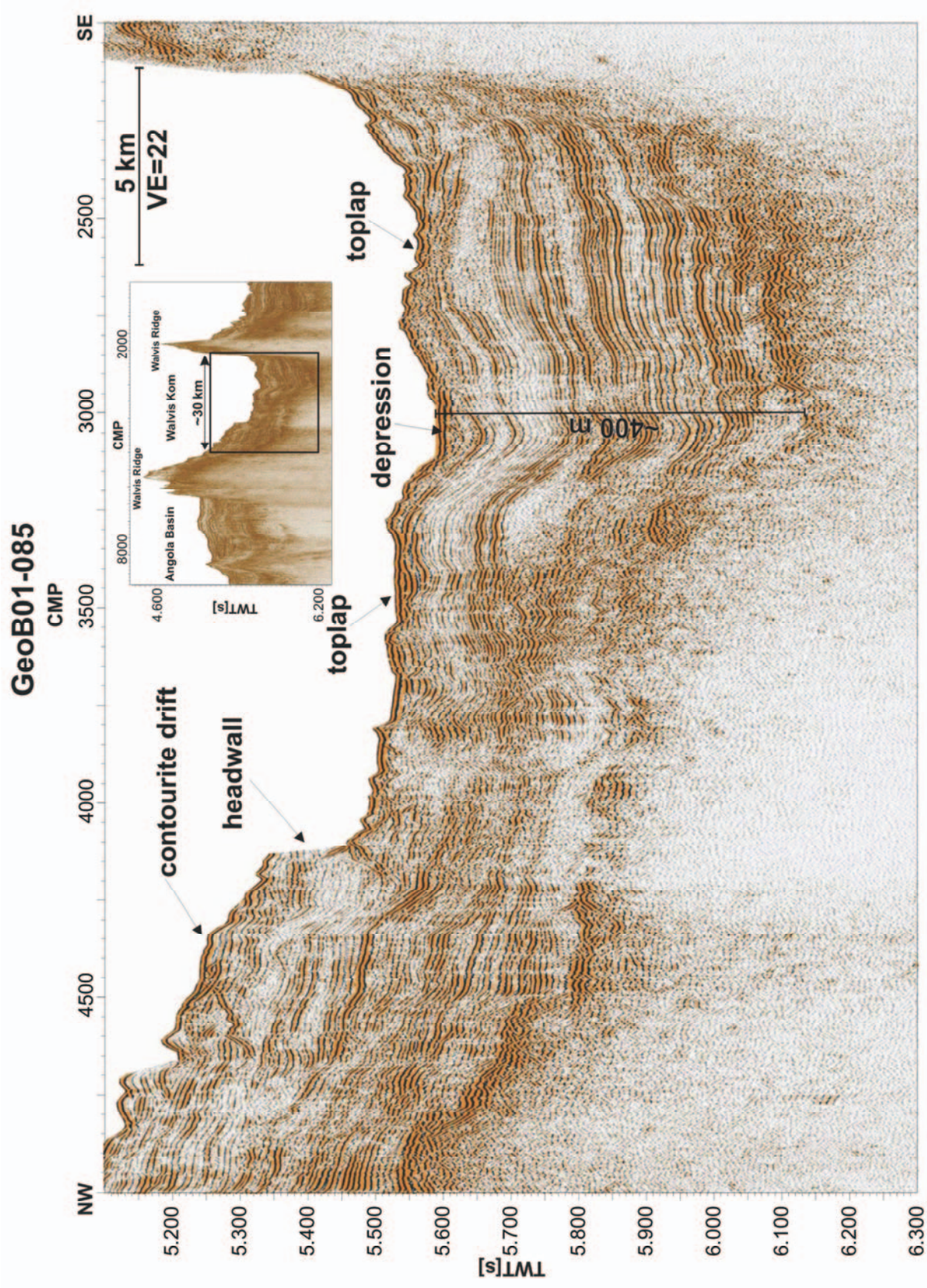
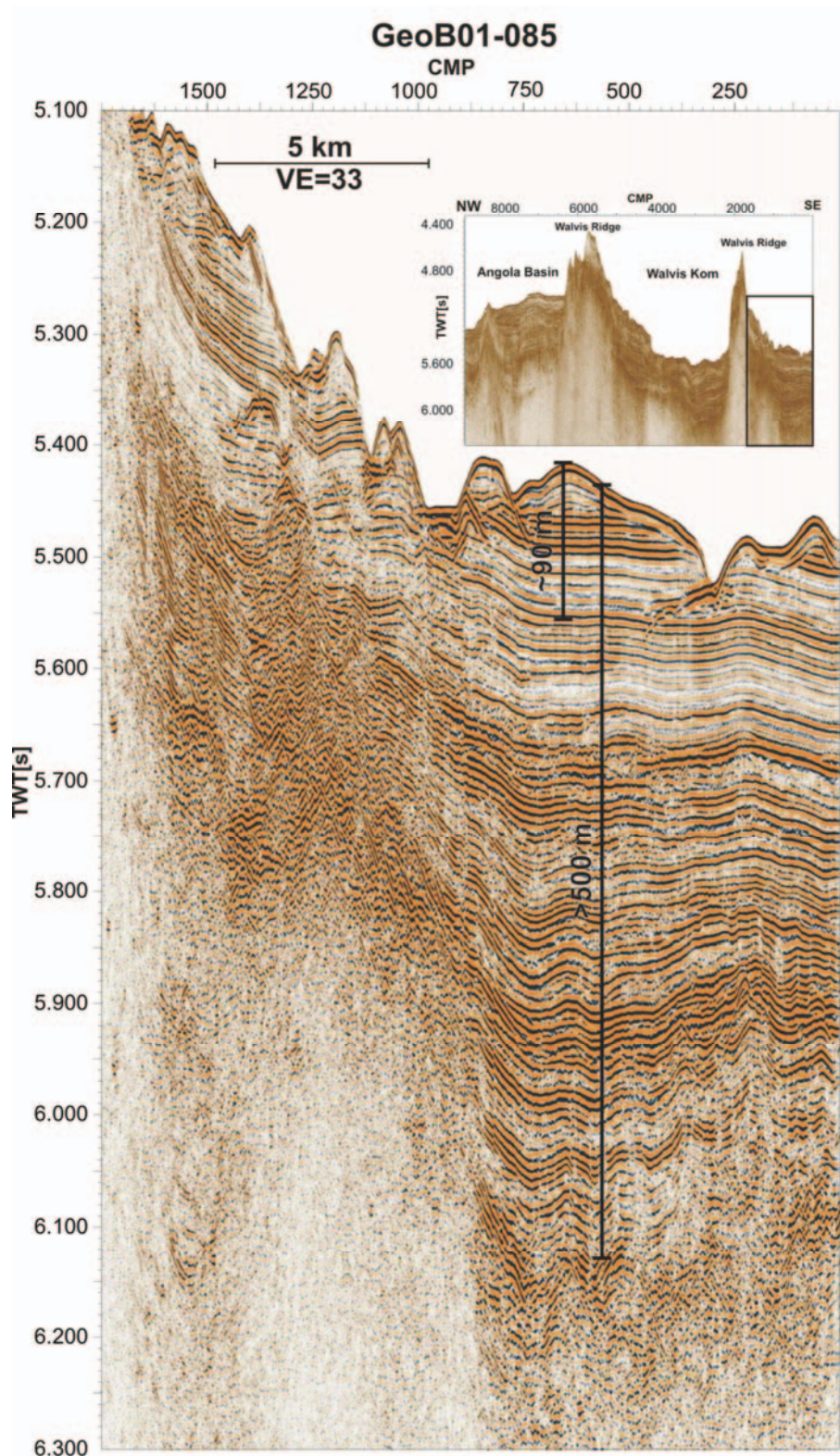


Figure 5.9: Central part of Seismic Profile GeoB01-085 with overview of Profile GeoB01-085.





**Figure 5.10:** South-eastern part of Seismic Profile GeoB01-085 with overview of Profile GeoB01-085.

Figure 5.11 shows the south-western part of Profile GeoB01-086 which corresponds to the outflow of the suggested path way into Angola Basin. The profile runs almost in perpendicular direction to the outflow into Angola Basin. The sedimentation pattern is dominated by the rough topography of Walvis Ridge. The maximum sediment thickness

amounts to ~250 m. The surface sediments are characterized by an undulating cover with a varying thickness. In the center of the profile probably at the outflow of AABW into Angola Basin it amounts ~40 m, but the determination of the boundary between the undisturbed pelagic sedimentary pattern and the disturbed surface sediments is difficult.

### 5.4.3 Stratigraphy

A regional stratigraphic concept has been developed for the area north-east in the vicinity of ODP Leg 208 drill sites, where borehole data had been used for precise age assignment to marker horizons within the Paleogene sequences (Bartels et al., 2007), where several anomalous climatic and oceanographic conditions led to a widespread drop in carbonate content (Zachos, Kroon, Blum et al., 2004). Assuming a regional or global origin of these changes in sediment composition, it can be expected to find the same marker horizon, e.g. the Eocene/Oligocene (E/O) boundary at 35.7 Ma, the ELMO event at 53.2 Ma, the Paleocene Eocene Thermal Maximum (PETM) at 55 Ma, and the Cretaceous/Tertiary boundary at 60 Ma, within the area around the Walvis Kom. A difference is, however, that the deposited sediment sequences in the southern part are under the influence of the Cape Basin oceanography.

In Figure 5.6 and Figure 5.7 on profiles GeoB01-081 and GeoB0-82 the marker horizons of Leg 208 are assigned to the sediments of the Walvis Kom. Both profiles are suited for this task because of the smoothest topography of the basement resulting in a mostly undisturbed sedimentation pattern. Hence, the seismic reflectors are characterized by a good continuity over several kilometers.

The K/T boundary occurs directly above the crystalline basement as a non-continuous reflector with high amplitudes on both profiles. Similar as on the north-eastern flank, the reflector is disturbed because of rough basement topography of Walvis Ridge. The next overlying characteristic horizon represents the PETM. It occurs as a continuous, reflector characterized by strong amplitudes. Different to the seismic data of the north-eastern flank, where the PETM occurs as a part of a reflector package with increasing amplitudes, the PETM at Walvis Kom is resolved as a singled reflector. The next seismic reflector represents the ELMO horizon. With a good continuity and strong amplitudes it has the same seismic attributes as at the north-eastern flank. It represents the last continuous single reflector in the Paleogene sediments. Like on Profile GeoB01-081 it is partly part of a package of high amplitude reflectors. In this case it is represented by the lowermost reflector (Bartels et al.,

2007). Typical for all seismic profiles at Walvis Ridge the E/O boundary occurs at the Walvis Kom as a sharp transition from a package of sediments imaged as reflectors with low amplitudes in the Eocene sediments to a thicker package of reflectors with high amplitudes in the Oligocene sediments (Bartels et al. 2007). It marks the most significant transition of the Neogene sediments and occurs well pronounced at Profiles (Fig. 5.6 and Fig. 5.7).

## 5.5 Discussion

In 1991, Shannon and Chapman provided the first evidence of AABW in the Angola Basin at 32°S. Temperature and salinity measurements along a suggested path way between Cape Basin and Angola Basin showed a possibly exchange of AABW and NADW between the two basins. The location of the measurements were based on echo sounder data, whereas the flow path of AABW trough the Walvis Kom and over the western sill of Walvis Ridge between 2° and 3° is still a matter of speculation (Fig. 5.2). Until now, no indications for current activities in the sediments are known (Shannon and Chapman, 1991).

AABW is pushed by the Coriolis force against Walvis Ridge (Dingle et al., 1977) and probably enters Walvis Kom, which builds a channel like structure for bottom waters. The summits of the surrounding blocks of Walvis Ridge rise to at least ~3000 m water depth, while some even show heights of <2000 m water depth. With water depth of 4150 m – 4500 m, the thalweg of the flow path (Fig. 5.3), represents a suitable flow path for a bottom water exchange between the Cape Basin and the Angola Basin. Confinements strengthen bottom water current flows (Wong et al., 2003) and bottom water models show that bottom water currents follow topography (e.g. Rhein et al., 2002), hence the blocks of Walvis Ridge probably lead AABW entering the Walvis Kom. The boundary between AABW and NADW at a water depth of 3800 m is constant along the flow path between the Cape Basin and the Angola Basin (Shannon and Chapman, 1991). The interaction of the decreasing water depth of the thalweg (Fig. 5.3) and the decreasing width of the path way, leads to a reduced cross-section of the flow of AABW between the two basins. Because of conservation of vorticity (e.g. Brown et al., 1993), this effect must lead to an increase of the current velocity of AABW through the Walvis Kom entering Angola Basin. As a result of this higher current velocity the sediment thickness decreases in the direction of Angola Basin (Fig. 5.3).



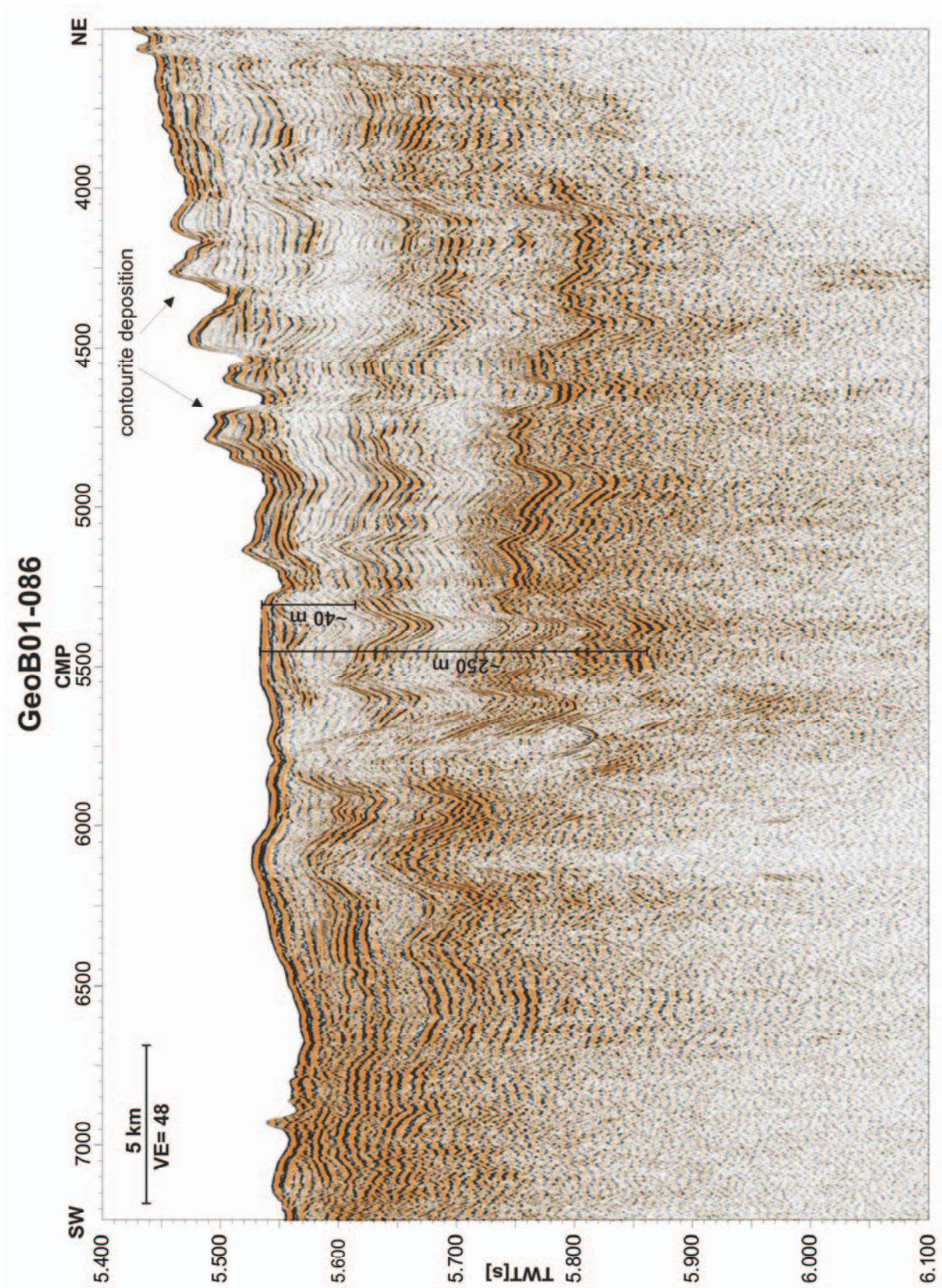


Figure 5.11: Seismic Profile GeoB01-086.

The pelagic sedimentation, which drapes the rough topography of the Walvis Kom at Walvis Ridge, is dominated by the interplay between production of biogenic carbon particles

and solution of carbon depending on a change of hydrography and water depth (e.g. Thunell 1982, Balsam and McCoy, 1987). With an increasing water depth and increasing solution of the carbonate content, the deeper parts of the Cape Basin are draped only with dark deep sea clay (Bickert, 1992). Therefore the sedimentation rates of the South Atlantic especially at Walvis Ridge are low and vary between 10 – 20 m ka<sup>-1</sup> (Embley and Morley, 1980). With an estimated age of the oldest sediments at Walvis Ridge of ~71 Ma (Zachos, Kroon, Blum, et al., 2004) and a maximal sediment thickness of ~600 m on Profile GeoB01-077, the average sedimentation rate at the Walvis Kom is even lower than 10 mm ka<sup>-1</sup>.

The Paleogene sediments of the Walvis Kom are undisturbed and obviously not influenced by bottom water activities or gravity driven sediment transports (e.g. slumps, turbidites, etc.). In contrast, the surface sediments show several indicators for current activities, which allude on bottom water activity:

### **Toplap structures**

Several toplap structures occur on almost all profiles along Walvis Kom at the base of the younger sediment sections at depth between 70 m and 30 m. Seismic reflectors are truncated probably because of non-deposition bottom currents and are covered by a subsequent sediment cover. The toplap structures mark the transition between an undisturbed sedimentation period and a current influenced sedimentation period. Hence they represent an unconformity which marks the beginning of the current activities.

### **Sediment waves**

On Profile GeoB01-077 (Fig. 5.5), the interaction of undulating sediment cover in the seismic data and linear elongated patterns in the bathymetry data indicates that sedimentary waves occur in the northern part of Walvis Kom. The waves have a height of 20-30 m and a wavelength of a few hundred meters. Such sedimentary waves are defined as large-scale (generally tens of metres to a few kilometres wavelength and several meters high), undulating, depositional bedforms which are generated beneath a current flowing at, or close to, the seafloor (Wynn et al. 2000). Besides turbidity origin they can have bottom water current origin, wherefore they are observed in places, where bottom currents play an important role in the depositional environment, e.g. at topography ridges and bottom current passages (e.g. Wynn et al. 2000, 2002). Sedimentary waves with regular structures in time and space

develop if bottom currents are extremely stationary over longer time periods (e.g. Flood and Shoor, 1988). Hence, the occurrence of such sedimentary waves suggests a constant flow of AABW through the Walvis Kom, which is recently still present.

### **Contourite Drifts**

Several sediment blocks were identified at the surface on the profiles at Walvis Kom. With their varying thickness between ~10 m and ~40 m and their different characteristics of their internal structures it is possible to group those bodies into three categories (compare Chap. 5.4.2). Category B and C with a thicknesses >25 m are characterized by internal structures of parallel seismic reflectors. Hence, all forms of gravity transports (e.g. turbidites, slumps, debris flows) as their origin can be excluded (Fig. 5.6-5.8). The examples show a distinct internal layering and a smooth transition to the older undisturbed pelagic sediments, wherefore the development of the sediment bodies is probably related to bottom currents. Deposits controlled by deep-water currents resulting from thermohaline circulation in the oceans form accumulations known as contourite drifts (Faugerès et al. 1999). Such abyssal contourite sheets have internal seismofacies, which are typically of lower amplitude and sometimes characterized by discontinuous reflectors thinned out at the margin of the drift (Faugerès et al. 1999). Sometimes they comprise or are covered by fields of sediment waves (e.g. Damuth, 1975, Mézerais, 1991, Faugerès et al. 1999). Both types of sediments bodies occur at Walvis Kom. Category B on Profile GeoB01-082 (Fig. 5.7 and Fig. 5.8) is characterized by internal structures with low amplitudes which are disturbed at the margin of the body. Category C is build out of sedimentary waves. Hence the sediment bodies at Walvis Kom probably represent contourite-sheeted drifts developed out of changing deposition conditions caused by constant bottom current activities. The continuity of the seismic reflectors along the drifts and the upper sediment sections indicate that the drifts are sedimented during the same time periods, caused by different current speeds along the flow path. The thickness of the bodies of the category A is too thin to analyze the internal structures in the seismic data as well as in the echo-sounder data. The surface indicates a wavelike cover. Potentially they represent a recent development of new drift bodies probably caused by changing depositional conditions.

As described above the sedimentary deposits can be separated into two units, separated by an unconformity indicated by several toplap structures along the seismic profiles.

Only Profile GeoB01-077 (Fig. 5.5) images no toplap structures, instead a change from an undisturbed sedimentation pattern to an undulating pattern (Fig. 5.5) occurs. This boundary probably represents the same time as the unconformity, which marks the beginning of the current activities.

The thickness of the sediment cover influenced by current activities varies between ~110 m and ~30 m along the path way from the Angola to the Cape Basin (Fig. 5.3). The northern part of Walvis Kom at Profile GeoB01-077 (Fig. 5.5) probably represents a sediment trap, where the current speed of AABW decreases and therefore resulted in the development of the sedimentary waves. The sediment thickness of the profiles along Walvis Kom decreases from ~70 m on Profiles GeoB01-079 – GeoB01-082 on ~30 m on Profiles GeoB01-085 and GeoB01-086. This decrease in the sediment thickness is probably a result of less- or non-deposition of the biogenic sediments resulting from increasing current velocities through the flow path caused by the decreasing cross-section of the current.

High current velocities may form erosional channel structures at the seafloor. Such channels would be carved into the seafloor cutting through existing sedimentary layers. In contrast, the observed structures in the surface sediments at Walvis Kom show mostly continuous seismic reflectors except the unconformity. This indicates that current velocities were too low for erosion leading to non-deposition and current influenced sedimentation on top of the unconformity. Recent current velocities are probably also relatively low.

Unfortunately no characteristic marker horizons exist for the Neogene sediment sections, wherefore the age of the unconformity must be evaluated out of the thickness of the Neogene sediments. The thickness of the sediment sequences above the E/O boundary on Profile GeoB01-082 (Fig. 5.8) varies between ~200 m at the center of the pathway and ~240 m at the edges. Assuming that current velocities in the middle of the path have been higher than at the margins of the flow path, the sediments in the middle of the profile represent thinned out sediments or even periods of non-deposition. The difference in sediment thickness on top of the unconformity sums up to 40 m between the center and the edges of the flow path. Hence the sediments sequences at the margin of the profile represent the most complete Neogene sections which were recorded. With a sediment thickness of ~240 m the average sedimentation rate during the Neogene amounts  $0.6 \text{ cm ka}^{-1}$ , which is less than the typical rates of  $1 \text{ cm ka}^{-1}$  for Walvis Ridge during the Neogene (Zachos, Kroon, Blum et al., 2004). Hence the deposition rates decreased during the Neogene, probably because of current activities along the Walvis Kom. Assuming a constant accumulation during the Neogene the initiation of the strong erosive current activities occurred at ~16 Ma (Lower Miocene), which



is reasonable because most important changes of the oceanography of the South Atlantic Ocean, e.g. the closure of the Central American Seaway between North and South America between 16 Ma (e.g. Duque-Caro, 1990; Droxler et al., 1998) and 3 Ma (Keigwin, 1982; Marshall et al, 1982; Coates et al, 1992) and a intensified production of NADW between 11-10 Ma (Woodruff and Savin, 1989), occurred during the Miocene. Recent current activities are too weak for erosion, because no erosive structures occur above the unconformity. However the contourite drifts and the sedimentary waves demonstrate the existence of recent bottom water activities. Stronger current activities during the Paleogene can be excluded because no indications or current influenced sediments were found in the deeper sediments.

In the southern part of the Walvis Kom, a smaller basin adjoins the thalweg of the suggested flow path (Fig. 5.4 and Fig 5.10). The sediment thickness exceeding 500 m is higher than in the flow path where the thickness amounts to ~400 m. The general sedimentary pattern in the adjoining basin, however, is very similar to all other profiles. The Paleogene sediments are undisturbed, whereas the near surface sediments show indicators for bottom current activities, i.e. contourite depositions. Probably a part of AABW flowing to Angola Basin is split from the main flow to pass through this basin (Fig. 5.4). This is presumably, because bottom water masses follow the topography (e.g. Rhein et al., 2002). A most likely meandering flow path through the basin causes lower current velocities which results in the higher sedimentation rates higher deposition rates of the upper sedimentary unit.

## 5.6 Conclusions

The results of the data collected during R/V Meteor Cruise M49/1 supports the hypothesis of Shannon and Chapman (1991) that a transfer of AABW at the Walvis Kom from the Cape Basin to the Angola Basin exists. The Walvis Kom is suitable for this bottom water transfer because blocks of Walvis Ridge form a channel like structure which leads the bottom water mass. AABW is pushed by Coriolis force into the flow path from the Cape Basin to the Angola Basin. Several toplap structures, contourite-sheeted drifts and sedimentary waves emphasize the hypothesis of recent bottom water activities. The results of the bathymetry data in combination with the seismic data show a decreasing width and a decreasing water depth of the flow path. This narrowing results in an increasing current velocity causing reduced deposition along the path way in direction to the Angola Basin. A rough age model determines the initiation of strong current activities during the Lower

Miocene at ~16 Ma. The current induced indicators e.g. the sedimentary waves and the contourite-sheeted drifts, suggest a recently weak bottom current activity.

A smaller basin adjoining the flow path to the south of the Walvis Kom indicates that AABW must be partly split during the exchange between the basins. AABW is mainly lead by the topography of the ridge into the adjoining basin and forms contourite depositions, which indicate lower current velocities, because of an increased thickness of the sedimentary sequence.

## 5.7 Acknowledgements

We are grateful for the support of the captain and the crew members as well as all cruise members of R/V Meteor Cruise M49/1 for their help during the expedition. We also want to thank the Scientific Shipboard Party of the ODP Leg 208, who did a great job. This research used samples and/or data provided by the Ocean Drilling Program (ODP). ODP is funded by the U.S. National Science Foundation (NSF) and participating countries under management of Joint Oceanographic Institutions (JOI), Inc. This research was funded by Deutsche Forschungs Gemeinschaft, Grant Sp 296/24-1, "Sedimentation processes on Walvis Ridge - correlation of high resolution seismic records with ODP Leg 208 physical properties data".

## 5.8 References

Arhan M., Mercier H., Park Y.H., 2003. On the deep water circulation of the eastern South Atlantic Ocean, *Deep-Sea Research I* 50, 889-916.

Balsam W.L., Mc Coy F.W.J., 1987. Atlantic sediments: Glacial/interglacial comparisons. *Paleocenography*, 2: 531-542.

Bartels T., Krastel S., Spiess V., 2007. A correlation of high resolution seismic data with ODP Leg 208 borehole measurements. ODP Leg 208 Scientific Results, Manuscript Number SR208-204, [http://www-odp.tamu.edu/publications/208\\_SR/204/204.htm](http://www-odp.tamu.edu/publications/208_SR/204/204.htm), Chapter 2).

Bartels T., Krastel S., Spiess V., 2006. Cenozoic evolution of central Walvis Ridge paleotopography, Chapter 4.

Borella P.E., 1984, Sedimentology, Petrology and cyclic sedimentation patterns, Walvis Ridge transect, LEG 74, Deep Sea Drilling Project, Initial reports of the Deep Sea Drilling Project, Leg 74, U.S. Govt. Printing Office, pp 645-666.

Brown J., Colling A., Park D., Phillips J., Rothery D., Wright J., 1989. Book: Ocean Circulation. The Open University, Walton Hall, and Butterworth-Heinemann.

Caress D.W., Chayes D.N., 1996. Improved processing of Hydrosweep DS Multibeam data on the R/V Maurice Ewing. *Marine Geophysical Researches*, 18, 631-650.

Coates A.G., Jackson J.B.C., Collins J.S., Cronin T.M., Dowsett H.J., Bybell L.M., Jung P., Obando J.A., 1992. Closure of the Isthmus of Panama: The near-shore marine record of Costa Rica and western Panama. *Geol. Soc. Am. Bull.*, 104, 814-828.

Connary S.D., Ewing M., 1972. The nepheloid layer and bottom circulation the Guinea and Angola Basins. *Studies in physical oceanography: a tribute to George Wüst on his 80<sup>th</sup> birthday*, Gordon and Breach, New York, 2, 169-184.

Connary S.D., Ewing M., 1974. Penetration of Antarctic Bottom Water from the Cape Basin into the Angola Basin. *Journal of Geophysical Research*, 79, 463-469.

Dammot J.E., 1975. Echo character of the western equatorial Atlantic floor and its relationship to the dispersal and distribution of terrigenous sediments. *Marine Geology*, Vol. 18, 17-45.

Dingle R.V., 1977. The anatomy of large submarine slump on a sheared continental margin (SE Africa). *J. Geol. Soc. London*, 134, 293-310.

Droxler A. W., Burke K.C., Cunningham A. D., Hine A. C., Rosencrantz E., Duncan D.S., Hallock P., Robinson E., 1998. Caribbean constraints on circulation between Atlantic and Pacific oceans over the past 40 million years, in *Tectonic Boundary Conditions for Climate Reconstructions*, edited by Crowley T.J. and Burke, K.C., 169-191, Oxford Univ. Press, New York, 1998.

Duque-Caro H., 1990. Neogene stratigraphy, paleoceanography and paleobiogeography in northwest South America and the evolution of the Panama Seaway. *Palaeogeogr., Palaeoclimatol. Palaeoecol.*, 77, 203-234.

Embley R.W., Morley J.J., 1980. Quaternary sedimentation and paleoenvironmental studies off Namibia (SW Africa). *Marine Geology* 36, 183-204.

Faugères J.C., Mezerai M.L., Stow D.A.V., 1992. Contourite drift types and their distribution in the North and South Atlantic Ocean basins. *Sedimentary Geology*, 82, 189-203.

Faugères J.C., Stow D.A.V., Imbert P., Viana A., 1999. Seismic features diagnostic of Contourite drifts. *Marine Geology*, Vol. 162, 1-38.

Flood R.D., Shor A.N., 1988. Mudwaves in the Argentine Basin and their relationship to regional circulation patterns. *Deep Sea Research*, Vol. 35, 973-983.

Fuglister F.C., 1960. Atlantic Ocean Atlas of temperature and salinity profiles and data from the International Geophysical Year of 1957-1958. Woods Hole Oceanographic Institution Atlas Series, 1, 209pp.

Grant J.A., Schreiber R., 1990. Modern Swath Sounding and Sub-Bottom Profiling Technology for Research Applications: The Atlas Hydrosweep and Parasound Systems. *Marine Geophysical Researches* 12, 9-19.

Keigwin L., 1982. Isotopic paleoceanography of the Caribbean and East Pacific: Role of Panama uplift in the Late Neogene time. *Science*, 217, 350-352.

Keller G., Barron J.A., 1983. Paleoceanographic implications of the Miocene deep sea hiatuses. *Geol. Soc. Am. Bull.*, 94, 590-613.

Marshall J., Shott F., 1982. Open-ocean convection: Observations, theory, and models. *Rev. Geophys.*, 37(1), 1-64, J.



Mézerais M.L., 1991. Accumulations sédimentaires profondes tubiditique (deep-sea fan du Cap Ferret) et contouritique (basin sud-brésélien) : géométrie, faciès, édification. Thèse, University Bordeaux I, 606, 301 pp.

Rhein M., Fischer J., Smethie W.M., Smythe-Wright D., Weiss R.F., Mertens C., Min D.-H., Fleischmann U., Putzka A., 2002. Labrador Sea Water: Pathways, CFC Inventory, and Formation Rates. *Journal of physical oceanography*, American Meteorological Society, Volume 32, 648-665.

Rogers J., 1987. Seismic, bathymetric, and photographic evidence of widespread erosion and manganese pavement along the continental rise of the southeast Cape Basin. *Marine Geology*, 78, 57-76.

Shannon L.V., Chapman P., 1991. Evidence of Antarctic Bottom Water in the Angola Basin at 32°S. *Deep Sea Research*, Vol. 38, No. 10, pp. 1299-1304.

Shannon L.V., van Rijswijk M., 1969. Physical oceanography of the Walvis Ridge region. Investigational Report of the Division of Sea Fisheries, South Africa, 70, 1-19.

Siedler G., Müller T.J., Onken R., Arhan M., Mercier H., King B.A., Saunders P.M., 1996. The Zonal WOCE Sections in the South Atlantic. From Wefer G., Berger W.H., Siedler G., Webb D.J., (eds) 1996, *The South Atlantic: Present and Past Circulation*. Springer-Verlag Berlin Heidelberg, 599-620.

Spiess V., Cruise Participants, 2003. Report and preliminary results of Meteor Cruise M49/1, Capetown (South Africa) - Montevideo (Uruguay), 04.01.2000 - 10.02.2000. *Berichte Fachbereich Geowissenschaften, Universität Bremen*, No. 205: 1- 57.

Suspan A., 1899. Die Bodenformen des Weltmeeres, *Petermanns Geogr. Mitt.*, 45, 117.

Tucholke and Embley, 1976. A continuous erosional zone in the Cape, Agulhas, and Mocambique Basins. *Geological Society of American Bulletin*, 88, 1337-1346.

Thunell R.C., 1982. Carbonate dissolution and abyssal hydrography in the Atlantic Ocean. *Marine Geology*, 47, 165-180.

Wessel P., Smith W.H.F., 1998. New, improved version of Generic Mapping Tools released. *EOS Transaction, American Geophysical Union*, 79(47), 579.

Wong H.K., Lüdmann T., Baranov B.V., Karp, B.Y., Konerding P., Ion G., 2003. Bottom current-controlled sedimentation and mass wasting in the northwestern Sea of Okhotsk. *Marine Geology* 201, 287-305.

Woodruff F., Savin S.M., 1989. Miocene deepwater oceanography. *Paleoceanography*, 4, 87-140.

Wüst G., 1936. Das Bodenwasser und die Gliederung der Atlantischen Tiefsee. *Wiss. Ergebnisse Deut. Atlantik Expeditionen Meteor*, 6(1),3-107.

Wynn R.B., Weaver P.P.E., Ercilla G., Stow D.A.V., Mason D.G., 2000. Sedimentary processes in the Selvage sediment wave-field, NE Atlantic: new insights into formation of sediment waves by turbidity currents. *Sedimentology* 47, 1181-1197.

Wynn R.B., Stow D.A.V., 2002. Classification and characterization of deep-water sediment waves. *Marine Geology*, 192, 7-22.

Zachos J.C., Kroon D. Blum P., et al., 2004. Proceedings of the Ocean Drilling Program, Initial Reports Volume 208, available on the web:

[http://www-odp.tamu.edu/publications/208\\_IR/VOLUME/CHAPTERS/IR208\\_01.PDF](http://www-odp.tamu.edu/publications/208_IR/VOLUME/CHAPTERS/IR208_01.PDF)

## 6. Final conclusions

Walvis Ridge is an aseismic ridge in the eastern South Atlantic Ocean, which separates the Cape Basin south of the ridge from the Angola Basin in the north. It is one of the few known locations where it is possible to recover undisturbed Paleogene sediments over a broad range of water depths ranging from roughly 2 km to more than 4.5 km. Hence, Ocean Drilling Project (ODP) Leg 208 was drilled in 2003 in order to sample “critical” climatic transitions, e.g. the Eocene/Oligocene (E/O) boundary, the ELMO horizon, the Paleocene Eocene Thermal Maximum (PETM), the Mid-Paleocene biotic event (ELPE event), and the Cretaceous/Tertiary (K/T) boundary. Site selection was mainly based on multichannel seismic GI-Gun data collected by Bremen University in 2001. This study represents a detailed analysis of the depositional history of Walvis Ridge by means of a joint interpretation of seismic and borehole data, which in turn allows to draw important conclusions on changes of the oceanographic regime.

Correlation between the six drill sites of ODP Leg 208 and seismic GI-Gun data was achieved by the calculation of synthetic seismograms. As a result of this correlation, it is possible to assign ages to significant reflectors in the seismic profiles. Target reflectors show similar seismic attributes at all drill sites, wherefore they were traced over the entire study area of Leg 208. The resulting depth maps of these dated seismic reflectors were used to construct a model of the paleoseafloor, which shows that the rate of subsidence during the last 50 Ma of the Angola Basin was almost compensated by the increasing thickness of the sedimentary succession. In addition the model illustrates that bottom water activities increased in the southeast of the study area between 28°S and 30°S. A channel developed across Walvis Ridge which is possibly related to an exchange of bottom waters between Cape Basin and Angola Basin. A stratigraphic analysis of the data shows that the current activities increased since the Middle Miocene, which is known as a dynamic period of the oceanography of the South Atlantic where significant changes, e.g. the closure of the Central American Seaway between North and South America, occurred.

Seismic imaging of sub-meter units in the deep sea at a sediment depth of several hundreds meters is an ambitious task, which cannot be solved using a GI-Gun as a source. Instead a higher resolution Watergun, which was also recorded in the study area of Leg 208, provides sufficient frequencies to resolve such thin sedimentary horizons. But, the vertical movements of the streamer and the gun due to wave action calls for additional static corrections of the Watergun data, which were successfully included into the standard seismic

processing steps. A comparison between these high resolution seismic images and the magnetic core measurements of Leg 208 shows, that it is possible to resolve such thin layers, in this study represented by “critical” climatic transitions like the PETM, the ELMO horizon, or the ELPE event, as singled seismic reflector packages clearly separated from each other in the deep sea sediments.

Farther southwest at 32°S the seismic profiles of Meteor Cruise M 49/1 cross a flow path between the Cape Basin and the Angola Basin in a region called Walvis Kom, where temperature and salinity measurements suggest an exchange of Antarctic Bottom Water (AABW) and North Atlantic Deep Water (NADW). The results of the seismic data in combination with bathymetric and echosounder data supports the idea that the Walvis Kom is a possible pathway for the transfer of AABW. Several toplap structures, contourite-sheeted drifts and sedimentary waves in the surface sediments indicate recent bottom water activities. A restriction of the cross-section of the pathway results in increasing current velocities, which are documented by smaller accumulation rates in the seismic data. A rough age model dates the initiation of these currents during the Lower Miocene at ~16 Ma.

In summary, the results of this study show that thin sedimentary layers (meter to sub-meter scale) can be resolved in a deep sea pelagic environment by very high resolution Watergun data. This knowledge will be very helpful for further drilling campaigns and positioning of drill sites.

In contrast to the classical assumption that Walvis Ridge builds an impassable barrier for bottom waters with possibly only two leakages (Walvis Passage and Namib Col), two additional potential regions of deep water exchange between the Cape and Angola Basins could be identified. One is located in the study area of ODP Leg 208 at 28°S and the second at the Walvis Kom at 32°S. The strength and the direction of the currents in both areas is still a matter of speculation, but non-deposition instead of erosion suggests relatively slow current velocities.

Because of the low dense of the seismic data a more detailed study including a detailed temporal evolution and spatial distribution of current induced structures is not possible. Hence, a higher dense of the seismic lines including some core samples of the surface sediments would be desirable to study the sedimentary evolution of both areas. Additional detailed oceanographic studies, including current measurements, temperature measurements and salinity measurements would be helpful to verify the suggested exchanges of the bottom waters between Angola Basin and Cape Basin.



## 7. Acknowledgements

I like to thank Prof. Dr. Heiner Villinger, who gave me the chance to finish this study. I am very thankful to him for being my advisor at a time, when I had almost lost hope to finish this study. Next I would also like to thank Prof. Dr. Thilo von Dobeneck for writing the secondary expertise.

Additionally I like to acknowledge with great thanks Dr. Sebastian Krastel for being a very supportive co-advisor, who was always able to find some minutes for useful and stimulating discussions during all my time at the University of Bremen.

Of course I thank all my colleagues from MTU/FB 5 at the University of Bremen for excellent cooperation and a good working relationship: Prof. Dr. Volkhard Spiess for giving me the chance to work on this study, Angelika Rinkel, who provided important administrative support, and especially Dr. Lars Zühlendorff, who thought me the basics of scientific working.

Collecting and processing of the data were funded by the DFG. All maps in this study were created using the public domain software Generic Mapping Tool (GMT) (Wessel and Smith, 1998). The seismic processing was made with the commercial software package `Vista` (Seismic Image Software LTD.), the interpretation was provided by the software `Kingdom Suite`, given as a donation of Seismic-Micro Technology, Inc. The hydrosweep data processing was carried out with the public domain software MultiBeam (Caress and Stockwell, 1996).

Finally I would like to thank my family, my wife Annika, my children Simon, Nora and Ida and my parents who provided me the basis to reach for a higher dream.